Combined MAGSAT and Aeromagnetic Investigation of the Alpha Ridge Crust

by

Henry Dilah Odwar

A thesis

presented to the University of Manitoba

in fulfilment of the

thesis requirement for the degree of

Master of Science

in

Geophysics

Winnipeg, Manitoba, Canada 1993

ISBN 0-315-81802-6

Canada

Name _____

Dissertation Abstracts International is arranged by broad, general subject categories. Please select the one subject which most nearly describes the content of your dissertation. Enter the corresponding four-digit code in the spaces provided.

GEOPHYSICS
SUBJECT TERM

|0|3|7|3| **U·M·I**
SUBJECT CODE

Subject Categories

THE HUMANITIES AND SOCIAL SCIENCES

COMMUNICATIONS AND THE ARTS
Architecture 0729
Art History 0377
Cinema 0900
Dance 0378
Fine Arts 0357
Information Science 0723
Journalism 0391
Library Science 0399
Mass Communications 0708
Music 0413
Speech Communication 0459
Theater 0465

EDUCATION
General 0515
Administration 0514
Adult and Continuing 0516
Agricultural 0517
Art 0273
Bilingual and Multicultural 0282
Business 0688
Community College 0275
Curriculum and Instruction 0727
Early Childhood 0518
Elementary 0524
Finance 0277
Guidance and Counseling 0519
Health 0680
Higher 0745
History of 0520
Home Economics 0278
Industrial 0521
Language and Literature 0279
Mathematics 0280
Music 0522
Philosophy of 0998
Physical 0523

Psychology 0525
Reading 0535
Religious 0527
Sciences 0714
Secondary 0533
Social Sciences 0534
Sociology of 0340
Special 0529
Teacher Training 0530
Technology 0710
Tests and Measurements 0288
Vocational 0747

LANGUAGE, LITERATURE AND LINGUISTICS
Language
  General 0679
  Ancient 0289
  Linguistics 0290
  Modern 0291
Literature
  General 0401
  Classical 0294
  Comparative 0295
  Medieval 0297
  Modern 0298
  African 0316
  American 0591
  Asian 0305
  Canadian (English) 0352
  Canadian (French) 0355
  English 0593
  Germanic 0311
  Latin American 0312
  Middle Eastern 0315
  Romance 0313
  Slavic and East European 0314

PHILOSOPHY, RELIGION AND THEOLOGY
Philosophy 0422
Religion
  General 0318
  Biblical Studies 0321
  Clergy 0319
  History of 0320
  Philosophy of 0322
Theology 0469

SOCIAL SCIENCES
American Studies 0323
Anthropology
  Archaeology 0324
  Cultural 0326
  Physical 0327
Business Administration
  General 0310
  Accounting 0272
  Banking 0770
  Management 0454
  Marketing 0338
Canadian Studies 0385
Economics
  General 0501
  Agricultural 0503
  Commerce-Business 0505
  Finance 0508
  History 0509
  Labor 0510
  Theory 0511
Folklore 0358
Geography 0366
Gerontology 0351
History
  General 0578

  Ancient 0579
  Medieval 0581
  Modern 0582
  Black 0328
  African 0331
  Asia, Australia and Oceania 0332
  Canadian 0334
  European 0335
  Latin American 0336
  Middle Eastern 0333
  United States 0337
History of Science 0585
Law 0398
Political Science
  General 0615
  International Law and
    Relations 0616
  Public Administration 0617
Recreation 0814
Social Work 0452
Sociology
  General 0626
  Criminology and Penology ... 0627
  Demography 0938
  Ethnic and Racial Studies 0631
  Individual and Family
    Studies 0628
  Industrial and Labor
    Relations 0629
  Public and Social Welfare 0630
  Social Structure and
    Development 0700
  Theory and Methods 0344
Transportation 0709
Urban and Regional Planning 0999
Women's Studies 0453

THE SCIENCES AND ENGINEERING

BIOLOGICAL SCIENCES
Agriculture
  General 0473
  Agronomy 0285
  Animal Culture and
    Nutrition 0475
  Animal Pathology 0476
  Food Science and
    Technology 0359
  Forestry and Wildlife 0478
  Plant Culture 0479
  Plant Pathology 0480
  Plant Physiology 0817
  Range Management 0777
  Wood Technology 0746
Biology
  General 0306
  Anatomy 0287
  Biostatistics 0308
  Botany 0309
  Cell 0379
  Ecology 0329
  Entomology 0353
  Genetics 0369
  Limnology 0793
  Microbiology 0410
  Molecular 0307
  Neuroscience 0317
  Oceanography 0416
  Physiology 0433
  Radiation 0821
  Veterinary Science 0778
  Zoology 0472
Biophysics
  General 0786
  Medical 0760

EARTH SCIENCES
Biogeochemistry 0425
Geochemistry 0996

Geodesy 0370
Geology 0372
Geophysics 0373
Hydrology 0388
Mineralogy 0411
Paleobotany 0345
Paleoecology 0426
Paleontology 0418
Paleozoology 0985
Palynology 0427
Physical Geography 0368
Physical Oceanography 0415

HEALTH AND ENVIRONMENTAL SCIENCES
Environmental Sciences 0768
Health Sciences
  General 0566
  Audiology 0300
  Chemotherapy 0992
  Dentistry 0567
  Education 0350
  Hospital Management 0769
  Human Development 0758
  Immunology 0982
  Medicine and Surgery 0564
  Mental Health 0347
  Nursing 0569
  Nutrition 0570
  Obstetrics and Gynecology .. 0380
  Occupational Health and
    Therapy 0354
  Ophthalmology 0381
  Pathology 0571
  Pharmacology 0419
  Pharmacy 0572
  Physical Therapy 0382
  Public Health 0573
  Radiology 0574
  Recreation 0575

Speech Pathology 0460
Toxicology 0383
Home Economics 0386

PHYSICAL SCIENCES
Pure Sciences
Chemistry
  General 0485
  Agricultural 0749
  Analytical 0486
  Biochemistry 0487
  Inorganic 0488
  Nuclear 0738
  Organic 0490
  Pharmaceutical 0491
  Physical 0494
  Polymer 0495
  Radiation 0754
Mathematics 0405
Physics
  General 0605
  Acoustics 0986
  Astronomy and
    Astrophysics 0606
  Atmospheric Science 0608
  Atomic 0748
  Electronics and Electricity 0607
  Elementary Particles and
    High Energy 0798
  Fluid and Plasma 0759
  Molecular 0609
  Nuclear 0610
  Optics 0752
  Radiation 0756
  Solid State 0611
Statistics 0463

Applied Sciences
Applied Mechanics 0346
Computer Science 0984

Engineering
  General 0537
  Aerospace 0538
  Agricultural 0539
  Automotive 0540
  Biomedical 0541
  Chemical 0542
  Civil 0543
  Electronics and Electrical 0544
  Heat and Thermodynamics ... 0348
  Hydraulic 0545
  Industrial 0546
  Marine 0547
  Materials Science 0794
  Mechanical 0548
  Metallurgy 0743
  Mining 0551
  Nuclear 0552
  Packaging 0549
  Petroleum 0765
  Sanitary and Municipal 0554
  System Science 0790
Geotechnology 0428
Operations Research 0796
Plastics Technology 0795
Textile Technology 0994

PSYCHOLOGY
General 0621
Behavioral 0384
Clinical 0622
Developmental 0620
Experimental 0623
Industrial 0624
Personality 0625
Physiological 0989
Psychobiology 0349
Psychometrics 0632
Social 0451

⊛

COMBINED MAGSAT AND AEROMAGNETIC INVESTIGATION

OF THE ALPHA RIDGE CRUST

BY

HENRY DILAH ODWAR

A Thesis submitted to the Faculty of Graduate Studies of the University of Manitoba in partial fulfillment of the requirements for the degree of

MASTER OF SCIENCE

© 1993

I hereby declare that I am the sole author of this thesis.

I authorize the University of Manitoba to lend this thesis to other institutions or individuals for the purpose of scholarly research.

I further authorize the University of Manitoba to reproduce this thesis by photocopying or by other means, in total or in part, at the request of other institutions or individuals for the purpose of scholarly research.

The University of Manitoba requires the signatures of all persons using or photocopying this thesis. Please sign below, and give address and date.

ABSTRACT

The subsurface structure of the Alpha Ridge in the Arctic Ocean was studied through an investigation of MAGSAT and aeromagnetic data. Both data sets were obtained from the Geophysical Division of the Geological Survey of Canada. In addition to analysis of the magnetic data, the study employs heat flow values for the ridge and the surrounding areas to estimate the thickness of the crust that gives rise to the observed magnetic anomalies over the ridge.

Investigation of the data included the inspection of a computer generated grey-level map, one- and two-dimensional spectral analysis, and forward modeling in two- and three-dimensions. The aeromagnetic data show that the positive magnetic anomalies are confined to a narrow zone of about 270-300 km that runs along the strike (crest) region of the ridge. The amplitudes of the anomalies reach up to 1800 nT peak to trough. The small almost-circular anomalies are up to 20 km in diameter while the elongated ones are about 80 km wide and up to 250 km long. The anomalies are thus irregular to sublinear. There is no clear pattern of alternating positive and negative anomalies as is expected of spreading ocean floors. The spectral analysis was limited to wavelength filtering. The results show that the positive anomalies dominate at longer wavelengths. This is consistent with the large positive observed MAGSAT anomaly over the ridge.

From Alpha Ridge heat flow data, about 36 km thickness of magnetic crust was estimated to lie above the curie level. This crust is the source of the observed MAGSAT and aeromagnetic anomalies. Forward modeling of the anomalies using the crustal blocks of this thickness shows that Alpha Ridge is made of an upper and and a

lower layer. The upper is estimated to be 8-12 km thick. It is more magnetic with magnetizations that vary laterally from zero to about 7 Am^{-1}. The variations in magnetizations indicate heterogeneity in either rock composition of this layer or thermal remanent magnetizations. This layer is responsible for the short wavelength aeromagnetic anomaly sources. Due to the ambiguity that is always inherent in modeling potential data, the lower layer could be one single homogeneous layer or consists of several sublayers. The lower layer is the one that contributes more to the observed MAGSAT anomalies.

Results of the investigation of the magnetic data, together with previous geological and geophysical information for the ridge, suggest that Alpha Ridge is a region that is highly affected by igneous intrusion. It was most likely formed by either a combination of sea-floor spreading and plate margin hotspot activity or by intra-plate hotspot activity.

ACKNOWLEDGMENTS

Contents

List of Tables

List of Figures

NOMENCLATURE

MAGSAT : MAGnetic SATellite

CESAR   : Canadian Expedition to Study Alpha Ridge

USSR   : Union of Soviet Socialist Republics

COSMOS : This acronym is derived from the spacecraft used by the then
           USSR.

LOREX   : Lomonosov Ridge EXperiment

NASA   : National Aeronautics and Space Administration

POGO   : Polar OrbitinG Observatory

Chapter 1

INTRODUCTION

1.1   Regional setting

The Arctic Ocean is the water mass around the North Pole. It is surrounded by Greenland, Canada, Russia (U.S.S.R) and Norway (Figure 1.1). The ocean itself is divided into two basins, namely the Amerasia and Eurasia Basins. Three near parallel submarine topographic highs run across the Arctic Ocean. These topographic highs are the Nansen, Lomonosov and Alpha-Mendelev Ridges. The Lomonosov Ridge runs across the ocean nearest the North Pole and divides the Amerasia Basin from the Eurasia Basin. The Nansen (Arctic mid-ocean) Ridge bisects the Eurasia Basin. It is a continuation of the North Atlantic mid-ocean ridge system. It is not known if the Alpha and the Mendeleev Ridges are one complex ridge or separate ridges. In this thesis, the two are treated as separate entities. The Alpha and Mendeleev Ridges divide the Amerasia Basin into the Canada and Makarov Basins. This study is focused on the magnetic nature of the subsurface beneath the Alpha Ridge.

1.2   Objective of the study

Alpha Ridge is one of the few large-scale submarine structures on earth whose tectonic evolution is still not fully known. Increase in knowledge about the Arctic region has been sporadic and not always progressive. This is attributed to the very harsh climatic environment and great distances involved that demanded special endeavour, often heroic, in order to discover and learn about the region. Modern technology has now provided aircraft, spacecraft, specialized ships and submarines, all of which have revolutionized research in the Arctic region. These innovations have now made the Arctic region accessible during most seasons of the year. In the past 40 years alone, a large quantity of geophysical and geologic data has been collected over the region. In particular, a vast amount of magnetic data has been acquired and constitutes the best, most extensive, yet detailed data set for the region (Coles and Taylor., 1990).

The purpose of studying the Arctic region is multifaceted. The reasons include, first, sheer scientific curiosity. Secondly, there is the need to understand the environmental impact of the cold regions on the rest of the globe. Thirdly, with the dwindling world resources and the continued improvements in technology, the Arctic region is a potential economic haven of the future in terms of mineral exploitation.

The primary objective of this research is to use information obtained from the investigation of both MAGSAT and aeromagnetic data so as to provide further information pertaining to the magnetic nature of the Alpha Ridge crust.

1.3 Data analysis

Data analysis in this work included visual inspection of computer generated grey-level maps, spectral analysis and 2-dimensional modeling of the aeromagnetic and MAGSAT data, and 3-dimensional modeling of the MAGSAT data. The spectral analysis provides the dominant wavelength and the pattern of magnetic signature when certain wavelengths are removed. The removal of short wavelength components of the anomaly field, which give results equivalent to upward continuation, reveals the dominant anomaly at higher elevations. In order to facilitate a better delineation of the crust that gives rise to the observed magnetic data, heat flow values over the Alpha Ridge are extrapolated to the Curie level. The crust above this level, with the exception of the sedimentary layer, constitutes the magnetic crust. This magnetic crust, used in conjunction with 2- and 3-dimensional modeling of the two magnetic data sets, provides the magnetizations associated with the Alpha crust.

Since this thesis is based on the magnetic method, some of the aspects involved in the magnetic method are reviewed in the following sections.

1.4 Magnetic studies

Since the first scientific investigation of the earth's magnetic field by Sir William Gilbert (1540-1603), magnetic studies have become a major branch of geophysics. The use of modern airborne and spacecraft magnetometers has permitted rapid acquisition of large volumes of magnetic data. The acquisition of magnetic data is quite inexpensive as compared to other geophysical methods such as seismic and gravity. Because magnetic data reflect rock composition and geologic structure, the magnetic method is an attractive tool for both reconnaissance and detailed exploration for minerals and petroleum on the one hand and, on the other, the general investigation

of the magnetic nature of the crust.

The following physical quantities are the parameters involved in magnetic studies. The units of the quantities, used throughout this thesis, conform to the SI units. However, due to the continued use of the cgs-emu system, the inter-relations between the two systems is given where necessary. Parkinson (1983) gives details pertaining to the outlined parameters.

Magnetic force $\vec{f}$

The magnetic force $\vec{f}$ acting on a circuit S_1 carrying a current $\mathbf{I_1}$ in the vicinity of circuit S_2 carrying current $\mathbf{I_2}$ is given by

$$\vec{f} = \frac{\mu_0}{4\pi}\mathbf{I_1}\mathbf{I_2} \oint \oint r^{-3}\vec{\mathbf{ds}}_1 \times (\vec{\mathbf{ds}}_2 \times \vec{\mathbf{r}}) \tag{1.1}$$

where $\vec{\mathbf{r}}$ is the position vector of $\vec{\mathbf{ds}}_1$ relative to $\vec{\mathbf{ds}}_2$. The above formula is true only in vacuum or in the absence of magnetic materials. $\vec{\mathbf{ds}}_1$, $\vec{\mathbf{ds}}_2$ and r are measured in meters (m), $\mathbf{I_1}$ and $\mathbf{I_2}$ are measured in amperes (A) and $\mathbf{f}$ is in newtons (N). The constant of proportionality, μ_0 (called the permeability of free space), is chosen to have the value of $4\pi \times 10^{-7}$ henry/meter (Hm^{-1}).

In the cgs-emu system, the force between two magnetic poles of strength p_1 and p_2, located r centimeters apart is given by

$$\vec{\mathbf{F}} = \frac{p_1 p_2}{\mu} \frac{\vec{\mathbf{r}}}{r^3}. \tag{1.2}$$

$\mathbf{F}$ is the force on p_2 in dynes. $\vec{\mathbf{r}}$ is a vector directed from p_1 toward p_2. μ is the magnetic permeability of the material and is dimensionless in the cgs-emu system.

Magnetic field (magnetic field intensity) $\vec{\mathbf{H}}$

The magnetic field intensity is expressed as the effect on circuit S_2 due to the presence of a magnetic field;

$$\vec{\mathbf{H}} = \frac{1}{4\pi}\mathbf{I_2} \oint \frac{\vec{\mathbf{ds}}_2 \times \vec{\mathbf{r}}}{r^3}. \tag{1.3}$$

The SI units of $\vec{\mathbf{H}}$ is ampere turn/meter. In the cgs-emu system, the magnetic field intensity is given as

$$\vec{\mathbf{H}}' = \frac{\vec{\mathbf{F}}}{p_2} = \frac{p_1}{\mu r^2}\vec{\mathbf{r}}_1. \tag{1.4}$$

The units of $\vec{\mathbf{H}}'$ in this system is given in oersteds or in dynes per unit pole.

Magnetization (or Intensity of Magnetization) $\vec{\mathbf{M}}$

If a magnetic material is present, a vector $\vec{\mathbf{M}}$ must be added to $\vec{\mathbf{H}}$ in equation (1.3). $\vec{\mathbf{M}}$ is a measure of the effect of the induced and remanent magnetization and its SI units is the ampere/meter (Am^{-1}). Magnetization in the cgs-emu system is defined in terms of the magnetic moment $\vec{\mathbf{m}}$ and the volume of the material. Given two poles of strength $+p$ and $-p$ that are separated by a distance l, the magnetic dipole moment is

$$\vec{\mathbf{m}} = lp\vec{\mathbf{r}}. \tag{1.5}$$

$\vec{\mathbf{m}}$ is in the direction of the unit vector $\vec{\mathbf{r}}$, and by convention extends from the negative pole towards the positive pole. The magnetization in the cgs-emu system is given by

$$\vec{\mathbf{M}}' = \frac{\vec{\mathbf{m}}}{v} \tag{1.6}$$

where v is the volume of the material.

Susceptibility k

For those materials and magnetic field strengths for which the magnetization $\vec{\mathbf{M}}$ is proportional to the magnetic field intensity $\vec{\mathbf{H}}$, the degree to which the material is magnetized is represented by its susceptibility k, which is defined as

$$\vec{\mathbf{M}} = k\vec{\mathbf{H}}. \tag{1.7}$$

In the cgs-emu system the susceptibility is defined as

$$\vec{\mathbf{M}}' = k'\vec{\mathbf{H}}'. \tag{1.8}$$

k and k' are dimensionless but not equal. The susceptibilities in the two systems are related by the following equation:

$$k = 4\pi k'. \tag{1.9}$$

Magnetic induction (magnetic flux density) $\vec{B}$

Magnetic induction is proportional to the sum of $\vec{H}$ and $\vec{M}$, and

$$\vec{B} = \mu_0(\vec{H} + \vec{M}). \tag{1.10}$$

The SI units of $\vec{B}$ is the tesla (T). In the cgs-emu system, the magnetic induction is given by

$$\vec{B}' = \mu\vec{H}' \tag{1.11}$$

where $\mu = 1 + 4\pi k'$. The units of $\vec{B}'$ is the gauss. This makes the units of μ gauss/oersted. But since μ is dimensionless, the gauss is equal to the oersted.

In this thesis, the main magnetic field of the earth F_e (the magnitude of $\vec{B}$) is taken to be vertical and 60000 nT. The main field, together with other components, constitute the magnetic field of the earth that is observable at the earth's surface.

1.5 The magnetic field of the earth

The magnetic field of the earth is divided into three parts. These are the main field, the external field and the lithospheric field. The following subsections are a brief description of the parts.

1.5.1 The main field

The dominant part of the main field of the earth can approximately be represented as the field of a dipole situated at the center of the earth with its magnetic moment

vector pointing towards the geographic south pole. It is thought to be caused by a system of currents in the outer core (Parkinson, 1983). Figure 1.2 illustrates the magnetic elements that are required to describe completely the main field at any point at the surface of the earth. These elements include the magnitude of the field F, the inclination (dip of the magnetic needle below the horizontal) I, and the declination (angle between the direction of the field and the geographic north direction) D. Other useful elements of the main field include the horizontal component H and the vertical component Z. H has components X which is positive to the north direction and Y which is positive in the east direction. The inclination I is given by $I = tan^{-1}(Z/H)$ and the declination is given by $D = tan^{-1}(Y/X)$. The points at which $I = 90°$ are called the magnetic north and south dip poles respectively. The main field varies slowly over time and has now been established to have reversed its polarity many times (Mankinen et al., 1985; Prévot et al., 1985; Mankinen et al., 1987).

1.5.2 The external field

The external field is a small portion of the earth's magnetic field and has its origin in the ionized parts of the upper atmosphere and in the magnetosphere. The time variations of the external field are more rapid than those of the main field. From the standpoint of magnetic surveys, the external field is treated as noise and has to be removed from the magnetic survey observations. The external field does not form part of this thesis and shall seldom be referred to.

1.5.3 The lithospheric field

The magnetic field originating from the lithosphere above the Curie isotherm (level or surface below which a ferromagnetic material loses it remanence) is known as the lithospheric field. It arises from variations in the magnetic mineral content of rocks.

The section below briefly describes the mineralogy which influences the magnetization of rocks.

1.6 Rock magnetization

There are five basic types of magnetization that occur naturally in minerals. These are diamagnetism, paramagnetism, ferromagnetism, antiferromagnetism and ferrimagnetism. The first two are related to the electron orbital motions and spins respectively and are present only in a magnetic field. Both are weakly magnetic and are usually of little consequence in magnetic surveys. The remaining three types of magnetism are due to alignment of spins by exchange forces (Parkinson, 1983).

The natural tendency in a structure to minimize the total energy results in domain structures. Substances in which there are an equal number of opposing spins that cancel one another exactly are called antiferromagnetic. Ferrimagnetic substances have unequal number of opposing spins yielding a net moment. Antiferromagnetic minerals sometimes contribute to anomalies in that they often alter into ferrimagnetic products or interact with existing ferrimagnetic minerals. The most important magnetic minerals are briefly discussed in the following section.

Alignment of electron spins is temperature dependent. At absolute zero of temperature, perfect spin alignment is achieved. Above this temperature, thermal energy prevents perfect alignment. The higher the temperature the less perfect the alignment. At a particular temperature, depending on the mineral, the ordered orientation of the electron spins become disordered. At this temperature, ferrimagnetism disappears and the substance becomes paramagnetic. This temperature is called the Curie point or Curie temperature.

A mineral's physical size also influences its magnetic character. At the atomic

level, the exchange energy is minimized by the alignment of dipoles. On a larger scale, it requires increasing energy to maintain a large number of free aligned dipoles. In order to achieve balance the mineral is segregated into discrete domains having internally consistent directions but externally opposing directions. The net result is that a large (multi-domain) ferrimagnetic grain may have only a weak overall magnetization whereas a very small (single domain) grain may have a much higher magnetization (Evans and McElhinny, 1969).

1.6.1 Magnetic minerals

The magnetic minerals that are of importance in magnetic prospecting and exploration are the oxides of iron, titanomagnetites and some iron sulphides. Of the sulphide minerals, phyrrotite is the most important mineral. Figure 1.3 shows a ternary diagram of the most important non-sulphide magnetic minerals. These minerals are discussed by Evans and McElhinny (1969) and Parkinson (1983). Within the FeO - TiO_2 - Fe_2O_3 ternary system, the important solution series are ilmenite ($FeTiO_3$) - hematite/maghemite (α-Fe_2O_3/γ-Fe_2O_3) and (Fe_2TiO_4) - magnetite (Fe_3O_4). Commonly, there is a wide range of intermediate titaniferous compositions with magnetizations and Curie temperatures decreasing with increasing Ti content. The +2 valence end members ilmenite and ulvospinel, and +3 valence end member hematite are antiferromagnetic and generate no magnetic anomalies. On the other hand, the +2, +3 mixed valence end member magnetite (titanomagnetite) and the short compositional range in ilmenite-hematite are ferrimagnetic. These are the minerals responsible for generating crustal anomalies.

Temperature dependent processes cause mineral alterations that result in the change of the magnetic nature of the original rock. In reviewing the processes, Bambrick (1984) lists four magnetic mineralogy changes resulting from differential cooling.

These are:

(1) *Exsolution.* At temperatures greater than 800°C, antiferromagnetic and ferrimagnetic phases separate from a single phase of intermediate composition and magnetic character. The ferrimagnetic material is typically magnetite.

(2) *High temperature deuteric oxidation.* This is a non-equilibrium reaction resulting from differential cooling and subsequent irregular entrapment of oxygen from primary magmatic water. It occurs at temperatures greater than 600°C.

(3) *Low temperature oxidation.* The process occurs at temperatures greater than 500°C and results in the formation of maghemite from ulvospinel assemblages upon diagenesis and subaerial alteration. The process is more common in mafic rocks where the relative abundance of Ti is higher.

(4) *Metamorphism.* This occurs at temperatures above 200°C and yields an overall degradation in magnetic characteristics due to oxide minerals reacting with other minerals to form amphiboles, pyroxenes and phyllosilicates. In general, metamorphism results in the formation of minerals of low magnetizations and hence a reduced magnetic anomaly. However, serpentinization (a hydrothermal process by which Mg-rich silicates like olivine, amphibole etc. are converted to or replaced by serpentine) results in multi-domain magnetite with high magnetization.

It is clear from the above considerations that magnetic anomalies can arise from a wide variety of rock types and can significantly change from time to time due to many external factors. Considering the mineral content and the ambient field, different rock magnetizations are obtained. The section below outlines the different types of magnetization acquired by rocks.

1.6.2   Remanent magnetization

The residual magnetism of a rock is known as the natural remanent magnetization (NRM). There are a number of different ways in which NRM is produced. These are:

1 *Thermal remanent magnetization* (TRM). This is the magnetization acquired when a magnetic material is cooled through the Curie point in the presence of the earth's field. This form of magnetization is stable and is the main process for the residual magnetization of igneous rocks.

2 *Detrital remanent magnetization* (DRM). This magnetization is also known as depositional remanent magnetization. It is acquired by sediments containing grains that have remanence as they settle in the water in the presence of the earth's magnetic field.

3 *Viscous remanent magnetization* (VRM). This is the form of magnetization acquired as a cumulative effect after a long exposure to an ambient field.

4 *Chemical remanent magnetization* (CRM). As a result of chemical action, CRM is acquired during growth or recrystallization of magnetic minerals (especially during metamorphism) at temperatures below Curie temperatures in the presence of an ambient field.
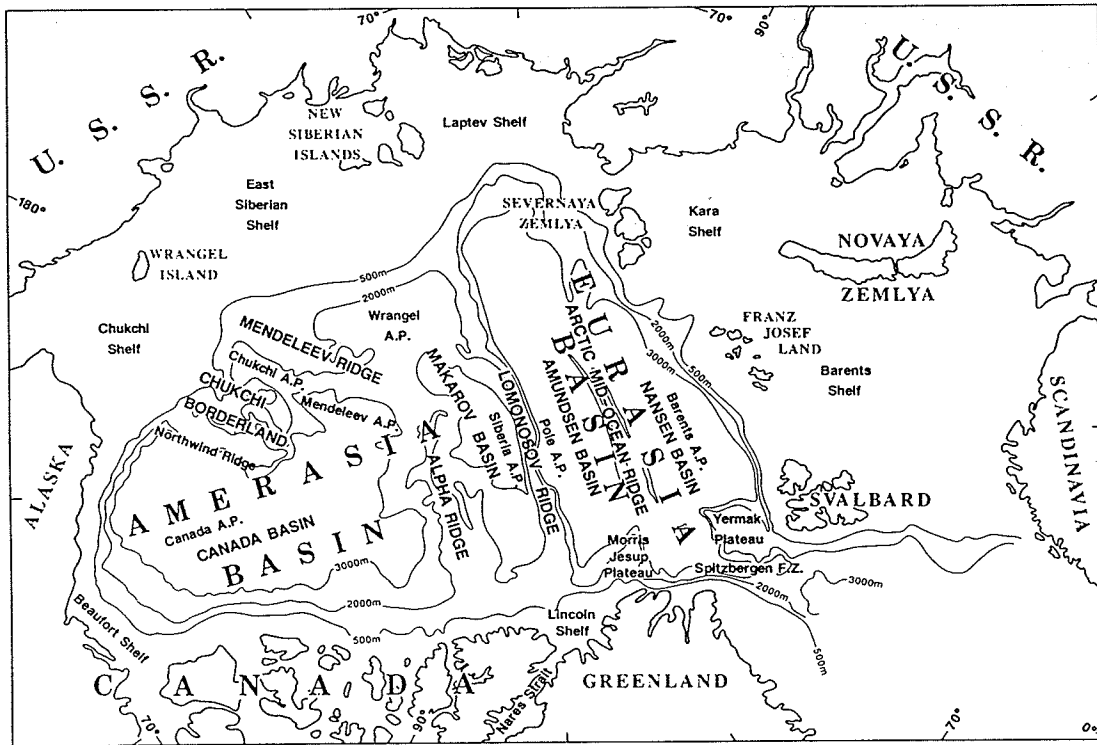
Figure 1.1: Map of the arctic region

Map of the Arctic region showing the location of Alpha Ridge and other features mentioned in the text (Grantz et al., 1990a).
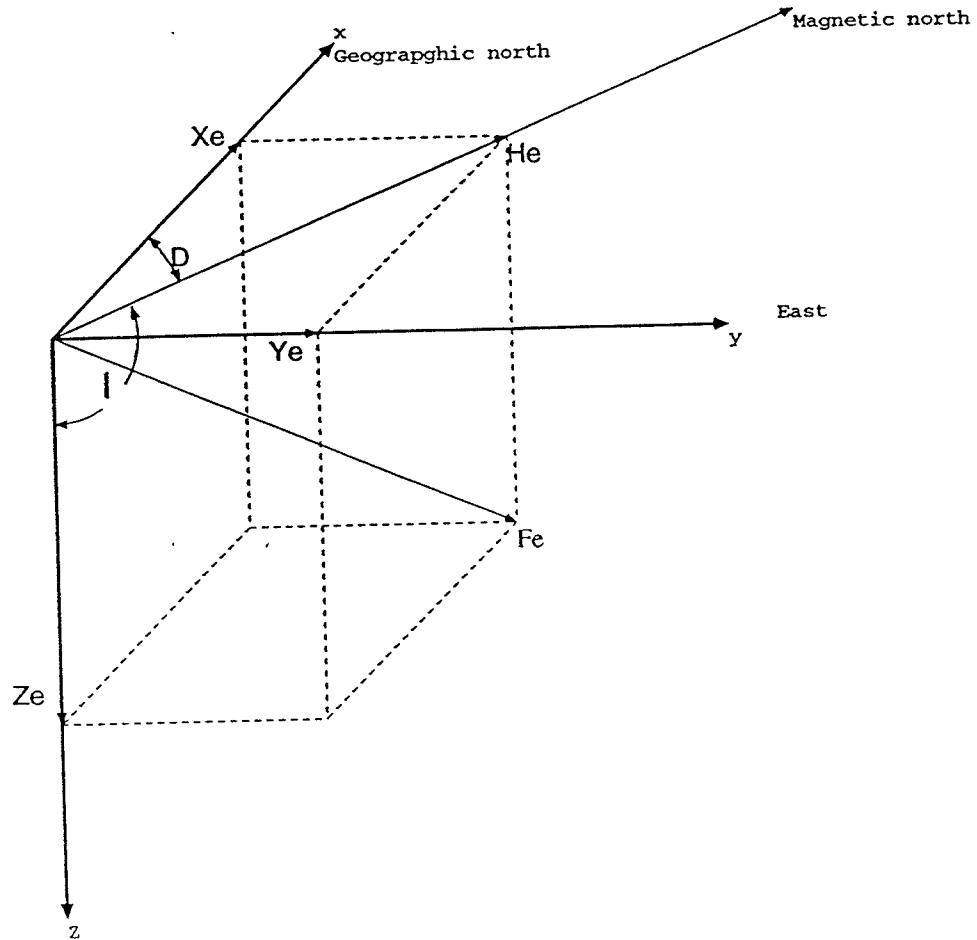
Figure 1.2: Elements of the earth's magnetic field

Magnetic elements used in the description of the earth's magnetic field. The symbols are explained in the text.
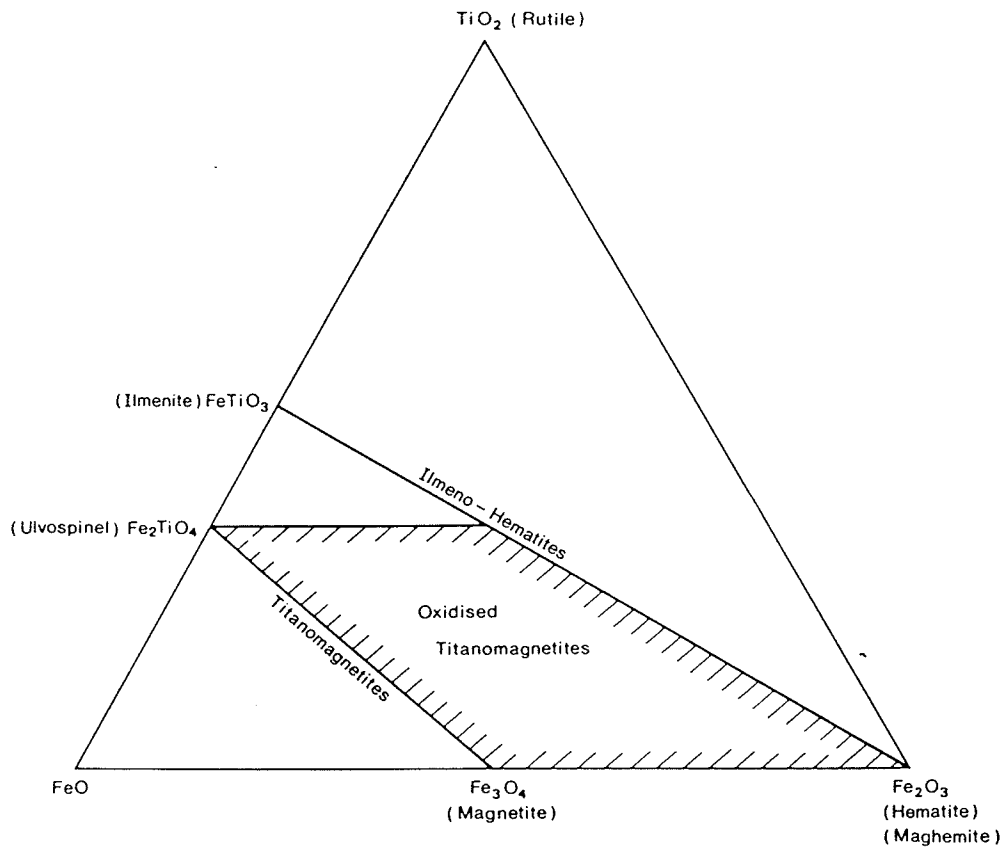
Figure 1.3: Ternary diagram

Ternary diagram showing the most important magnetic minerals (from Parkinson, 1983).

Chapter 2

PREVIOUS WORK

Weber and Roots (1990) have given an exhaustive review of all the geological and geophysical exploration of the Arctic basin. Most of the bathymetric, gravity, seismic, heat flow and some magnetic data were taken from floating ice stations. The use of aircraft and satellites has tremendously increased the amount of magnetic data acquired in the region. Aircraft have done the same for gravity data. Bathymetric data were also taken by submarines. Geological data are still few and are limited in areal coverage. The available data are drill and gravity sediment cores and a few bedrock samples dredged from the ocean floor. The following section is a summary of the geological and geophysical information on the Alpha and Mendeleev Ridges.

2.1   Physiography and bathymetry

The Alpha and Mendeleev Ridges are the largest submarine mountains in the Arctic Ocean. Johnson et al. (1990), have presented a summary of the bathymetry in the region. Detailed but limited bathymetric soundings of Alpha Ridge were obtained during the LOREX survey (Sweeney et al., 1982) and during the multidisplinary

15

CESAR expedition (Weber and Jackson, 1985).

Figure 2.1 shows bathymetry of the Amerasia Basin. The Alpha Ridge starts in the vicinity of the Ellesmere Island. It is separated from the island by a relatively smooth trough which is between 1500 and 2000 m deep. The crestal region of the ridge is delineated by the 2000 m isobath. The ridge strikes in a predominantely east-west direction from the vicinity of the island to approximately 165°W longitude, spanning a length of about 1000 km. Its width averages around 360 km. It is broadest near the Ellesmere Island where it reaches 800 km. It is narrowest near 80°N, 180°W and the width in this vicinity is about 250 km. In cross-section, the ridge is roughly symmetrical (Figure 2.2). Superimposed on and striking parallel to the main ridge are a series or chains of topographic highs and depressions (Hall, 1973; Weber and Jackson, 1985). Some of the structures on the ridge were identified to be seamounts. The shallowest point on the ridge is 1169 m. At about 83°N, 180°W, the ridge is deepest. This depression is known as the Cooperation Gap (see Figure 2.6a). At Cooperation Gap, Alpha Ridge joins with or is continuous with the southsouth-east striking Mendeleev Ridge. The Mendeleev Ridge connects with the continental margin of Siberia in the vicinity of Wrangel Island. Like the Alpha Ridge, the Mendeleev Ridge is similarly segmented by depressions and topographic highs that are parallel to the ridge.

2.2 Geological data

The only bedrock samples ever recovered from Alpha Ridge are 20 samples dredged from the bottom of a major depression on the ridge during the CESAR expedition (Van Wagoner and Robinson, 1985). Comprehensive analysis of the samples has been done by Van Wagoner et al. (1986). The samples are found to be composed of volcanic clasts of alkalic basalts. Textural interpretation of the samples suggest that

the clasts were a result of volcanic eruption in relatively shallow water. The alkalic affinity of the bedrock led to the suggestion that the Alpha Ridge is formed from an intra-plate tectonic setting and rules out its formation by volcanic activity at an island arc, a mature spreading center or a fracture zone (Van Wagoner et al., 1986).

In addition to the bedrock samples, 28 gravity and drill sediment cores were obtained during the CESAR expedition (Mudie and Blasco, 1985). The cores contained siliceous fossil forms that are well preserved. The well-preserved state of the fossils together with results of textural and geochemical analysis of the sediments suggest that the eastern part of Alpha Ridge was formed before 80 to 40 million years ago (Mudie et al., 1986).

2.3 Geophysics

Only a limited amount of ground geophysical work has been done in the Amerasia Basin due to the prevailing harsh cold climatic conditions. Thus geothermal and seismic data which are collected from the surface of the water or floating ice are sparse. Gravity and magnetic data on the other hand are relatively abundant because they are remotely collected by aircraft and spacecraft. The following sections are a review of the available geophysical information.

2.3.1 Seismic data

Seismic reflection data over the Alpha and Mendeleev Ridges have been reported by Hall (1973) and Jackson (1985). The sediment cover on the ridges is found to be layered and is mostly flat lying or conformable to basement structures. The thickness of the sediments is less than 1 km. A thicker sequence of less regularly bedded sediments occurs in the troughs. The most valuable seismic data has been the refraction

data acquired during operation CESAR. Ray tracing, amplitude modeling, and other processing techniques were applied to this data. These processing methods permitted the recognition of velocity gradients within layers and two-dimensional structures. Asudeh et al. (1988) have reported the results of their analysis of the refraction data. The results show that the basement material immediately below the sediment cover has a velocity ranging from 5.0 to 5.2 kms^{-1} at a depth of only about 8 km. The velocity increases smoothly and rapidly to about 6.5 kms^{-1}. Below this layer, the velocities continue to increase relatively smoothly, reaching values of about 7.0 kms^{-1} at depth ranging from 14 to 19 km. This layer also indicates lateral velocity variations ranging from 6.45 to 6.8 kms^{-1} with both negative and positive velocity gradients. Below about 20 km depth, a more laterally consistent velocity of 7.3 kms^{-1} is determined. Depth to mantle-type velocities of about 8.0 kms^{-1} or more are not well constrained. These velocities are found at depths of 36 - 44 km beneath crestal regions of the northeastern and central Alpha Ridge and depths of 21 - 25 km beneath the southeast flank facing Makarov Basin. Figure 2.3 shows a column diagram summarizing the crustal structure of the northeast portion of the Alpha Ridge.

2.3.2   Gravity data

Gravity data over the Alpha and Mendeleev Ridge have been discussed by Vogt and Ostenso (1970), Hall (1973), and Weber (1986). Figure 2.4 a-b show free air anomalies over the eastern parts of Alpha Ridge. The gravity anomaly fields vary from 80 to -50 mgal. The anomalies correlate with the sea bed topography (Figure 2.5); high anomaly values over the ridges and low values over the depressions. This trend of highs over ridges and lows over depressions appear to extend across the Mendeleev Abyssal Plain to the Chukchi borderland and the eastern part of the Mendeleev Ridge (Sobczak et al., 1990). Over the continental margin (Figure 2.4a), the gravity

anomaly field is characterized by elliptically-shaped positive anomalies of up to 60 mgal centered over the continental shelf break. These anomalies appear to be the eastern continuation of positive elliptically-shaped anomalies located all along the polar margins and may be traced along the 1000 m isobath. The elliptically-shaped anomalies are a typical feature of passive continental margins and are believed to be caused by the combined gravitational effect of the thickening of the sediments and thinning of the crust across the margins (Weber, 1986). The implication for this region of the Alpha Ridge is that the adjoining continental shelf appears to be a normal passive margin structurally not connected to the ridge. On a regional scale, the anomaly field over the Alpha and Mendeleev Ridges is positive.

Figure 2.6b shows the gravity-derived crustal structure of the Alpha Ridge. The model is derived from CESAR gravity measurements and is constrained by seismically determined depths of 23 km and 38 km, respectively (Forsyth et al., 1986a). The 23 km depth is located on the Alpha Ridge north flank at S2 and the 38 km depth is at position S1 (Figure 2.6a). The observed free air anomaly is thus accounted for by the following structural layers. Immediately beneath the sea water is a thin layer of sediments of up to 0.5 km thick with an average density of 2.0 Mgm^{-3}. The sediment layer overlies an upper crust of average density of 2.88 Mgm^{-3} and a lower crust of average density 3.04 Mgm^{-3}. The boundary between the upper and lower crust occurs at a depth of about 26 km. Below the 38 km depth mark, mantle densities of 3.17 Mgm^{-3} are encountered.

2.3.3 Magnetic data

The magnetic anomaly field, satellite and aeromagnetic, is the only geophysical parameter in the Arctic that has been uniformly measured. Quantitative compilation of the aeromagnetic data has however proved to be a formidable task. This is due

to the varying conditions of data acquisition (flight altitude, navigation, etc) and the difficulties of correction for temporal field variations at high latitudes.

Vogt et al. (1979), Taylor et al. (1981) and Vogt et al. (1982) have discussed aeromagnetic data from the Amerasia Basin. Figure 2.7 shows a zebra-strip aeromagnetic map of the Arctic. The Eurasia Basin shows a lineated anomaly pattern while the Amerasia Basin does not. The Atlantic Geoscience Center (a Division of the Geological Survey of Canada), is currently involved in acquiring and merging data sets from numerous organizations in order to create a digital data base of coherent magnetic observations (Macnab et al., 1992). Figure 2.8 shows one of the preliminary magnetic representations of the Arctic. From the figure, the anomaly over the Alpha Ridge exhibits characteristics that are continental in nature unlike the lineated nature exhibited by the Eurasia Basin and the North Atlantic Ocean. The anomaly over the Alpha Ridge is also similar to the one over Iceland which is an oceanic feature. This suggests that the magnetic structure of Alpha Ridge is similar to that of Iceland.

Over the Alpha Ridge, the aeromagnetic anomaly amplitudes and wavelengths are extremely variable. The largest amplitudes, peak to trough, are 1000 nT and over, while the smaller amplitudes are about 100 nT or less (Vogt and Ostenso, 1970; Taylor et al., 1981; Hall 1973). Anomaly wavelengths vary from 20 to 75 km. The long wavelength anomalies are strongly correlated to the bathymetry of the ocean bottom (Figure 2.5). The high-amplitude, short-wavelength anomalies associated with the Alpha Ridge extend into the Canada Basin. Some of the anomalies along both the Alpha and Mendeleev ridges exhibit short lineated segments that are parallel to the regional strike of the ridges (Taylor et al., 1981; Hall 1973). The lineations however do not reveal any consistent pattern of lineations such as would be expected for a normal mid-ocean spreading center, whether active or dormant (Riddihough et al. 1975). The aeromagnetic data show that the Alpha Ridge basement rocks below the sediment cover are highly magnetized (Vogt et al., 1979). The magnetization

varies from 20 to 30 Am^{-1}. Kovacks and Vogt (1982) analysed aeromagnetic data for regional magnetic source depth over the Canada Basin and found that the Alpha Ridge appeared as a high in the calculated magnetic basement topography while the zone between the ridge and the Ellesmere Island appeared as a low (Figure 2.9). The regional magnetic source depth analysis thus also show that the Alpha Ridge is not connected to the Ellesmere Island.

Analysis of satellite magnetic anomalies began with the reduction of the magnetic data from the POGO satellite (Cain and Langel, 1971). The POGO data were obtained at altitudes ranging between 400 and 700 km. Based on the POGO data, Langel and Thorning (1982), and Langel (1990) have published polar magnetic anomaly maps. The MAGSAT mission was dedicated to the measurement of the near-earth magnetic field (Langel et al., 1982). Since this thesis work also involves the modeling and interpretation of the MAGSAT data over Alpha Ridge, the MAGSAT mission is comprehensively covered in Chapter 5. Preliminary northern polar magnetic maps from MAGSAT data have been published by Coles et al. (1982), Coles (1985), and Haines (1985b). The maps confirm the major features of the POGO maps and add more details in some areas. The maps show a very large satellite magnetic anomaly over the Alpha-Mendeleev ridge complex (see also Figure 5.1). The concept of a magnetic province (Hall, 1968) may be applied to this large anomaly and thus qualifying the ridge complex to be a magnetic province.

In order to compare aeromagnetic and satellite magnetic data, Coles and Haines (1979) and Langel et al. (1980), upward continued the aeromagnetic data to an altitude of 500 km. At this altitude, the amplitude over Alpha Ridge (about 12 nT) from the two data sets is in good agreement (Figure 2.10).

2.3.4 Heat flow data

A considerable number of heat flow determinations have been made in the Amerasia Basin. On the Alpha and Mendeleev Ridges, heat flow measurements have been determined by Lachenbruch et al., (1966), and recently during the multidisplinary CESAR expedition (Taylor et al., 1986). Figure 2.11 shows the locations of the heat flow values in the Amerasia Basin. Over much of the length of Alpha and Mendeleev Ridges, a mean heat flow value of 49 ± 3 mWm^{-2} was obtained (Langseth et al., 1990). This mean heat flow value is significantly lower than that obtained for the Canada Basin (56 ± 1.5 mWm^{-2}). Along the strike of Alpha Ridge heat flow values show a tendency towards higher values eastward. This suggests that the crust thins eastwards. At the vicinity of Alpha Ridge - Ellesmere Island junction, the heat flow values are anomalously high with a mean value of 72.5 mWm^{-2}. This high heat flow value indicates that the crust at this vicinity is thinnest thereby implying that the ridge and the islands are different tectonic features.

2.3.5 Magnetotelluric (MT) data

The only available MT data over the Alpha Ridge was collected during the CESAR expedition. The data has been processed and interpreted by Niblett et al. (1987). Depth to the ocean bottom agreed remarkably well with the known bathymetry. The thickness of the sediments was determined to be 100 m. This result is in agreement with that obtained from seismic data. Below the sediment layer, the MT data revealed that the Alpha Ridge lithosphere is homogeneous and extends to a depth of 70-85 km.

2.4 Nature, origin and age

The nature, origin and age of the Alpha/Mendeleev Ridge complex is still a subject for debate. Thus a wide variety of models have been proposed to explain the nature of the ridge complex. Prior to CESAR and the refinement of previous data, the ridge complex had been suggested to be:

1. Of continental origin (King et al., 1966; Sweeney et al., 1982; Taylor et al., 1983).

2. A result of hotspot activity (Vogt et al., 1979; Vogt et al., 1982).

3. An extinct spreading ridge (Vogt and Ostenso, 1970; Hall, 1973; Ostenso and Wold, 1977).

4. A former island arc or subduction region (Heron et al., 1974).

Results from the analysis of CESAR data and the refinement of satellite and aeromagnetic data has greatly improved the number of constraints imposed on the evolution of the Alpha and Mendeleev Ridges. Comparison of geological and geophysical data from the ridge complex with data from other crustal blocks has also contributed in understanding the ridge complex.

Gravity and bathymetric results from CESAR confirm earlier suggestions derived from depth-to-magnetic basement calculation that the Alpha Ridge is not structurally connected to North America (Weber, 1986). This evidence casts further doubt as to the continental nature of Alpha Ridge. The basement material of the ridge on which the sediment cover was deposited is determined to have a velocity of 5.3 kms^{-1} (Forsyth et al., 1986a; Asudeh et al., 1988). Inspite of the layer being thicker than the usual oceanic layer-2, the velocity of 5.3 kms^{-1} is typical of this layer (Jackson et al., 1986). Below the 20 km depth, Alpha Ridge has a layer of between 10 to 16 km

thick that has a laterally consistent velocity of 7.3 kms^{-1}. This velocity is diagnostic of all plateaus believed to be formed of oceanic crust (Carlson et al., 1980). Heat flow values from the Alpha and Mendeleev Ridges point to a crust that is not purely continental in nature. The heat flow values for continental (shields and platforms) and normal oceanic crusts are respectively 38-44 and 66 mWm^{-2} (Bott, 1982). The average heat flow value of 49 mWm^{-2} over the two ridges is lower than the values determined for the adjacent Canada Basin (about 56 mWm^{-2}) but larger than for a purely continental fragment (Taylor et al., 1986).

All the evidence so far considered point to the oceanic affinity of the Alpha and Mendeleev Ridges. Comparisons of the ridges to other crusts in other locations with oceanic affinities have been made to reinforce the oceanic origin of the ridges. The morphology of the Manihiki plateau, which is an oceanic plateau, has striking similarities to that of the Alpha Ridge (Jackson et al., 1986). Seismic refraction studies show that the Alpha Ridge crustal structure is very similar to that of Iceland and the Ontong-Java Plateaus (Forsyth et al., 1986b). In Figure 2.12 the Alpha Ridge is compared with continental crustal sections (2.12b) and with thick oceanic crusts (2.12a). Although Alpha Ridge is similar in some aspects to both categories, the evidence presented earlier points to its character being oceanic in nature. The similarities between Alpha Ridge and Iceland and the series of large satellite anomalies traceable from the ridge to Iceland lead Forsyth et al. (1986b) to suggest that both the Alpha Ridge and Iceland crustal blocks are a product of the same hotspot activity.

If the Alpha and Mendeleev Ridge are oceanic in nature and a thermal origin is assumed, the time of their formation can be estimated from magnetic measurements plus studies based on heat flow measurements, biostratigraphy and palynology of sediment cores recovered during CESAR. The strong, mainly positive magnetic anomalies over the ridges indicate that they formed during an interval dominated by normal geomagnetic polarity. Two candidate time spans within the Cretaceous

period seem likely for the formation of the ridges: 122-84 and 80-72 Ma (Weber and Sweeney, 1990). From heat flow-versus-sediment thickness curves, a crustal age of between 60 and 120 Ma is obtained (Langseth et al., 1990). Paleontological studies indicate that the retrieved shallow sea-bed samples from CESAR are late Campanian (about 78 Ma) in age (Mudie et al., 1986). The combined age constraints therefore seem to place the formation of the Alpha and Mendeleev Ridges within the Cretaceous normal polarity Superchron between about 122 and 84 Ma.

Heat flow values versus sediment thickness curves also indicate that the Canada Basin was formed at the same time as the Alpha and Mendeleev Ridges (Langseth et al., 1990). The higher heat flow values in the Canada Basin is attributed to radioactive heat production in the thick sediments in the basin. The greater thickness of crust below the Alpha Ridge, together with the evidence that the age of the ridge is comparable to the Canada Basin, support the hypothesis that the Alpha (and Mendeleev) Ridge was formed as an aseismic ridge by an anomalously high magma generation at a hotspot on the spreading center that formed the Amerasia Basin in a manner analogous to the formation of the Faroes Island-Greenland Ridge at the Iceland hotspot (Forsyth et al, 1986b).

The information reviewed in this chapter points to the oceanic nature of the Alpha Ridge, and that it likely formed due to hotspot activity during the Cretaceous period of normal geomagnetic polarity. This information is important and shall form part of the basis of modeling aeromagnetic and MAGSAT data from the ridge.
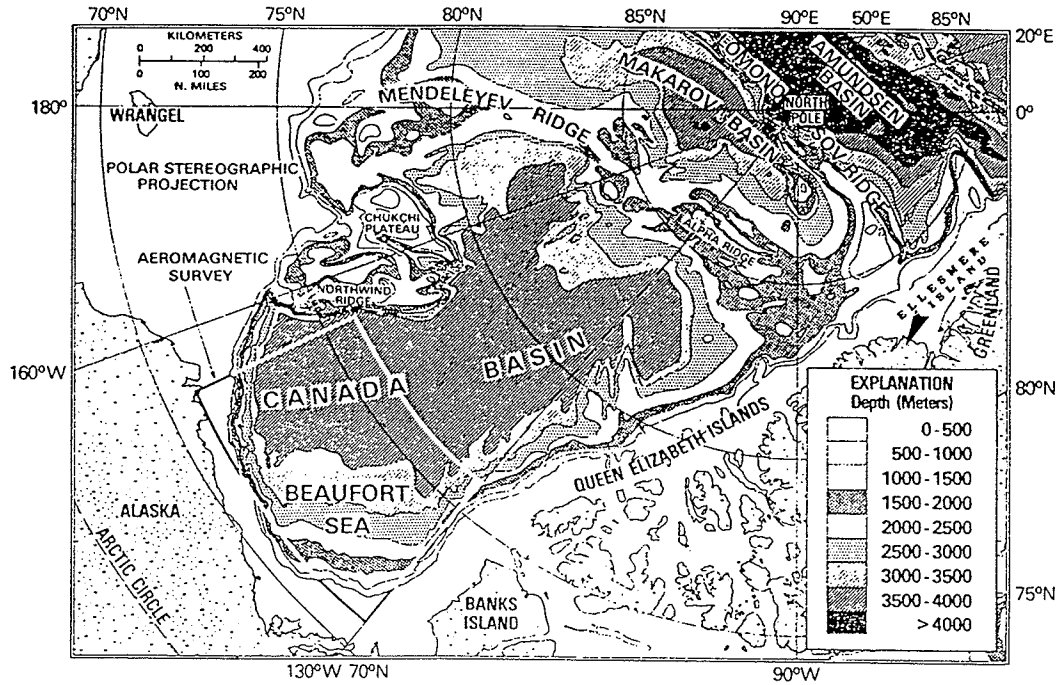
Figure 2.1: General bathymetry

Map showing the general bathymetry of the Amerasia Basin and the location of Alpha Ridge (from Taylor, 1983).
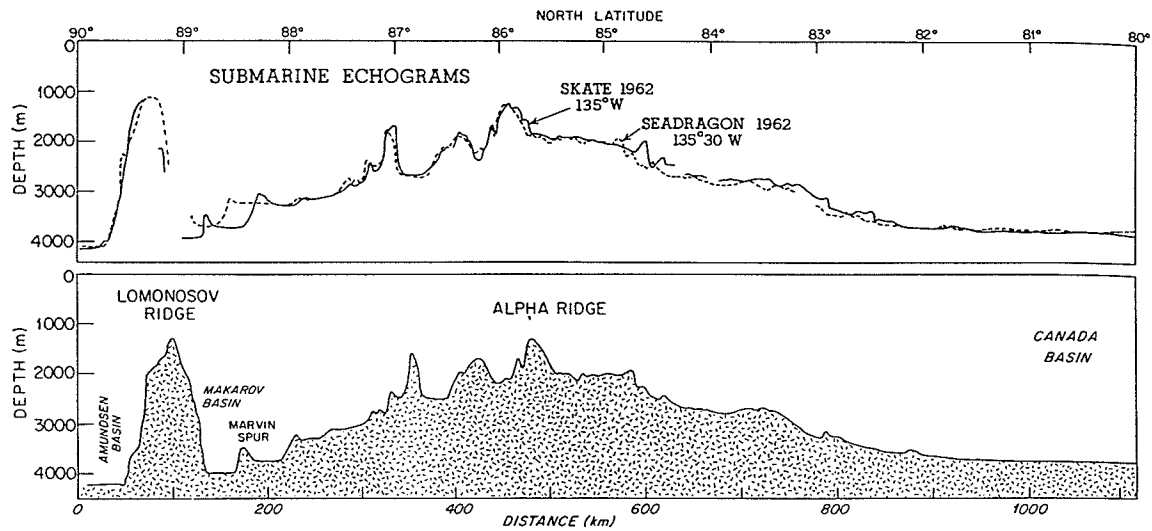
Figure 2.2: Cross-section of Alpha Ridge

Top: Echograms from the United States nuclear submarines Skate and Seadragon that sailed from the North Pole along the 135°W meridian. Bottom: Bathymetric profile compiled from echogram data from Skate (From Weber,1986).
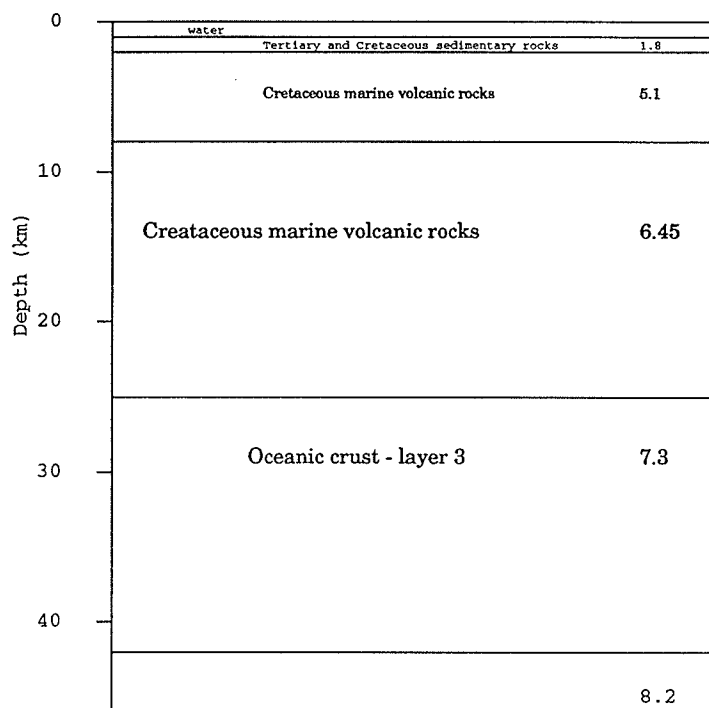
Figure 2.3: Seismic structure of Alpha Ridge

The subsurface structure of the of Alpha Ridge as delineated by seismic data. The numbers are the P-wave velocities in kms^{-1}. The layers are interpreted by Grantz et al. (1990b).
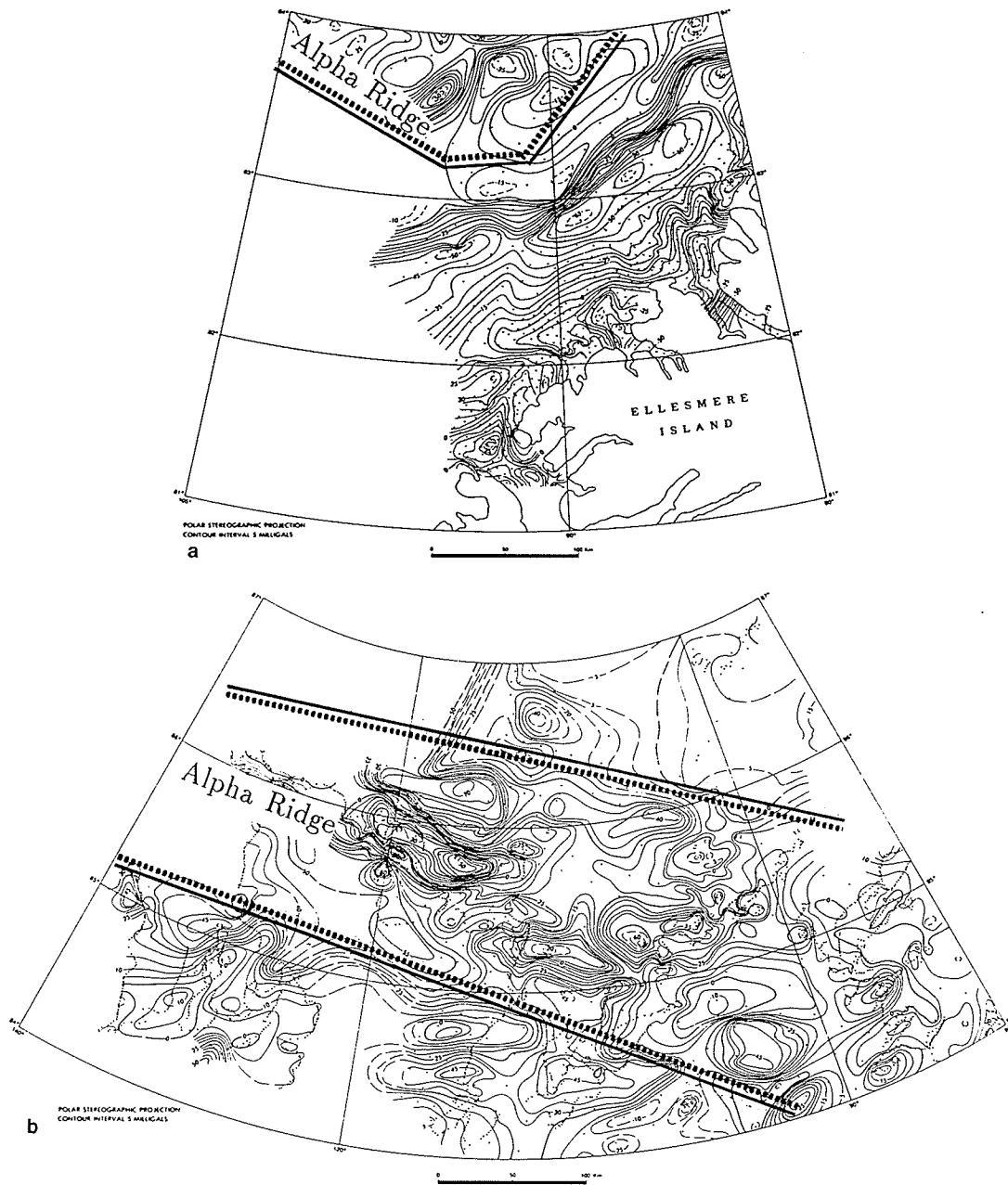
Figure 2.4: Free-air gravity anomalies

a: Anomalies north of Ellesmere Island and b: Anomalies over the north eastern
Alpha Ridge. The gravity measurements are in mgal (from Weber and Sweeney,
1990).
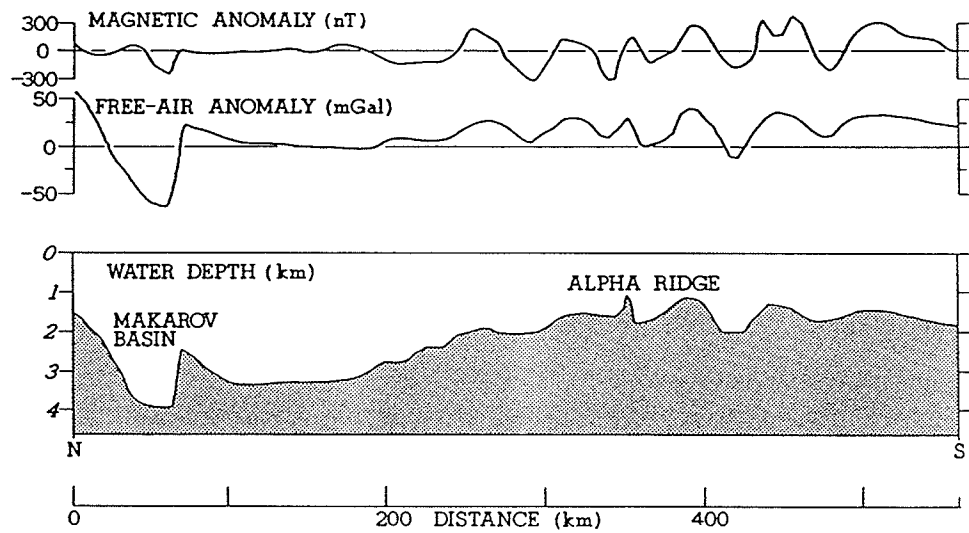
Figure 2.5: Correlation of magnetic and gravity data with bathymetry

The figures shows the correlation of magnetic and free-air gravity anomalies over a section of Alpha Ridge. The anomaly lows correspond to topographic lows and the highs correspond to the topographic highs (from Weber, 1986).
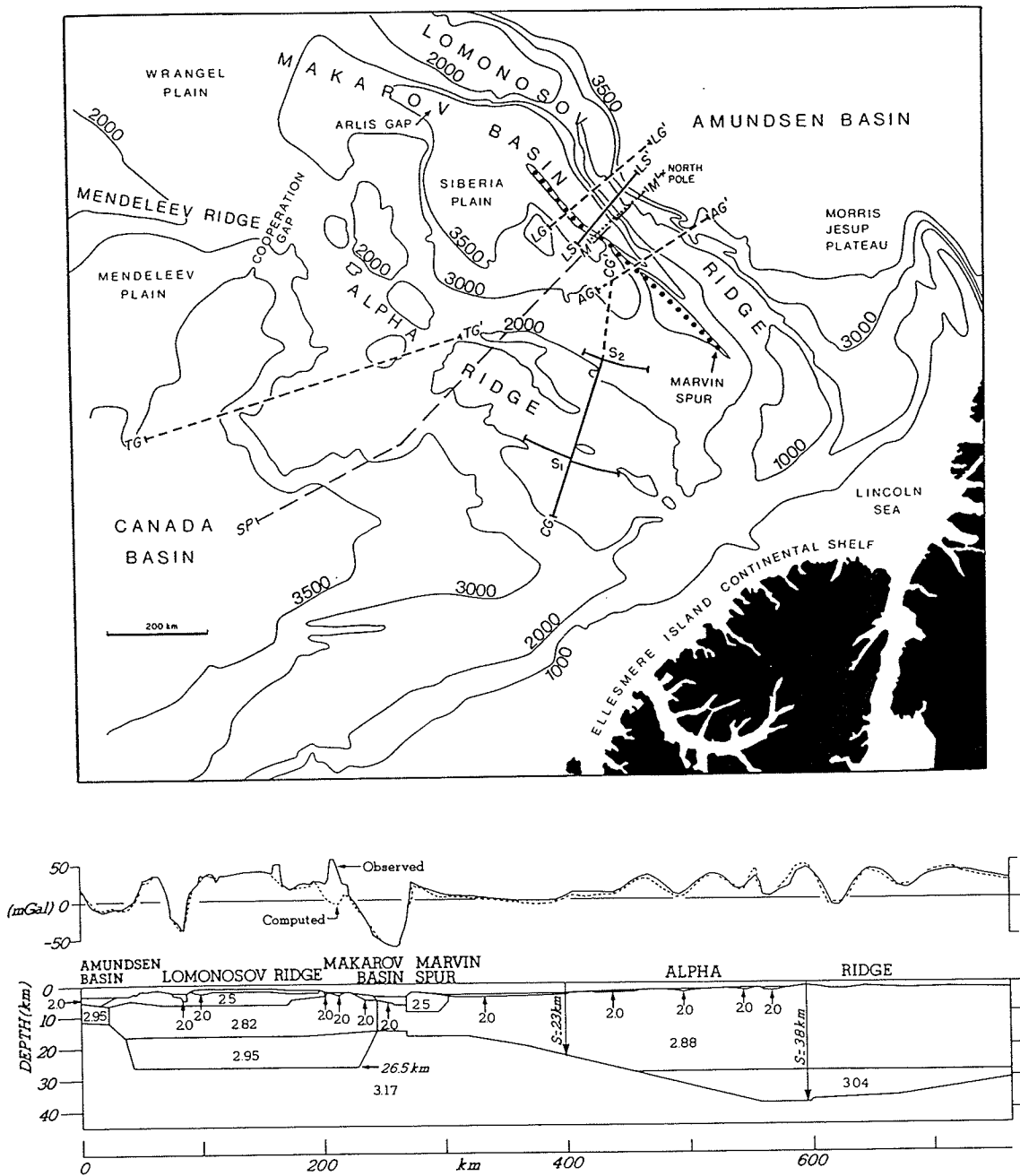
Figure 2.6: Alpha Ridge gravity structure

a: Map showing profiles AG' - AG, CG' - CG and LG' - LG indicate locations of gravity profiles, and b: gravity density model across Alpha Ridge, Makarov Basin and the Lomonosov Ridge along above profiles (from Weber, 1986).
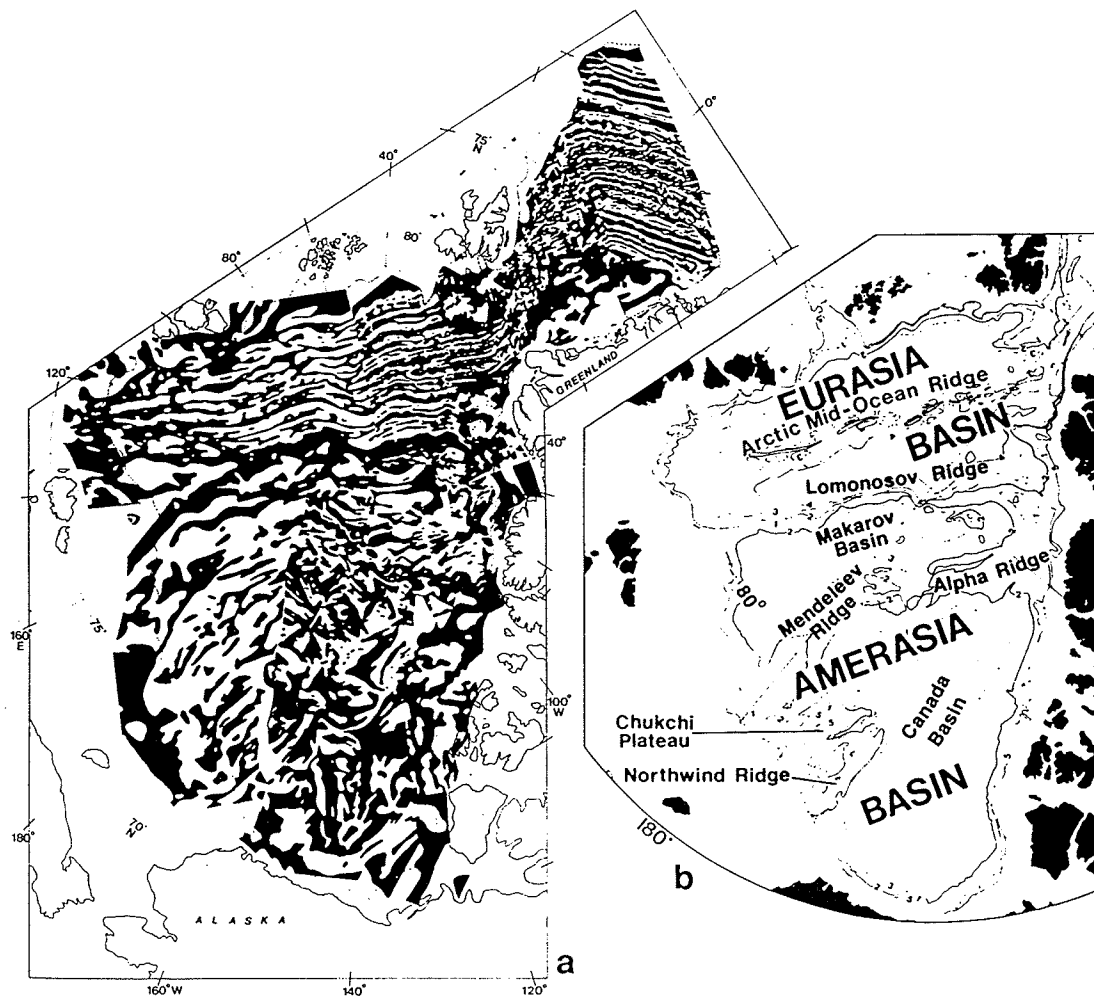
Figure 2.7: Arctic Basin aeromagnetic signature

a: Residual (zebra-strip) magnetic anomaly pattern from aeromagnetic surveys over the Arctic Ocean. The anomalies over the Eurasia Basin are lineated while there is little or no lineations over the Amerasia Basin. b: Simplified map of the Arctic corresponding to the area over which the anomalies are taken (from Vogt et al., 1982).
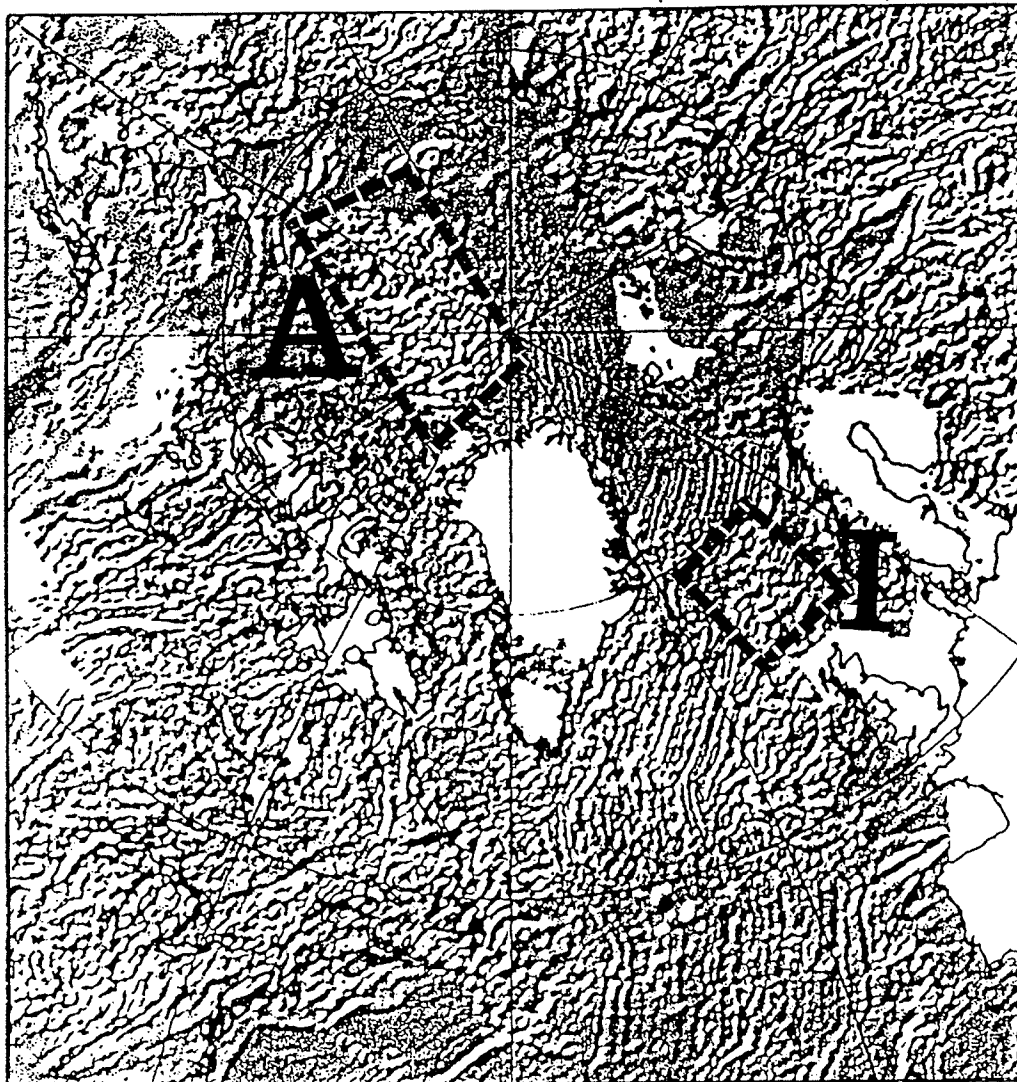
Figure 2.8: Preliminary aeromagnetic derivative map

The map shows a plot of the first derivatives of aeromagnetic data over the the
Arctic Ocean and the surrounding land masses. The pattern of the plotted data
over Alpha Ridge (region marked A) is continental (not lineated). The anomaly
is similar to the Iceland anomaly (region marked I). The Eurasia Basin and the
North Atlantic Ocean are lineated, exhibiting typical spreading ocean floors (from
Mcnab et al, 1992).

Figure 2.9: Estimated depth to magnetic basement

Estimated depth to magnetic source over Alpha Ridge, Makarov Basin, and areas
north of Ellesmere Islands. The lines L - L show a group of highs along the crestal
region of Alpha Ridge. The line C - C is the group of lows north of Ellesmere
Island discussed in the text (from Kovacks and Vogt, 1982).
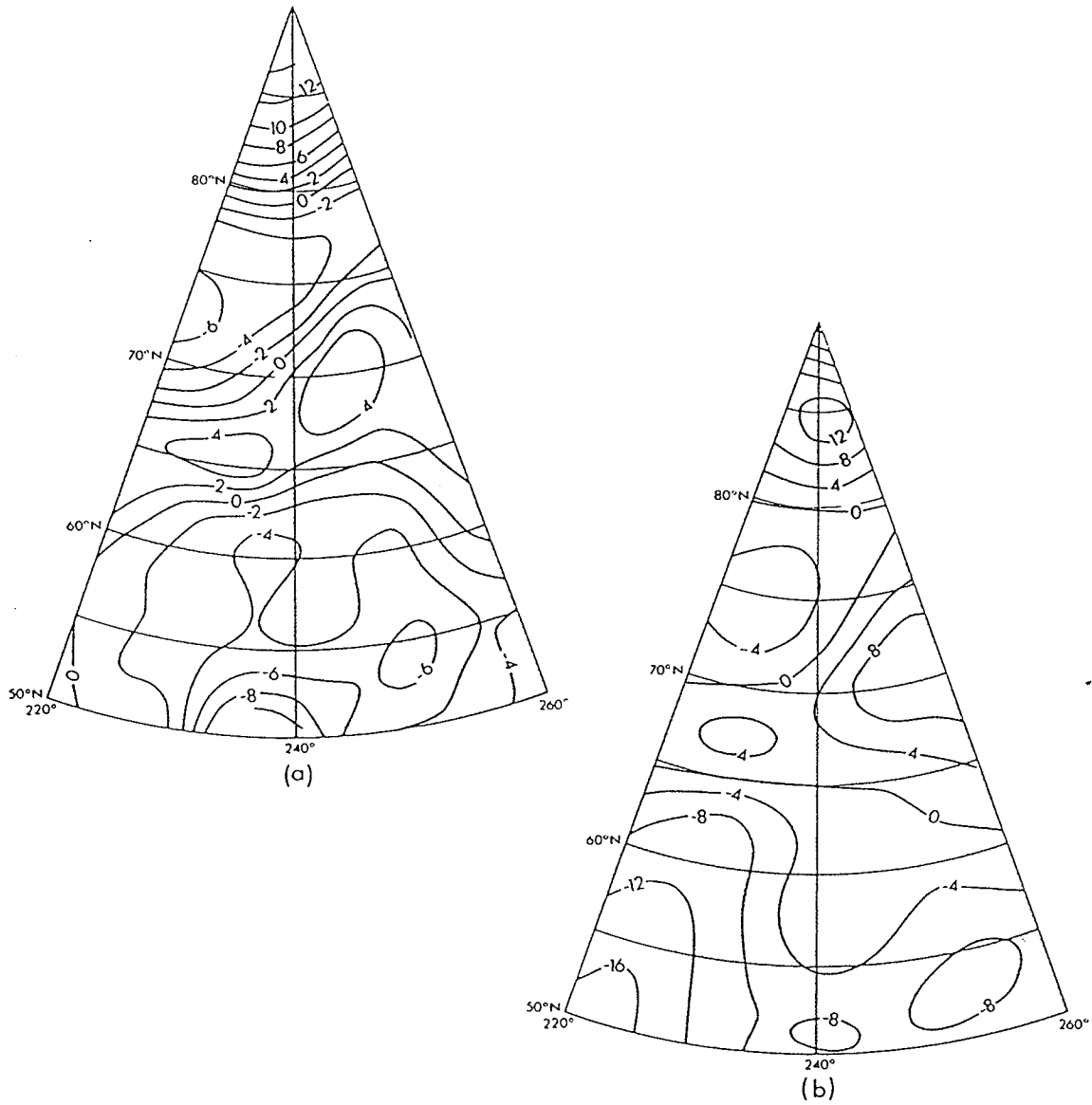
Figure 2.10: Comparison of Alpha Ridge satellite and aeromagnetic data

a: Average scalar magnetic anomaly from POGO at 500 km altitude and b: aero-magnetic data upward-continued to the altitude of 500 km. The two anomaly maps are in good agreement (from Langel et al., 1980).
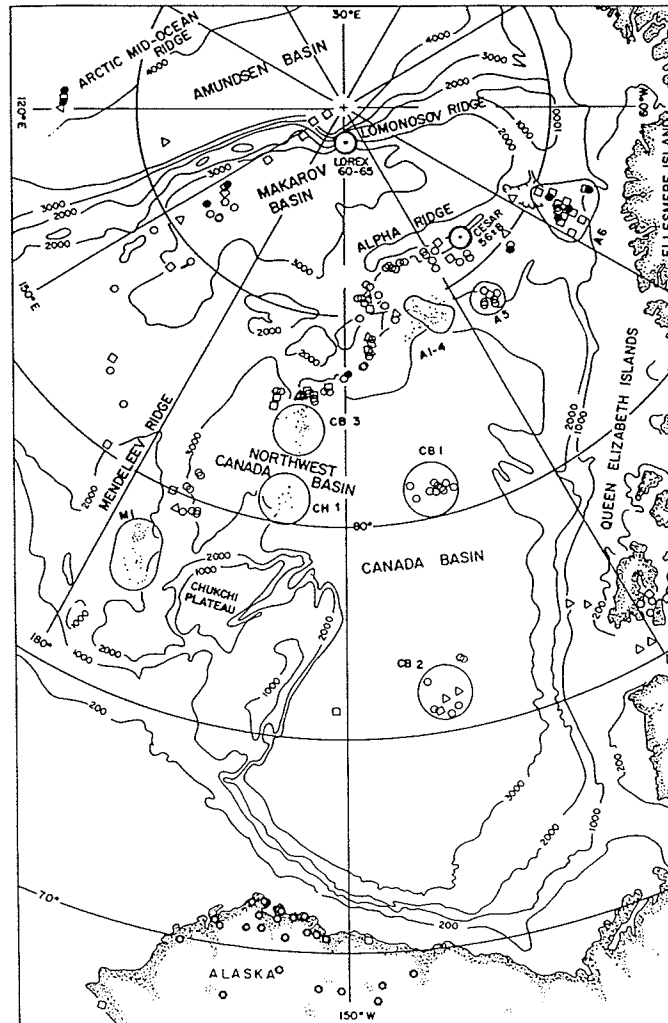
Figure 2.11: Map of heat flow measurements

Map showing the heat flow values in the Amerasia basin. The values are coded to indicate the range in mWm^{-2}. Traingle are less than 40, circles range from 40 to 60, squares range from 60 to 80 and solid circles are greater than 80 (from Langseth et al., 1990).
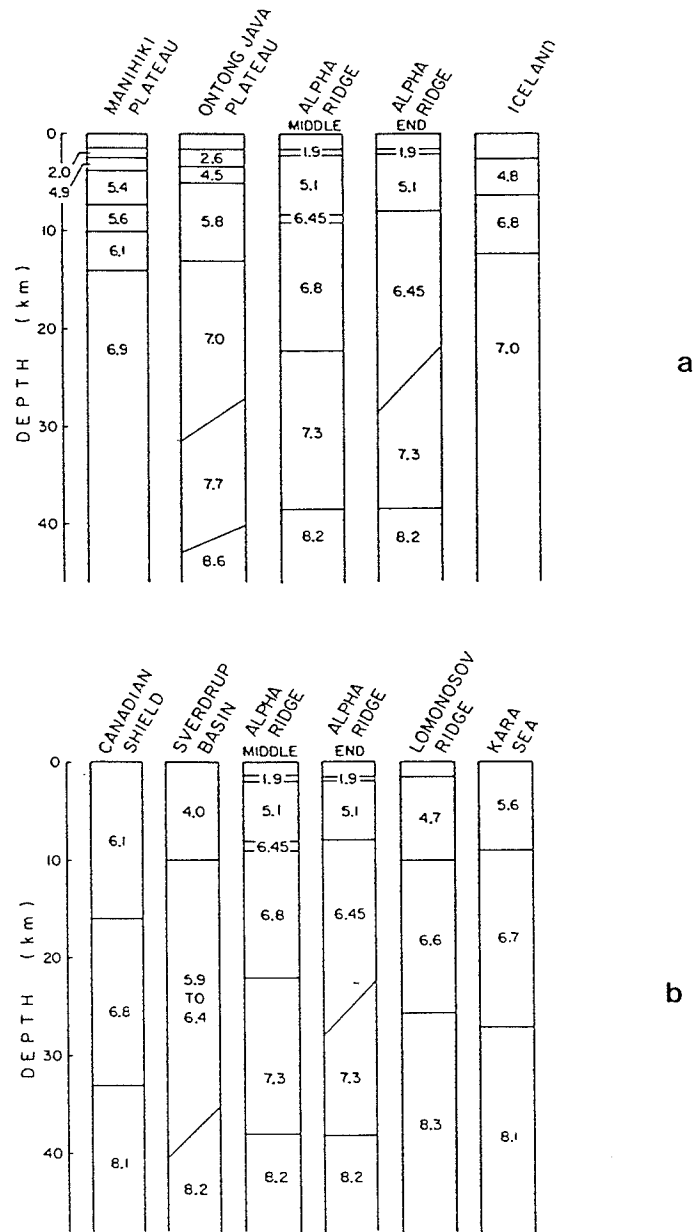
Figure 2.12: Alpha Ridge, continental and oceanic structures

Comparison of Alpha Ridge seismic crustal structure within thick oceanic (a) and continental (b) crusts. The values indicate crustal velocities in kms^{-1}. Alpha Ridge is similar to both types of crust (from Jackson et al., 1986).

Chapter 3

THE MAGNETIC CRUST

The residual magnetic anomalies observed at the earth or near-earth surface are caused by magnetic minerals already reviewed in Chapter 1. Above their Curie temperatures, the minerals lose their magnetism. The heat required to achieve Curie temperatures emanate from crustal radiogenic sources (80%) plus a contribution (20%) from internal heat from accretion, core formation, etc. Thus, depending on the amount of heat available, the depth at which Curie temperatures are achieved varies. The crust above the Curie level or surface is henceforth referred to as the magnetic crust. Some investigators have taken the Moho as the Curie level in the modeling of continental magnetic crusts (Wasilewski et al., 1979; Mayhew, 1979). This criterion was used by Taylor (1983) in modeling the Alpha Ridge satellite magnetic anomaly. However, since the Curie temperature determines the thickness of the magnetic crust, the Curie surface may occur below or above the Moho. In this chapter the approximate Curie level beneath the Alpha-Mendeleev Ridge complex and the adjacent Canada and Makarov Basins is determined. The resulting estimate of magnetic crust thickness is then used in modeling both Alpha Ridge satellite and aeromagnetic data.

3.1 Simple heat flow model

The determination of sub-surface temperature distribution by extrapolating heat flow values measured at the earth surface to some depth has been discussed by Lachenbruch (1970), Čermák (1975) and Rao and Jessop (1975). In addition to the heat flow values, the determination requires the knowledge of the layers that constitute the magnetic crust, the thermal conductivities of the layers, and the heat production within the layers.

Figure 3.1 shows a simple model for heat flow and heat production of a magnetic layer. Assuming steady state conditions, the following simplified general heat equation is used to model the temperature-depth relations (Čermák, 1975).

$$\frac{d}{dz}(k\,\frac{dT}{dz}) = -H \tag{3.1}$$

where

T = temperature (K),

k = thermal conductivity $\mathrm{mWm^{-1}K^{-1}}$ and

H = heat production $(\mathrm{mWm^{-3}})$.

The solution of equation (3.1) is given by

$$k(T - T_u) = Q_u(Z - Z_u) - \frac{H}{2}(Z - Z_u)^2 \tag{3.2}$$

where

T_u = temperature at the surface of layer (K),

T_l = temperature at the bottom surface of layer (K),

Z_u = depth to the upper surface of layer (m),

Z_l = depth to the bottom surface of layer (m),

Q_u = the heat flow observed at the surface of layer (mWm^{-2}) and

Q_l = the heat flow extrapolated at depth Z_l (mWm^{-2}).

The following parameters are determinable at the surface; the temperature Tu, the heat flow value Qu, and the thickness of a layer Z_l. The conductivity k is not easily determined especially for deeper layers and often has to be estimated on the basis of the expected geology. Using equation (3.2), the temperature at depth Z_l is given by

$$T_l = T_u - \frac{1}{k}Q_u(Z_l - Z_u) - \frac{H}{2k}(Z_l - Z_u)^2 \tag{3.3}$$

and the heat flow Q_l is calculated from

$$Q_l = Q_u - (Z_l - Z_u)H. \tag{3.4}$$

For a multiple layer crust, the temperature T_l from equation (3.3) is used as the temperature (Q_u) at the surface of the next layer and the new heat flow value at this surface is given by Q_l. Thus in a similar manner, the temperatures can be calculated for any arbitrarily layered model representing the earth's crust and composed of a number of layers such as sedimentary, granitic, basaltic, etc.

3.2   Oceanic, continental and ocean ridge layering

This section is a review of the crustal layering beneath oceans, in continents and in ocean ridges.

3.2.1   Oceanic crust

The structure of the ocean crust is well understood from the various seismic refraction and magnetic anomaly studies (Bott, 1982; Banerjee, 1984). Beneath the ocean floor, the crust is composed of three layers that lie above the Moho. Layer 1 is composed of unconsolidated sediments. The average thickness of this layer is about 0.4 km. Layer 2 extends from below the sediments to a depth of about 2 km. The layer includes pillow lavas (layer 2A) and doleritic sills and sheeted dikes (layer 2B). The third layer in the structure is gabbroic and is further divided into layers 3A and 3B.

3.2.2   Continental crust

Whereas an oceanic crust is remarkably uniform in structure and thickness, the continental crust is varied and much more complex in structure. Away from mountain ranges, the average thickness of a continental crust is about 35 to 40 km. Young folded mountain ranges reach some 70 to 80 km in thickness. On the basis of geophysical data such as gravity and seismic, the continental crust is petrologically divided into an upper and a lower crust (Bott, 1982). The upper crust is suggested to be a layer of intermediate metamorphic rocks containing granitic intrusions which grade down to a more felsic migmatitic zone. The lower crust on the other hand is thought to consist of a heterogeneous mixture of high grade metamorphic and subordinate igneous rocks. Seismic studies conducted in Europe and Canada show that the continental crust may have up to 7 layers (Berry and Mair, 1980). From the surface downwards,

the layers include sediments, crystalline basement, laccolithic zone, migmatitic zone, amphibolites, granulites and ultramafics.

3.2.3   Oceanic ridge crust

Some ocean regions are underlain by anomalously thick crust. The best known regions are Iceland-Faeroe, Manihiki, Hess, Magellan and Shatsky Plateaus (Jackson et al., 1986). Seismic studies show that these Icelandic types of crust may be divided into two or three layers (Bott, 1982). Beneath the Iceland-Faeroe Ridge, the Moho is found at a depth of 30-35 km, a depth comparable to that beneath the continents. The crust itself is divided into three layers. The upper two layers are formed by lava flows which outcrop at the surface and are associated with minor intrusive rocks. These layers are regarded as a thick representative of oceanic layer 2, and the thickness reaches a depth of 7-9 km. The third layer is is inferred to be oceanic layer 3 (Bott, 1982).

3.3   Alpha Ridge crust

The heat flow values and crustal layering used for modeling the magnetic crust beneath the Alpha Ridge and the Canada and Makarov Basins were obtained from previous studies. The heat flow values used are obtained from Figure 2.11. The values are heat flow averages for the locations CESAR, A1 - 4, CB1, CB3 and LOREX and are summarized in Table 3.1. The crustal layering of Alpha Ridge and Canada and Makarov Basins is based on the interpretation of Grantz et al. (1990b). For Alpha Ridge the first layer is composed of sediments. Oceanic layers 2 and 3 are marine volcanics and gabbros respectively. Table 3.2 summarizes the crustal layers and the respective thicknesses in km for the ridge and the basins.

3.4 Magnetic crust determination

Čermák and Rybach (1982) have compiled thermal properties of minerals and rocks. Heat production of each of the crustal layers for the Alpha Ridge and the Canada and Makarov Basins are estimated from the compilation and are shown in Table 3.3. The thermal conductivity of the sediment layer obtained from CESAR results is 1.3×10^3 mWm^{-1}K^{-1}. The conductivities of the rest of the layers are assumed to be equal to 2.5×10^3 mWm^{-1}K^{-1}. The sea bottom temperature used in the calculation, determined during the CESAR expedition, is $-0.42°$ C. Using these known parameters and equations (3.3) and (3.4), the temperature at various depths is computed.

Figure 3.2 shows a plot of temperature versus depth for the A1-4 heat flow values. The magnetic crust is estimated using the Curie temperature of magnetite (550° C). This temperature is chosen because it gives the maximum possible thickness of the magnetic crust. From the figure, the depth at which the temperature of 550°C is reached is 36 km below the ocean bottom.

Similar processing is done for CESAR and the Makarov (LOREX) and Canada (CB1,CB3) Basins. The results for all the determinations are summarized in Table 3.4.

The results show that for Alpha Ridge, the Curie level is within layer-3 and varies from 28 km (for CESAR) below the ocean bottom to about 36 km (for A1-4). The difference in the Curie levels indicates that the Curie surface for Alpha Ridge as a whole is not a flat surface. In some areas of the ridge, the Curie level is shallower than in others: a situation similar to having an undulate topography.

The Curie levels for the Canada and Makarov Basins vary from 18 to 23 km below the ocean bottom. These levels are shallower than the Alpha Ridge levels. This should be expected since the mantle and therefore higher temperatures is found at shallower depth beneath the oceans.

Verba et al. (1990) include the Curie level for Alpha Ridge and the Canada and Makarov Basins in their summary of the Arctic geophysics. The Curie level for Alpha Ridge is found at a depth of about 25 km below the sea level. The level is more shallow than that determined in this chapter. It may be attributed to the interpretation of the crustal layering of the ridge. In this chapter the layering of the crust is as interpreted by Grantz et al. (1990b). The shallow Curie level in the summary of Verba et al. (1990) could be for an area where the Curie surface is much shallower than for the rest of the ridge.

In their summary, Verba et al. (1990) give a Curie level of about 20 km below the sea level for the Canada and Makarov Basins. The result is in agreement with the one determined in this chapter. This is most likely due to interpreting the oceanic layering in the same way as is done in this chapter.
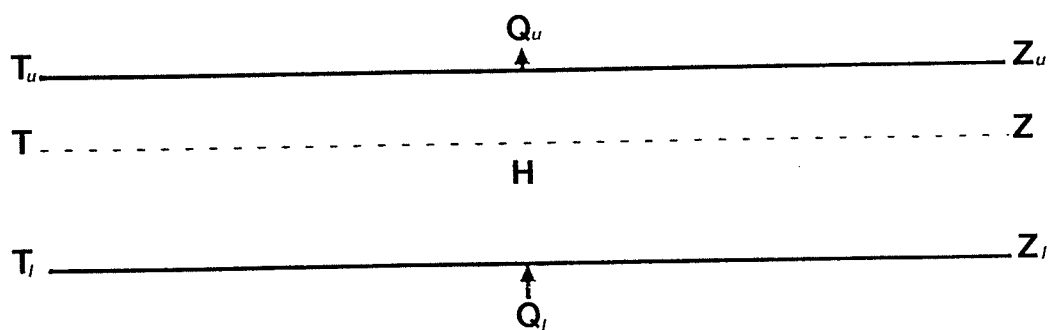
Figure 3.1: One-dimensional heat flow model

One-dimentional temperature-depth model. T_u and Q_u respectively denote the temperature and heat flow at the surface of the layer. Z_u is the depth to the layer surface. At the bottom of the layer, these are repevtively T_l, Q_l and Z_l. The heat production of the layer is H.

Table 3.1: Table of heat flow values

Heat flow values in the Amerasia Basin used for the Curie level calcualtions. The regions where the measurements are taken from are shown in Figure 2.11. The values (in mWm^{-2}) are compiled from Langseth et al., 1990.

Region	Mean Lat., N	Mean Lon., W	Heat Flow
ALPHA RIDGE			
A1-4	84°45'	129°55'	48.6
CESAR	85°50'	108°40'	56.0
MAKAROV BASIN			
LOREX	88°32'	150°	60.0
CANADA BASIN			
CB1	80°36'	137°16'	55.0
CB3	82°22'	157°40'	67.2

Table 3.2: Layer thicknesses of Alpha Ridge crust

Summary of crustal layer thicknesses beneath the Alpha Ridge and the Makarov Basins. The thicknesses are in km (compiled from Grantz et al., 1990b).

LAYER	CANADA BASIN	ALPHA RIDGE	MAKAROV BASIN
Sediments	5.7	0.67	3.84
Oceanic layer 2	1.5	0	0
Marine volcanics	0	22.7	0
Oceanic layer 3	5.7	13.8	5.17

Table 3.3: Heat productions

Heat productions of the various rock types, in mWm^{-3} (compiled from Čermák and Rybach, 1982).

LAYER	HEAT PRODUCTION
Sediments	1.5
Oceanic layer 2	0.63
Marine volcanics	0.63
Oceanic layer 3	0.33
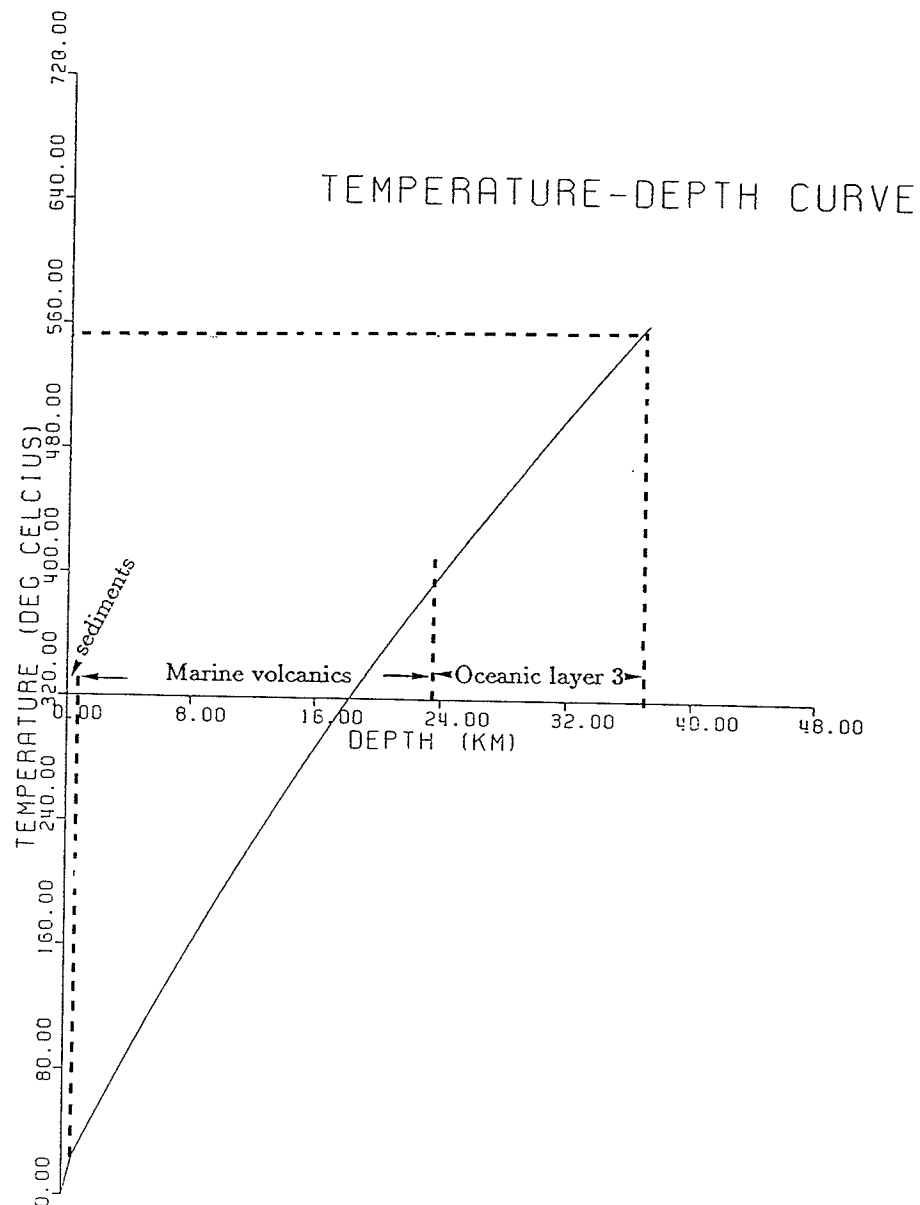
Figure 3.2: Temperature-depth profile of Alpha Ridge crust

Temperature-depth relationship beneath Alpha Ridge calculated using A1-4 heat flow values (see Table 3.1). The magnetite Curie temperature of 550° C is determined to be at the 36 km depth.

Table 3.4: Curie level approximation

Depth to the curie level (in km) beneath the Makarov and Canada Basins and the Alpha Ridge. Determinations of the curie level is discussed in the text.

REGION	DEPTH
ALPHA RIDGE	
A1-4	36
CESAR	28
MAKAROV BASIN	
LOREX	23
CANADA BASIN	
CB1	23
CB3	18

Chapter 4

AEROMAGNETIC DATA

4.1   Area and data coverage

A diskette containing aeromagnetic data covering the eastern part of Alpha Ridge was obtained from the Geophysical Division of the Geological Survey of Canada. The data consist of the aeromagnetic total field digitized at an interval of 2 km. The areal extent of the data is shown in Figure 4.1. The area covered extends from latitudes 83° to 87°N, and from longitudes 90° to 141°W. The initial data was acquired by different sources. In merging the initial data sets, any discrepancies were empirically adjusted (Riddihough et al., 1973). The corrected flight height is 3.5 km above sea level. The reference field used to derive the residuals was the International Geomagnetic Reference Field (IGRF). The digitization of this data set was completed by the end of August, 1989. By then, not all data sets had been merged and as a consequence, there are large gaps in the map in which no data is available. Nonetheless, the available data provides significant information as to the nature of Alpha Ridge. The location and some of the parameters of the gridded data, together with the program that reads the data, are provided in Appendix A. A copy of the data set may be obtained

either from the Geophysical Division of the Geological survey of Canada or from the
Department of Geological Sciences at the University of Manitoba.

4.2   Examination of the raw data

The area covered by the aeromagnetic data is located at very high latitudes (83° −
87°N). For such an area, reduction to the pole of the aeromagnetic data is not nec-
essary (Langel, 1974; Taylor, 1983). The areas on the map marked by light tones
indicate features having positive magnetic anomalies while the dark tones indicate
features having negative anomalies. The following characteristics are derived from
visual inspection of the raw data.

 i. Features having positive magnetic anomalies are confined to a narrow zone of
    about 270-300 km (between lines L1 and L2, Figure 4.2). This zone is along
    the general trend of Alpha Ridge. There are smaller positive anomalies outside
    the zone.

 ii. The magnetic features are of various shapes and sizes. The small near circular
     positive anomalies are about 20 km in diameter while the elongated broader
     ones are about 80 km wide and about 250 km long. The positive anomalies
     have an irregular to a sublinear pattern that trends west to southwest. There
     is no clear pattern of alternating positive and negative anomalies as is seen at
     active mid-ocean ridges.

 iii. The anomaly amplitudes are extremely variable. Examination of eight profiles
      (S1-S5 and W1-W3; see Figure 4.3) show that the highest amplitudes are
      over the Alpha Ridge. These amplitudes reach some 1800 nT peak to trough

while the smallest are about 100 nT. The anomalies that flank Alpha Ridge have very low amplitudes and are generally negative. To the north, the low amplitude negative anomalies are over the Makarov Basin and to the south and southwest, they are over Canada Basin.

4.3   Spectral analysis

Since the development of the fast Fourier transform by Good (1958) and its subsequent modifications by Cooley and Tukey (1965) and many others in the field of time series analysis, the spectral representation of potential field data has gained an important role. The potential anomaly field represents the composite effect due to subsurface sources of various wavelengths (Gupta and Ramani, 1980; Darby and Davis, 1967). The wavenumber (frequency) representation of the potential field data is obtained by taking the Fourier transform of the data. This frequency representation is simple and allows immediate recognition of the characteristic harmonics. There are three main categories in which the spectral representation has been applied to the potential field. The first category involves the interpretation of single anomalies which are interpreted in terms of a single homogeneous body by means of certain spectral characteristics. Examples of this category are discussed by Odegard and Berg (1965), Bhattacharryya (1966), Sharma et al. (1970), Sengupta (1974), Collins et al. (1974), Bhattacharryya and Leu (1977), Bhimasankaram et al. (1977) just to mention a few. The second category involves the interpretation of anomaly assemblies which are interpreted on a statistical basis in which main features (e.g. the estmation of depth to the magnetic basement) are extracted from the average spectra. Examples of this second category of potential data analysis have been dealt with by Spector and Grant (1970), Treitel et al. (1971), Cassano and Rocca (1975), Hahn et al. (1976), Pedersen (1978), Wang and Hansen (1990). The third category of potential field spectral representation

involves the speed of the fast Fourier transform and the ease with which complicated operations in the space or time domain become simple mathematical manipulations in the wavenumber or frequency domain. Taking advantage of these simplifications in the frequency domain are operations involving data filtering (Agarwal, 1968; Darby and Davies 1967), upward (downward) continuation and calculation of derivatives (Agarwal, 1968; Gunn 1975), and the transformation of data such as reduction to the pole and conversion between components (Agarwal 1968; Gunn 1975; Lourenco and Morrison, 1973; Roy and Aina,1986).

In this thesis the aeromagnetic data were analyzed in the wavenumber domain in order to examine the dominant wavelengths of the large scale anomalies and i-dentify wavelengths that constitute geological noise. Identification of wavelengths constituting noise allows the separation of the magnetic anomalies due to subsurface sources from the noise. Filtering of the data may also give insight into the subsurface distribution of the sources.

The sampling interval of the aeromagnetic data is 2 km. Based on the Nyquist principle, the smallest identifiable magnetic feature has a wavelength of 4 km. This wavelength is considerably smaller than the size of the magnetic anomalies over Alpha Ridge, which are of the order of 15-270 km. In order to check that the spacing interval thus chosen does not introduce aliasing at wavelengths greater than 4 km, power spectra of the profiles were examined. If the energy does decrease such that at the Nyquist wavelength there is little energy, it may be concluded that any aliasing or folding back of energy is negligible.

The fast Fourier transform programs used in the analysis of the data are entirely those developed by Agarwal (1968).

4.3.1 One-dimensional FFT analysis

The eight profiles (extracted along S1-S5 and W1-W3; Figure 4.2) were used in the spectral analysis. First, linear trends were fitted to the profiles using a robust method (Press et al, 1986; also see Appendix B for for the program). The robust method performs better than least squares methods in the presence of geological and non-gaussian noise (Silva and Cutrim, 1989). Figure 4.4 shows an example of a profile to which a linear trend has been fitted using the robust method (least squares fitting is included for comparison). The trends fitted are characterized by small slopes of up to about 1.0 nT/km in magnitude. The trends were then subtracted from the profiles. Subtracting a trend is in effect a filter operation in which long wavelength effects are suppressed (Dobrin,1988), that is, operation reduces leakage from strong spectral lines at long wavelength into short wavelength.

Having removed the trends, the eight profiles were then Fourier transformed. Figure 4.5 shows the relative amplitude spectra. In addition to the eight profiles, sixteen other profiles were subjected to trend removal and Fourier transformation. In Figure 4.5, some of the profiles have dominant wavelengths that are easy to identify. The dominant wavelengths vary from 80 to 100 km. There are also a few spectral highs at wavelengths of 15 and 45 km. At shorter wavelengths of between 5-8 km, there are a few spectral peaks. These peaks are either due to digitization, instrumental and navigational errors or due to the effects of topography and small scale geological features such as very thin dikes and thus constitute noise that has to be removed before any further work is done on the data.

A better statistical examination of the signals is provided by the power spectra. Here, the power spectra is estimated by averaging FFT results from line S1-S5. The average power spectra of the profiles is shown in Figure 4.6. Most of the energy is concentrated at wavelength of 100 km or greater. At shorter wavelength the energy

falls very rapidly. Reaching the Nyquist wavelength of 4 km, the energy is about 5 orders of magnitude less than at 40 km. It is therefore concluded that aliasing or folding back of the energy is negligible.

The power spectra show that the signal drops beneath the noise level at wavelengths less than about 8 km. To reduce the effect of noise on the profiles, a high-cut filter was applied to retain wavelengths greater than 8 km. Figure 4.7 shows a profile in which a high-cut filter is used. Removal of wavelengths less than 8 km leaves signals that reflect the subsurface magnetic sources at depth. Examination of all the profiles spectra show that there are no particular wavelengths at which signals from the subsurface magnetic features are concentrated.

4.3.2   Two-dimensional FFT analysis

An attempt was made to apply a band-pass filter so as to isolate the magnetic features of particular wavelengths. In particular, the application of a band-pass filter would reveal, if present, any lineations as is found in mid mid-ocean ridges. The aplication of a wide variety of band-pass filters did not show any lineations.

The application of a high-cut filter suppresses noise and the effect of near surface contributions. The application of a such a filter also give results similar to upward continuation (Dobrin, 1988). By increasing the wavelength at which the anomalies are cut, the equivalent in upward continuation would be to observe the anomalies at higher elevations. Thus the resulting anomaly field becomes broader as the signals from the sources merge. Also, the amplitudes of the signals are reduced.

Figure 4.8 is an extract from the original data to which several high-cut filters are applied. The results of applying the various filters are shown in Figure 4.9. Removal of the average regional value (Figure 4.9a), which is equivalent to removal of a constant in the case of profiles, does not provide any new information as compared to the

original data (Figure 4.8). Removal of wavelength of up to about 16 km (Figures 4.9b, 4.9c) show that the anomalies are still of the same dimension as at the near surface. Noticeable changes due to the merging of the anomalies start to show when wavelength of up to 25 km are cut-off (Figure 4.9d). The features become broader and reduced in amplitude.

Subsequent filtered data (Figures 4.9e-h) for the Alpha Ridge region show that the positive anomalies dominate at long wavelength. This is equivalent to saying that positive anomalies dominate when observed at higher elevations. This filtering result shows Alpha Ridge may be a broad structure with numerous sources near the surface. Since deep anomaly sources are more observable at higher elevations, the sources of Alpha Ridge anomalies may be located at the deeper parts of the ridge. It is also possible that near surface and deeper sources all contribute to the Alpha Ridge anomaly; the short wavelength components being due to shallow sources while the long wavelength components are due to deeper and possibly more uniform sources.

4.4 Spectral analysis results

From the spectral analysis of data, the following conclusions are derived.

i. There is little noise in the data, characterized by wavelength of up to 6-8 km. This noise may be due to digitization, instrumental and navigational errors or due to effects that can be attributed to topography or small geological features such as thin intrusives. The noise is not significant to spectral analysis results at wavelengths greater than 8 km.

ii. The wavelengths of most the anomalies vary from 80 to 100 km. A few have wavelength of 15 and 45 km. This result shows that the subsurface magnet-

ic sources are complex. These may be small, broad, near surface and deep sources.

iii. Positive anomalies become dominant at higher elevations (e.g. when wavelength components greater than 25 km are removed) over the Alpha Ridge. The dominance of the positive anomalies is due to the merging of anomalies when observed at higher elevations. The amplitude of the resulting anomalies are reduced.
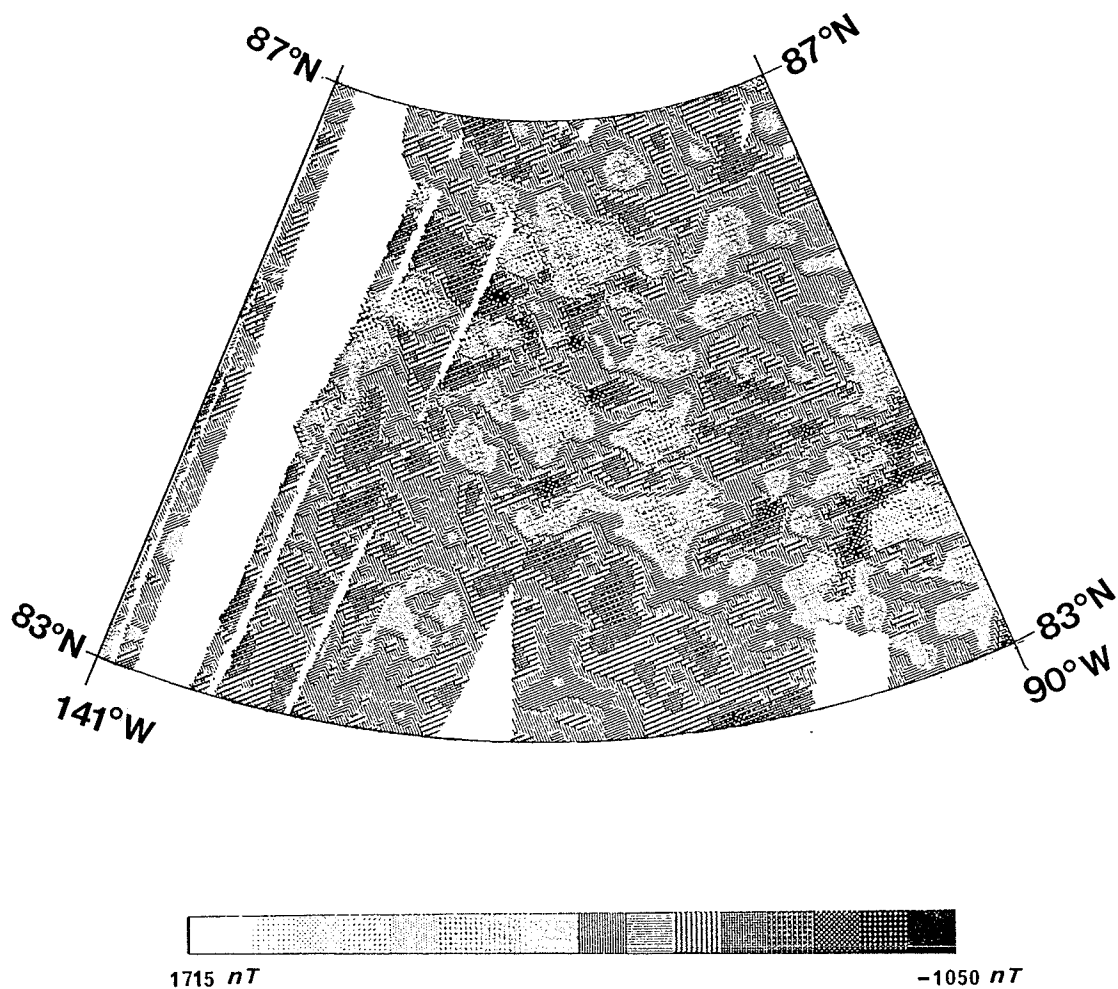
Figure 4.1: Aeromagnetic map

Map showing the area covered by the aeromagnetic data. The location of Alpha Ridge is shown in Figure 4.2.
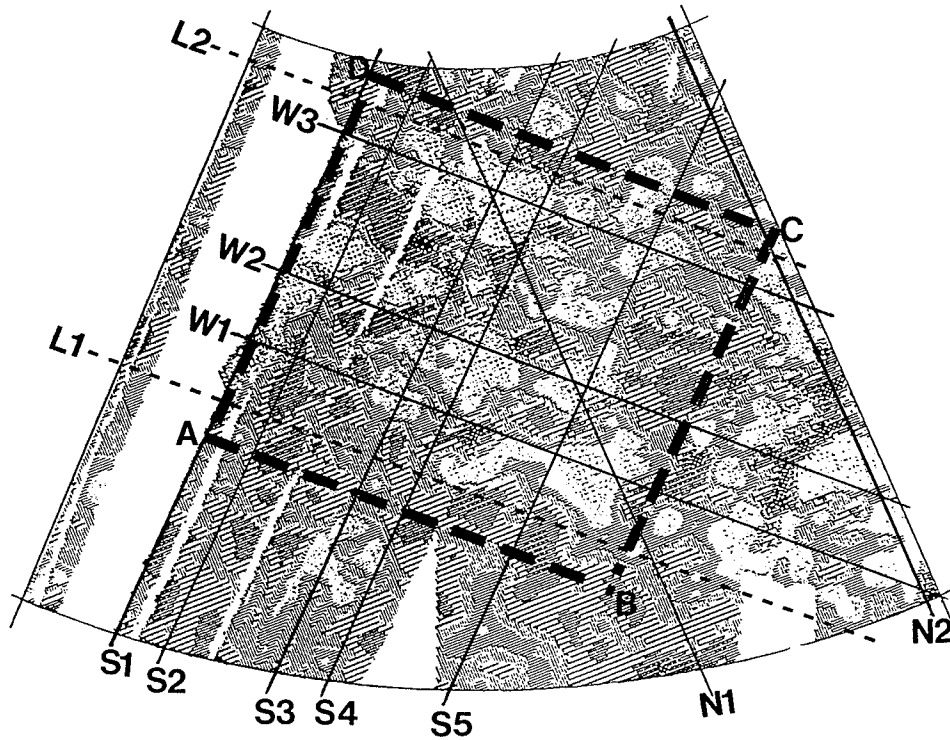
Figure 4.2: Aeromagnetic map for profile extraction

This map is the same as the original map (Figure 4.1) except that this shows specifications that are discussed in the text. The narrow zone between lines L1 and L2 define the Alpha Ridge zone to which the positive anomalies are confined. Profiles for investigation are extracted along lines S1 to S5, W1 to W3 and N1, N2. The area ABCD marks the zone from which data is extracted for 2-D spectral analysis.
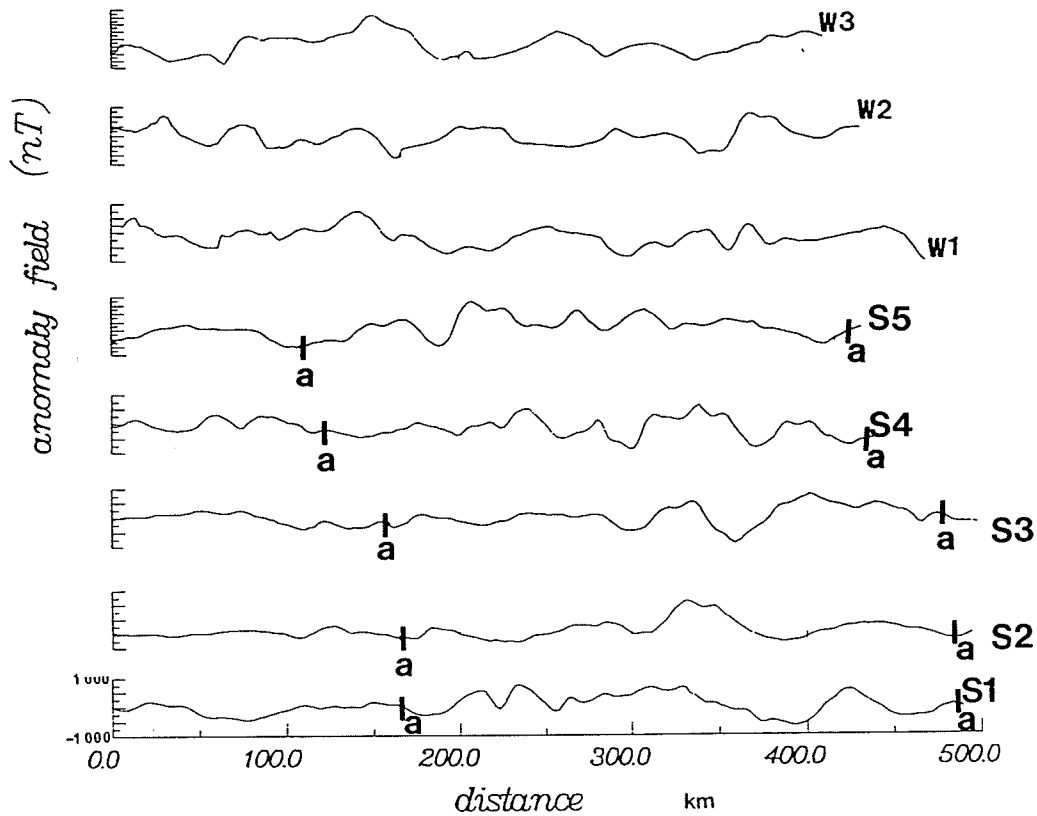
Figure 4.3: Anomaly amplitudes

Anomaly amplitudes of profiles along S1-S5, and W1-W3 extracted from Figure 4.2. Profiles W1-W3 are taken along the strike of Alpha Ridge while S1-S5 are extracted across the strike. The approximate width of the ridge (a-a) is indicated on profiles S1-S5.
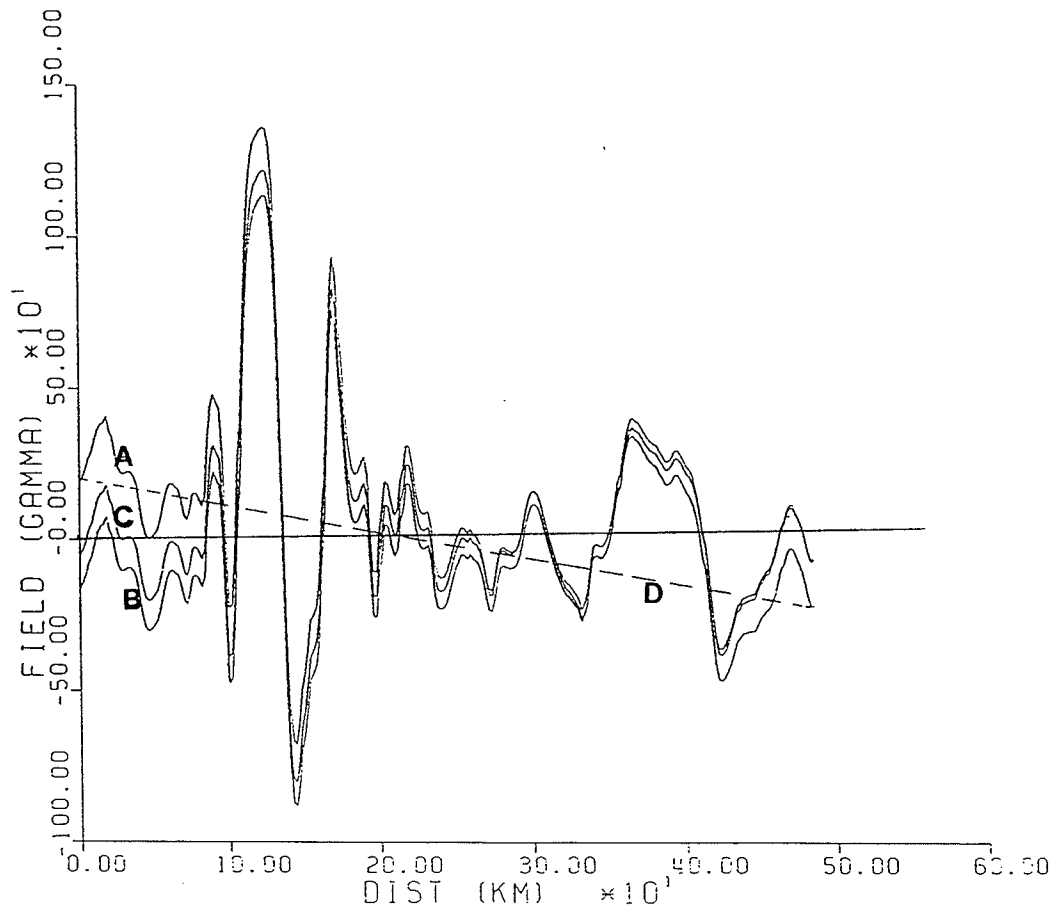
Figure 4.4: Linear trend removal

Plot A is the original profile (N2, Figure 4.2). B is the plot in which a linear trend is removed using least squares while C is the plot when the trend is removed using a robust method. D is the slope of the fitted trend.
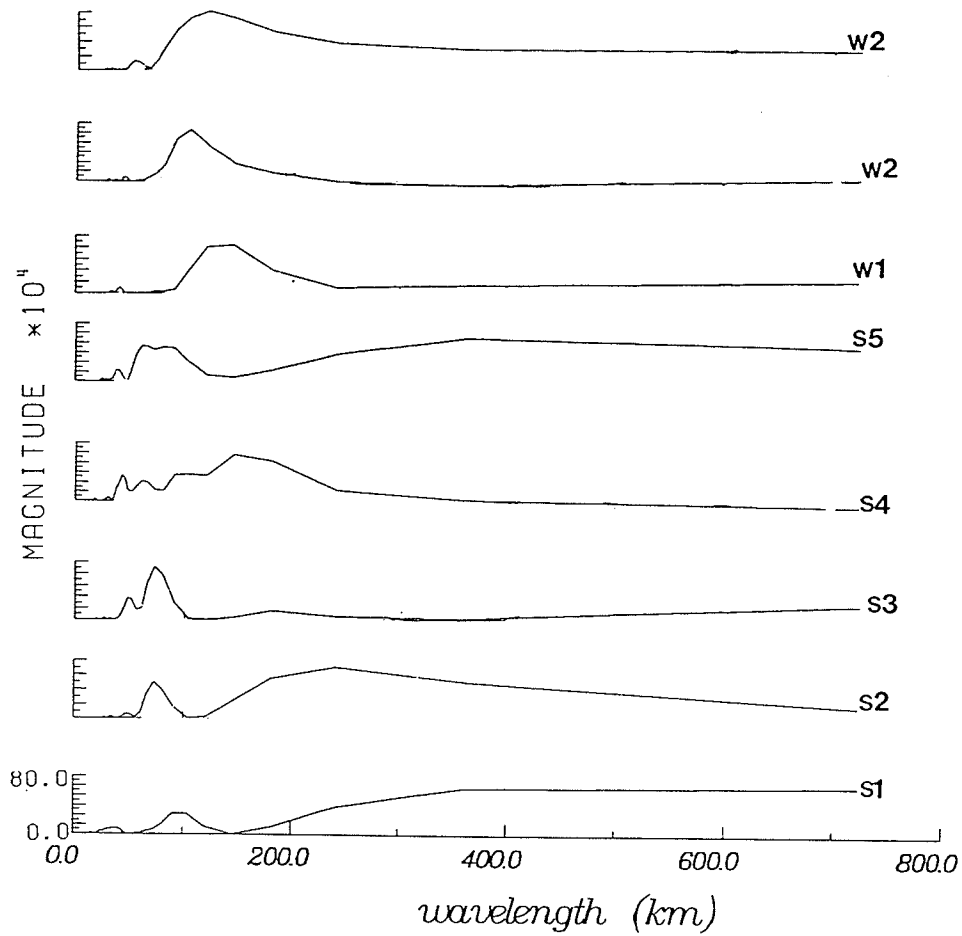
Figure 4.5: Relative amplitude spectra

The relative amplitude spectra are for the profiles shown in Figure 4.4. The wavelengths of the anomalies are varied. For S2, the dominant wavelength is 80 km.
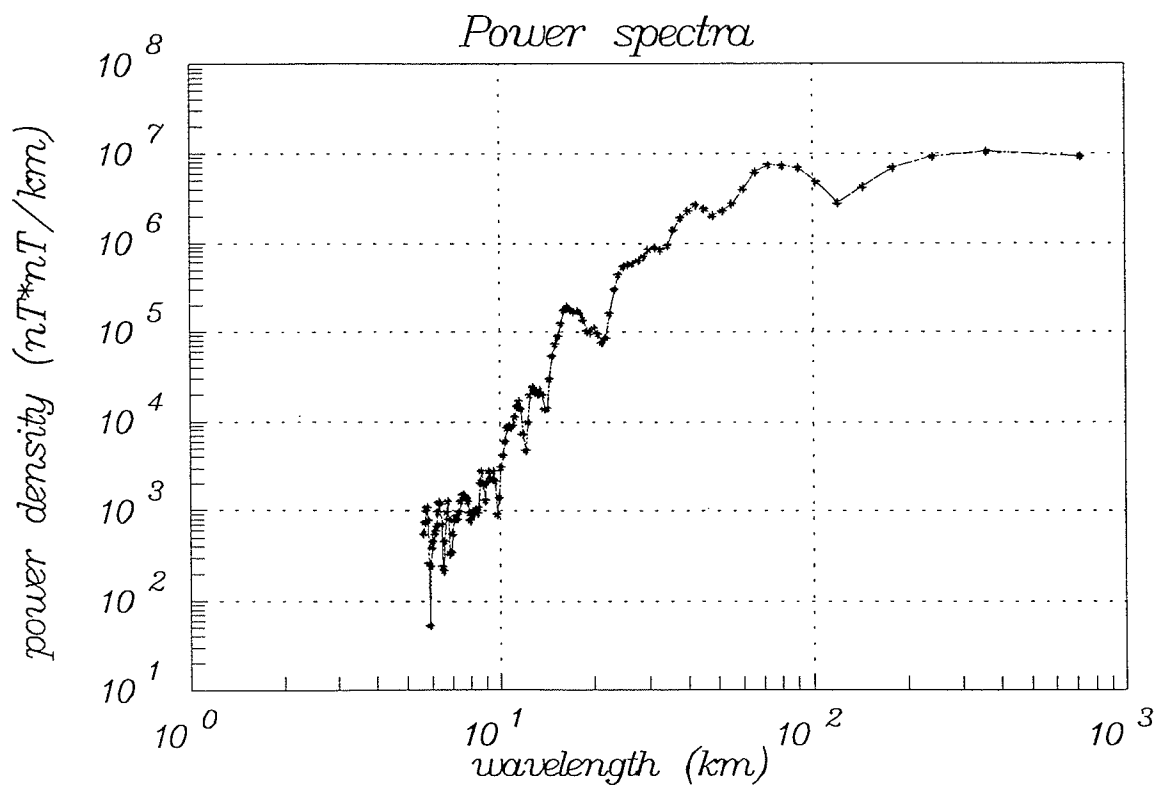
Figure 4.6: Average power spectra

The Figure shows a plot of the average power spectra of the profiles S1-S5 and W1-W3 (Figure 4.2). Most of the power is concentrated at wavelengths of 100 km or greater. At the Nyquist wavelength of 4 km, the energy is about 5 orders of magnitude less than at 40 km.
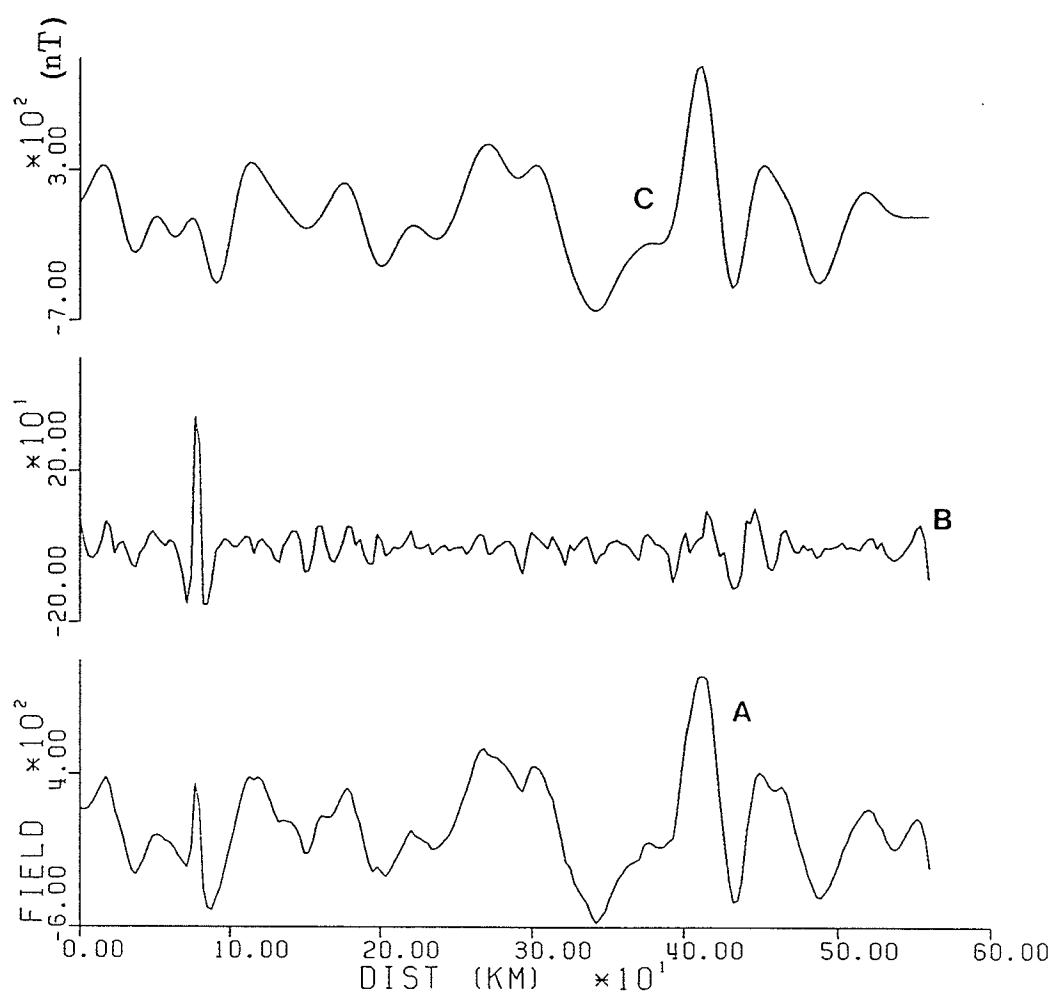
Figure 4.7: Wavelength filtering

This figure illustrates the application of wavelength filtering. A high-cut filter retaining wavelength greater than 8 km is applied to profile **A** (profile N1, Figure 4.2). The noise removed is **B**. The final result is profile **C**.
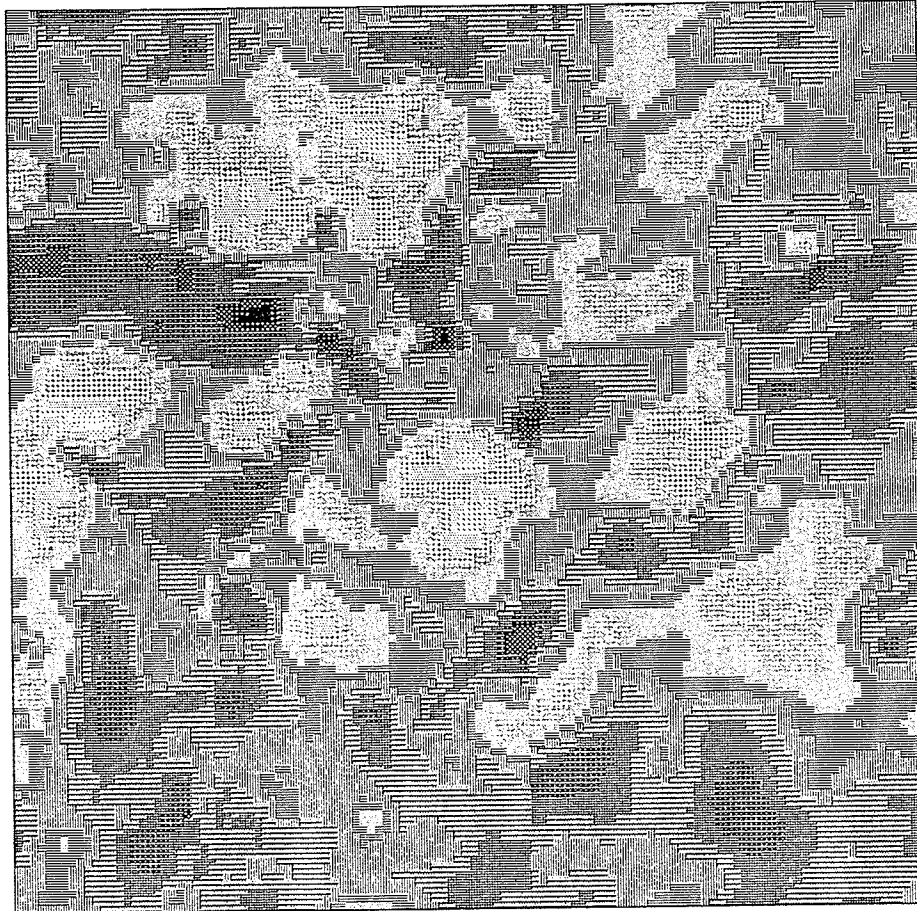
Figure 4.8: Map extract for 2-D FFT analysis

This map is extracted from Figure 4.2 (area ABCD) . It covers an area of $333.75 \times$ 333.75 km^2. The map is used for 2-D FFT analysis.
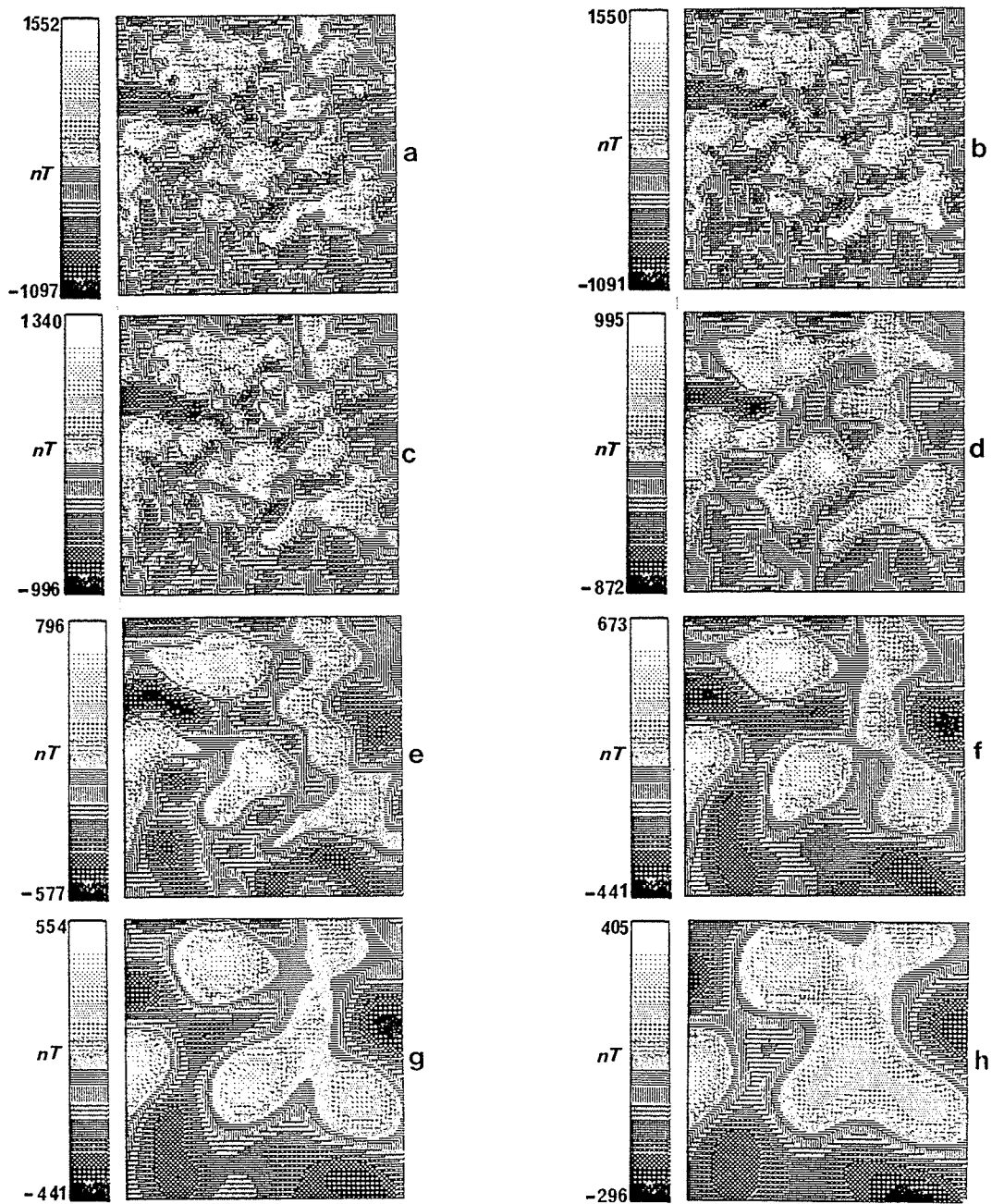
Figure 4.9: Maps of filtered aeromagnetic data

The grey-level maps are a result of applying different filters to the data of Figure 4.8. The individual maps are explained in the text.

Chapter 5

MAGSAT DATA

5.1 MAGSAT mission

The measurement of the geomagnetic field on a global scale, in a short time span, and at satellite heights began with Sputnik 3 in May 1958. This was followed by subsequent satellites such as COSMOS 49 and the POGO satellites which operated from 1965 to 1971. The POGO satellites provided a global set of magnetic measurements of uniform precision and accuracy thus enabling the first satellite magnetic anomalies to be computed (Regan et al., 1975). Encouraged by the results of this earlier satellite magnetometry, NASA launched the spacecraft MAGSAT on October 30, 1979. The satellite stayed in operation for $7\frac{1}{2}$ months until June 11, 1980. It had an initial orbit with 561 km apogee and 352 km perigee (Langel et al., 1982). The orbit decayed to an approximately circular shape (apogee less than 400 km) as the mission neared completion. While in operation, MAGSAT was in a twilight, sun-synchronous orbit with an inclination of 96.76°.

There were two objectives of the MAGSAT mission. The first being the acquisition of data for the study of the magnetic field generated at the core of the earth. The

second objective was to use the acquired data for the study of the distribution and significance of crustal magnetization. Both scalar and vector magnetometers were used in the measurement of the magnetic data. The scalar magnetometer was accurate to about $\pm$ 1.5 nT while the vector magnetometer was estimated to be accurate to within $\pm$ 3 nT in each of the axes (Langel et al., 1981). MAGSAT has surpassed its expectations. Main field models derived from it are the most accurate to date (Langel and Estes, 1985). Crustal studies using MAGSAT data number in the hundreds. Table 5.1 summarizes some of the work that has been done using the MAGSAT data as of 1990.

5.2 Crustal fields

The magnetic field measured at the surface of the earth and at satellite heights is composed of the earth's main field, the lithospheric field, and the fields originating from outside the earth. The first two fields constitute the geomagnetic field. In order to better understand the geomagnetic field, it is generally described with a mathematical model. The potential of the geomanetic field is represented by a spherical harmonic analysis of the form (Langel and Estes, 1982):

$$V = a \sum_{n=1}^{N} \sum_{m=0}^{n} (\frac{a}{r})^{n+1} \{g_k^m cos(m\phi) + h_k^m sin(m\phi)\} P_n^m(cos\theta) \qquad (5.1)$$

where

V : magnetic scalar potential,

a : mean radius of the earth,

r, θ, ϕ : standard spherical coordinates,

m : order of the spherical harmonic,

n : degree of the spherical harmonic and

$P_n^m(cos\theta)$: The Schmidt quasi-normalized spherical functions.

Langel and Estes (1982) examined the power spectra of the field models given by equation (5.1). The form of the power spectra they examined is given by:

$$R_n = (n + 1) \sum_{m=0}^{n} \{(g_n^m)^2 + (h_n^m)^2\} \qquad (5.2)$$

where R_n is the mean square over the earth's surface of the magnetic field intensity produced by the harmonics of the nth degree. They found a distinct change of slope at $n = 14$ which they interpreted to mean that the field from the core dominates at $n \leq 14$ and the field from the crust dominating for $n \geq 15$ (Figure 5.1). Based on the interpretation of the geomagnetic power spectra, the lithospheric field may be separated from the core fields.

Many procedures have been developed for separating lithosperic fields from the core field and the fields due to external currents from the geomagnetic field (Regan et al., 1975; Mayhew, 1979; Langel et al., 1980). A novel method of representing the geomagnetic field has also been developed by Haines (1985a). Known as the 'spherical cap harmonic analysis', the method solves Laplace's equation for a spherical cap using associated Legendre functions of integral order but nonintegral degree.

The basic mathematical formulation for spherical harmonic analysis consists of expressing the internal magnetic scalar potential $V(r, \theta, \lambda)$ as

$$V = \sum_{k=0}^{K} \sum_{m=0}^{k} a(\frac{a}{r})^{n_k(m)+1} P_{n_k(m)}^m(cos\theta).\{g_k^m cos(m\lambda) + h_k^m sin(m\lambda)\} \qquad (5.3)$$

where

r : polar spherical coordinates radius,

θ : polar spherical coordinates colatitude,

λ : polar spherical coordinates longitude,

a : reference radius,

$P^m_{n_k(m)}(cos\theta)$: associated Legendre functions and

g^m_k, h^m_k : spherical harmonic coefficients.

The parameters n and m are generally referred to as the degree and order respectively. k is an index that is used to order the various n at a given m. The degree n is thus denoted $n_k(m)$. In fitting a potential with an arbitrary value at the spherical cap boundary, the values of the spherical degree n for a particular value of m are chosen as the root of the equations:

$$P^m_n (cos\theta_0) = 0 \qquad (5.4)$$

and

$$dP^m_{n_k(m)} (cos\theta_0) /d\theta = 0. \qquad (5.5)$$

θ_0 is the half-angle of the spherical cap. The vertical field B_z is then obtained by taking the vertical derivative of equation (5.3), namely

$$B_z = -\frac{\partial V(r, \theta, \lambda)}{\partial r} \qquad (5.6)$$

$$= \sum_{\substack{k=0 \\ k-m=even}}^{k} \sum_{m=0}^{k} (n_k(m) + 1)(\frac{a}{r})^{n_k(m)+2} P^m_{n_k(m)}(cos\theta).\{g^m_k cos(m\lambda) + h^m_k sin(m\lambda)\}.$$

$$(5.7)$$

If the value of n determined from equations (5.4) and (5.5) are written down in increasing order, the solutions of (5.4) and (5.5) alternate in the series. The smallest

value of n at each m is the solution of equation (5.5). The index k is used to order the values of n at each m. The solutions of equation (5.4) are characterized by $k - m = odd$ and those of equation (5.5) by $k - m = even$.

Haines (1985b) applied the method of spherical cap harmonic analysis to MAGSAT data selected by Coles (1985) to obtain the vertical field anomaly above 40°N at $r = 6700$ km using a maximum index of $k = 22$. For this choice of k and the spherical half-angle of $\theta_0 = 50$, the corresponding maximum degree n is 39.97, permitting representation of anomalies with wavelengths of $2\pi r/39.97$ or 1000 km at the earth surface. The vertical anomaly field at $r = 6700$ km was made available on disk by G. V. Haines and is used in this study (see appendix C). Although there was no MAGSAT data above 83.24°N since the inclination of MAGSAT was 96.76°, the method of spherical cap harmonic analysis permitted analytical lateral continuation of the field to the pole. Figure 5.2 shows the anomaly field over the Alpha and Mendeleev Ridges at an elevation of 328 km above the earth surface. It is the most intense anomaly observed by MAGSAT.

Some large regions of the earth's lithosphere exhibit characteristic magnetic signatures whether it be in terms of trend, wavelength, relief, shape or a combination of these factors. Hall (1968) terms such regions as magnetic provinces. Because of the large anomaly intensity over it, the Alpha-Mendeleev Ridge complex qualifies as a magnetic province. Modeling of this magnetic province is described in the following Chapter. The modeling is done so as to obtain and examine the magnetic nature of the Alpha Ridge.

5.3   Alpha-Mendeleev Ridge models

Taylor (1983) modeled the Alpha and Mendeleev Ridges using two large homogeneous spherical prisms. The dimensions of the prisms were controlled by the known

bathymetry and crustal thickness determined from seismic soundings. The effective bulk susceptibility used was based on the LOREX results (Sweeney et al., 1982). The modeling produced a good match for Alpha Ridge but a poorer one for the Mendeleev Ridge. On the basis of this matching result, Taylor (1983) concluded that the two ridges are different geological entities.

An averaging technique, that of upward continuing aeromagnetic data to satellite elevations, is useful in comparing aeromagnetic data with satellite magnetic data at the same elevation. Coles and Haines (1979) and Langel et al., (1980) showed that aeromagnetic data over the Alpha Ridge when continued to an elevation of 500 km is similar to the POGO data at the same elevation (see also Figure 2.10). In the next Chapter a different approach of comparing the aeromagnetic and satellite magnetic data is presented. The effective magnetizations and crustal prisms obtained from the modeling of the aeromagnetic data are used to calculate an average anomaly field of the prisms at satellite elevations. By using the same magnetizations and crustal models, it is possible to investigate whether the calculated aeromagnetic and MAGSAT data match the observed data.

Table 5.1: Summary of work based on MAGSAT

Summary of publications based on the MAGSAT program (from Langel et al., 1991). 'Bckgnd/programatic' refers to information about MAGSAT prior to its launching. 'Using models' refers to studies using MAGSAT-based main field models while 'crust and main' refers to combined main and crustal field studies.

YEAR	78	79	80	81	82	83	84	85	86	87	88	89	90	Total
CLASSIFICATION														
Backgnd/programatic	0	1	2	0	0	0	0	0	0	0	0	0	0	2
Instrumental	1	0	11	1	0	0	1	0	0	0	0	0	0	14
Data description	0	0	0	1	2	0	0	0	0	0	0	0	0	3
Review	0	0	1	1	3	3	2	2	1	1	1	2	3	20
Crustal studies	0	0	1	6	23	16	20	34	32	21	13	14	30	209
Main field	0	0	2	0	9	5	2	4	4	7	2	6	3	44
Crust and main	0	0	0	0	0	1	0	0	0	0	0	0	0	1
using model	0	0	0	0	2	2	4	5	8	13	3	4	2	43
External field	0	1	1	2	10	4	14	16	5	3	1	2	4	63
Earth induction	0	0	0	0	1	1	0	0	0	0	0	0	0	2
Total	1	2	17	11	50	32	43	61	50	457	20	28	42	402
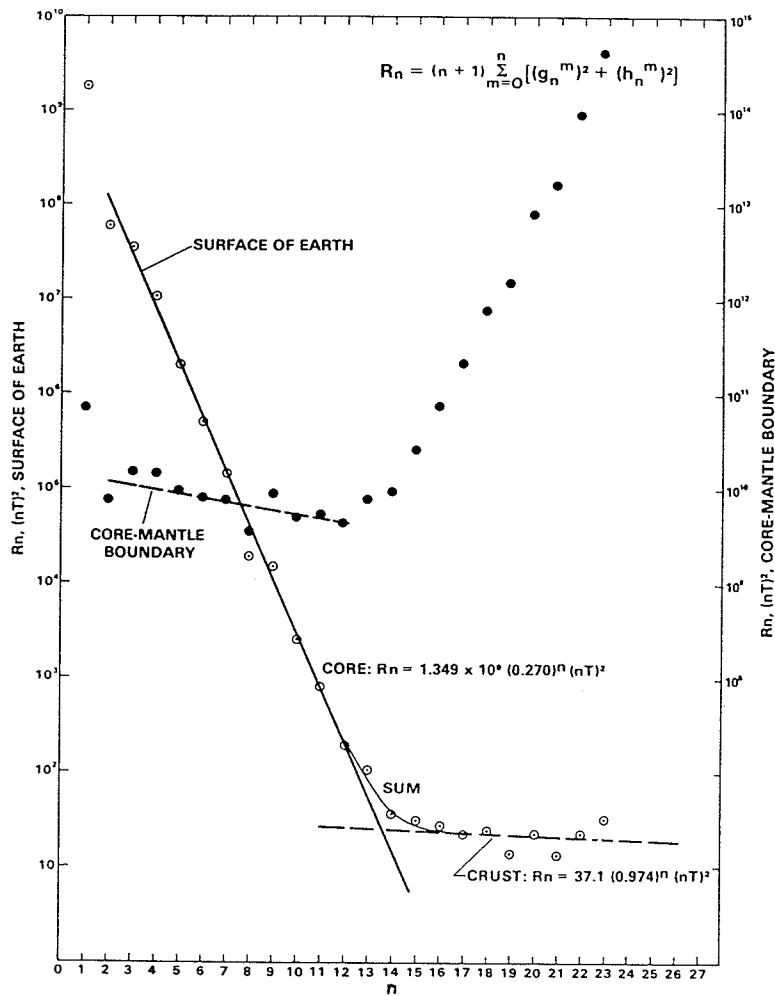
Figure 5.1: Geomagnetic field spectrum

The power spectra of the geomagnetic field. The crustal field dominates at $n \geq 15$ while the core field dominates at $n \leq 13$ (from Langel and Estes, 1982).
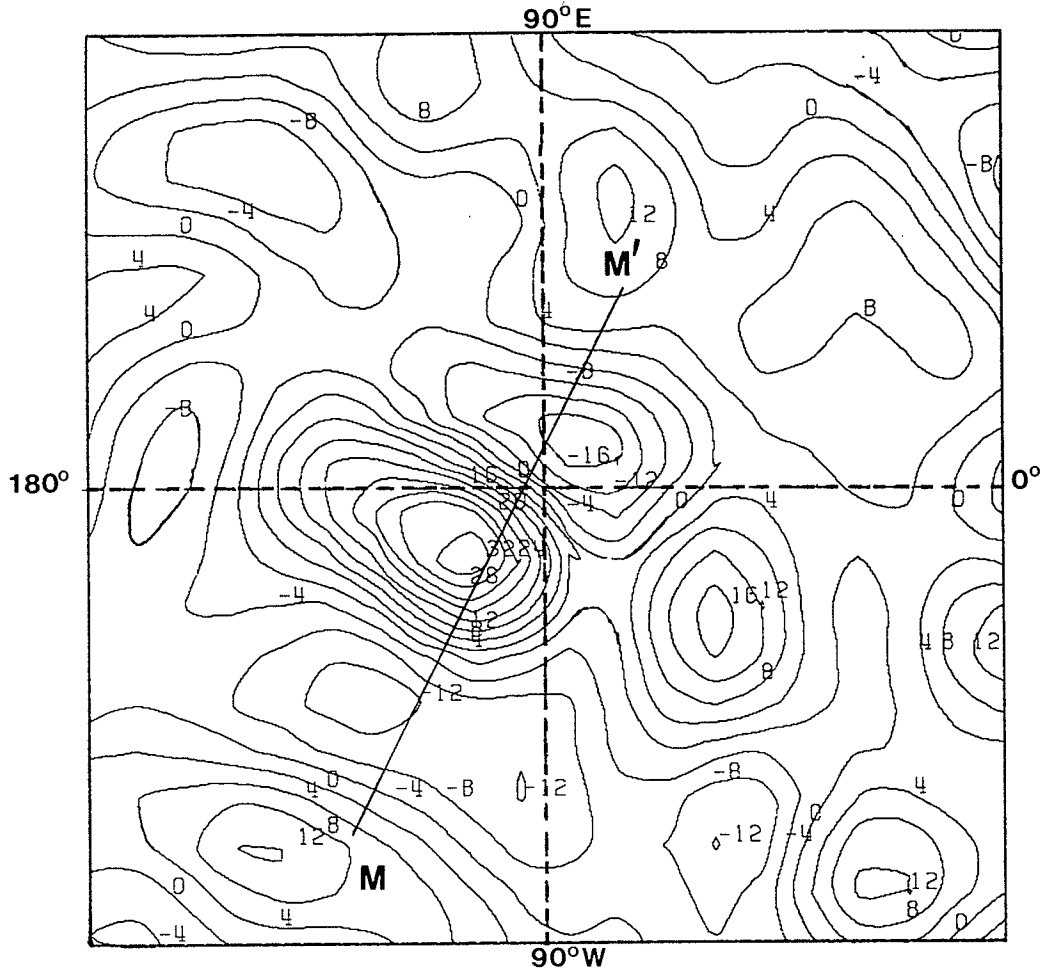
Figure 5.2: Alpha Ridge MAGSAT anomaly

MAGSAT vertical component anomaly field over the Alpha-Mendeleev Ridge complex at an altitude of 328 km above the earth surface. The contour interval is 4 nT. The data was obtained from G. V. Haines (see text).

Chapter 6

AEROMAGNETIC AND MAGSAT DATA MODELING

6.1 Sources delineated by aircraft and satellite

A magnetic anomaly map reflects the properties of the rocks in which the anomaly field originates. As has already been discussed in Chapter 3, the source of the observed magnetic anomalies lies above the Curie surface in the crustal portion of the lithosphere. The question that needs to be answered therefore pertains to the type of crust that would provide a fit to the recorded anomalies at both satellite and aircraft elevations. The following is a review of magnetic sources in oceanic and continental crusts that are observable by aircraft and satellites.

6.1.1 Magnetic sources delineated by aircraft

At aircraft elevations, magnetic sources located in the oceanic and near-surface continental crust are observed as strong anomalies when compared to those that are

77

located at the deeper parts of the continental crust (Thomas, 1987).

Oceanic sources that are resolved at aircraft elevations are located in layers 2A and 2B. For a typical oceanic crust such as the Atlantic Mid-Ocean Ridge, these sources give an anomaly pattern of alternating positive and negative strips. The strips are a record of the earth's field at the time of emplacement of the crust. Magnetizations for such sources are typically TRM in nature (Banerjee, 1984).

Continental sources on the other hand generally do not give a particular pattern of anomalies. Strong anomalies are mostly due to extrusive and intrusive igneous rocks and near surface metamorphic rocks. Sedimentary basins in general have low amplitude anomalies.

6.1.2 Magnetic sources detectable at satellite elevations

Many researchers now agree that the major source of satellite anomalies is an induced crustal magnetization aligned to the present main magnetic field (Wasilewski et al., 1979, Mayhew et al., 1985, Thomas, 1987). The sources of these long-wavelength anomalies are largely in the lower parts of continental crusts, and oceanic crusts and oceanic plateaus/ridges.

In reviewing the likely sources of satellite anomalies of oceanic crustal magnetization, Thomas (1987) suggested that the total magnetization in layers 2A, 2B and 3A all contribute to the anomaly recorded at satellite elevations. At heights greater than 200 km, the striped oceanic anomaly pattern cannot be resolved. The magnetizations (due to TRM) of the various strips algebraically add to zero (Thomas, 1987).

Continental magnetic anomaly sources measurable at satellite elevations emanate from the deeper parts of the crust. Mayhew at al. (1985) give a comprehensive review of these long-wavelength anomaly sources. Large magnetization in the range

2-6 Am^{-1} at depth directed along the main earth magnetic field is required to explain long-wavelength anomalies that are observable at satellite elevations.

6.2 Modeling constraints

Modeling of the subsurface structures that give rise to the observed anomalies is done in terms of magnetization contrasts of the modeled structures relative to their surroundings. For any potential field data such as magnetic or gravity, an infinite number of models may be generated which fit the same data. It is therefore necessary to impose certain constraints in the modeling so as to develop a meaningful interpretation of the data. The following facts, deduced from gravity, seismic, heat flow and bathymetric studies, are used in developing models for the Alpha Ridge data.

i. Seismic and gravity soundings show a thickened Alpha Ridge crust that thins towards the Makarov and Canada Basins. Figures 2.3 and 2.6b show that the crust reaches a thickness of about 38-42 km beneath the crest of Alpha Ridge and about 20 to 30 km beneath the Canada and Makarov basins.

ii. From heat flow values (Chapter 3) the calculated depth to the Curie level is about 36 km within the Alpha Ridge crust. This depth rises to about 20 to 25 km beneath either of the Canada and Makarov basin flanks. The crust that gives rise to the observed magnetic anomalies thus lies above this depth.

iii. Bathymetry (Figure 2.1) is used to define the upper magnetic boundary of the crust. The depth from the ocean surface to the top of the magnetic crust varies from 3 km over the Canada and Makarov Basins to about 2 km over Alpha Ridge.

iv. P-waves traveling through the Alpha Ridge crust show lateral variations in velocity. These lateral variations are interpreted in terms of changes in the

subsurface rock types and hence different magnetizations. The depth extent of the lateral inhomogeneity is up to 8-25 km. Therefore, for the crustal rock layers of down to 8-25 km deep, crust reflecting the positive and negative anomalies are modeled by vertical blocks to which different magnetizations are assigned. The horizontal distances (the width of the blocks) in which the velocities remain homogeneous reach up to 100 km.

In addition, the following assumptions are also used as modeling criteria.

i. The average magnetization of the crustal blocks is assumed to be constant in direction throughout the blocks and parallel to the present earth's field. Any remanence is therefore accounted for in the average magnetization.

ii. The sediment layers, the mantle and the lithospheric layers below the Curie level are all assumed to have zero magnetizations (Wasilewski et al., 1979).

6.3 Two-dimensional modeling of the data

A 2-dimensional forward modeling technique was used to compute both the aeromagnetic and MAGSAT data. The modeling uses Cartesian coordinates in which the earth is assumed to be flat. The surface on which the anomalies are computed is also assumed to be flat. In the following section, a justification is developed for using such a 2-D modeling program in the modeling of both the aeromagnetic and MAGSAT data.

6.3.1 Anomalies of simple geometries

In the following sections, simplified geometries are used to synthesize anomalies so as to see the effects of strike lengths and the effects of surface at which the anomalies are

calculated. Investigating the later effect is especially required because the MAGSAT anomalies are measured over a curved surface.

6.3.2   Anomaly due to a horizontal sheet

Figure 6.1 illustrates the geometry used in the calculation of the anomaly field of a thin horizontal sheet of infinite strike extent. The vertical magnetic field $Z(x, d)$ at the observation position $O(x, d)$ is given by (Telford et al., 1990) as

$$Z = -2ktF_e[(1/r_1)(cosIsin\beta sin\theta_1 + sinIcos\theta_1) - (1/r_2)(cosIsin\beta sin\theta_2 + sinIcos\theta_2)]$$

$$(6.1)$$

where

I : inclination of the geomagnetic field,

k : susceptibility,

t : thickness of sheet,

F_e : geomagnetic field strength,

x : distance between reference and observation points,

β: strike angle of prism,

$r_1^2 = x^2 + d^2$,

d : depth to top of sheet,

$r_2^2 = (x - l)^2 + d^2$,

l : width of sheet (traversed across strike),

$sin\theta_1 = d/r_1$,

$cos\theta_1 = x/r_1$,

$sin\theta_2 = d/r_2$ and

$$cos\theta_2 = (x-l)/r_2.$$

Eliminating θ_1 and θ_2 from equation (6.1), the following equation is obtained.

$$Z = -2ktF_e[(1/r_1)^2(d\ cosI\ sin\beta + x\ sinI) - (1/r_2)^2(d\ cosI\ sin\beta + (x-l)\ sinI)] \quad (6.2)$$

If the horizontal sheet is of finite strike length 2L, the anomaly field is approximated by

$$Z = 2ktLF_e[Q\ cosI\ sin\beta + S\ sinI)] \quad (6.3)$$

where

$$Q = \frac{d}{r_2^2(r_2^2 + L^2)^{\frac{1}{2}}} - \frac{d}{r_1^2(r_1^2 + L^2)^{\frac{1}{2}}} \quad (6.4)$$

and

$$S = \frac{x - l}{r_2^2(r_2^2 + L^2)^{\frac{1}{2}}} - \frac{x}{r_1^2(r_1^2 + L^2)^{\frac{1}{2}}}. \quad (6.5)$$

The vertical field profiles for an infinite strike length and for a finite strike length with $2L = 1000$ km were computed using equations (6.2) and (6.3) respectively for a horizontal sheet 36 km thick and 400 km wide and at the elevation of 328 km. A magnetization of 2.82 Am^{-1} was used in the computation. The computed profiles (Figure 6.2) agree to within 92% of peak value. Since the strike extent of Alpha Ridge is about 1000 km, the magnetic data (from the middle of the ridge) may be modeled with a 2-D program without using an end correction. Unless the strike length is less than the width of the sheet, the finite length does not affect the final results more than 20% (Telford et al., 1990).

6.3.3 Anomaly measurement on curved surface

In calculating the anomalies in the preceding section, a model for a horizontal sheet with plane boundaries and traverse parallel to the plane (a flat-earth model) is used.

However the MAGSAT trajectory shows significant curvature when orbiting the study area. The models presented in the previous section can be used for MAGSAT with appropriate modification. In this section, the measurement of anomalies on a curved surface while keeping the sources in Cartesian geometry is investigated. The anomaly observation positions are specified in Cartesian coordinates but the positions are on a curved level. Figure 6.3 shows the configuration of obtaining observation positions on a curved level. The curve joining C_1 and C_2 defines a segment of the great circle at the earth surface. The straight line joining C_1 and C_2 defines the surface of the flat-earth. Anomaly (prismatic blocks) sources are located below this surface. R_e is the radius of the earth (6356.912 km at the poles). The observation elevation is at $R_o = R_1 + R_2$. The distance from the center of the earth to the flat surface is given by $D = 2R_e cos(\phi/2)$. The curved surface is separated from the flat surface by a distance of $d = R_e - D$. The observation positions are obtained as follows. The angle θ defines the intervals at which the anomalies are calculated. Since D is known, x_1 and R_1 are calculated. R_2 is obtained by subtracting R_1 from the observation radius R_o (say at $R_o = 6684$ km, MAGSAT value for the Arctic). h and x_2 are then calculated. The observation position O is at (h, x) where $x = x_1 + x_2$.

Having fixed the relative positions of the sheets, the anomaly field at the curved surface (say at MAGSAT elevations) is then calculated. Figure 6.4 shows a comparison of the anomaly fields calculated for a flat and a curved observation levels. The anomaly fields are not significantly different. The difference, peak to peak, is about 1.5%. The use of a flat earth and a flat observation level is therefore justified for 2-D modeling of the aeromagnetic and MAGSAT data.

6.4 Modeling the data

A 2-dimensional forward modeling program (developed by T.A. Larson and L.L. Malinconico Jr., Southern Illinois University, 1988) was used to model both the aeromagnetic and MAGSAT data. The program is available at the department of Geological Sciences, University of Manitoba for research purposes and as a teaching aid. With the program, it is possible to use a particular crustal model to calculate magnetic anomalies at both aeromagnetic and MAGSAT elevations. The crustal model is adjusted until the calculated anomalies at the two elevations match the observed data sets. Inherent in the modeling program is the assumption that the strike length of the crustal layers is infinite and the calculation of the anomalies is done on a flat source and observation level. The use and justification of the infinite strike model (instead of finite strike approximation), and flat source and observation levels has already been discussed in the last two sections.

Although several profiles were extracted from the aeromagnetic and MAGSAT data, the results herein presented are for one MAGSAT and one aeromagnetic profile. Each profile is extracted approximately along the same line and direction over Alpha Ridge. For the MAGSAT data, the profile being discussed is along M - M' (see also Figure 5.1), while for the aeromagnetic data, the profile is extracted along S4 (see also Figure 4.2). It should be noted that the aeromagnetic profile is shorter than the MAGSAT profile.

In matching the observed and calculated anomalies, a relative error e_r value was computed as follows:

$$e_r = \left(\frac{1}{N} \sum_{i=1}^{N} (o_i^2 - c^2)_i \right)^{1/2} \tag{6.6}$$

where

e_r : relative error value,

N : number of data points,

o_i : observed data value and

c_i : calculated data value.

A small or zero e_r value would indicate that the observed data matches the calculated while a large e_r value would indicate that the data do not match.

6.4.1   Modeling aeromagnetic data

Figure 6.5a shows a crustal layer about 8 km in thickness. The layer is divided into vertical blocks so as to represent lateral variations in the uppermost crust. This lateral variation was made because the seismic data (discussed in Chapter 2) show a lateral variation in the P-wave velocities in this zone for Alpha Ridge. Positive magnetizations (Table 6.1) were used for all the crustal blocks (with two exceptions which have negative magnetizations). These magnetizations are in the range 0 - 7 Am^{-1}. The calculated magnetic field matched the observed field quite well, with a small e_r value of 5.333 nT (Figure 6.5b).

Having obtained the fit for the aeromagnetic data, the same crustal layer was then used for calculating the anomaly at MAGSAT elevation (328 km above the earth surface). Figure 6.5c shows that the calculated anomaly field does not match the observed MAGSAT data. The crustal blocks were then extended to depth deeper than 8 km, including a test in which the blocks reach 36 km. Subjecting the crustal layers to the same analysis as for the 8 km thick layer produced similar results, that is, a good match for aeromagnetic data but a poor match for MAGSAT data.

From these results, it is concluded that the MAGSAT magnetic anomaly over Alpha Ridge cannot be explained by vertical sided crustal blocks whether of limited depth extent or blocks that extend down to the Curie level.

6.4.2 Modeling MAGSAT data

Five homogeneous crustal blocks are used in the modeling of the MAGSAT data (Figure 6.6). Alpha Ridge is represented as the middle crustal block that is broad at the surface and becomes narrower in the deeper parts of the lithosphere (block a1, Figure 6.6a). The magnetization of the block is 1.818 Am^{-1}. Canada Basin is represented by a crustal block with a magnetization of 0.179 Am^{-1} (block a3, Figure 6.6a). Representing the Makarov and the Eurasia Basins is a crustal block with a magnetization of 0.000 Am^{-1} (block a2, Figure 6.6a). Crustal blocks a4 (with a magnetization of 4.6 Am^{-1}) and a5 (with a magnetization of 5.2 Am^{-1}) were used to represent the continental crusts of North America and Eurasia respectively. The thicknesses and widths of the blocks are not necessarily continental. The blocks are used for the sole purpose of modeling the MAGSAT data which shows positive anomalies (with magnitudes of up to 12 nT) over the continental crust portions (see also Figure 5.2, line M - M').

The calculated and the observed anomaly matched quite well with an e_r value of 0.1 nT (Figure 6.6b). It should be noted that the crustal block which partly represents the Eurasia Basin was not constrained by heat flow values. However, that the thickness of the magnetic block is about 16-18 km is supported by data compiled by Verba et al. (1990).

The same crustal arrangement was then used to obtain an anomaly at the aeromagnetic elevation of 3.5 km. The calculated and observed anomalies do not match (Figure 6.6c).

These results indicate that Alpha Ridge is not wholly homogeneous since the model does not explain the aeromagnetic anomaly.

6.5 Simultaneous modeling of aeromagnetic and MAGSAT data

Since the aeromagnetic model does not explain the MAGSAT anomaly and vice versa, both the aeromagnetic and MAGSAT data are modeled simultaneously. The modeling is explained in the following subsections.

6.5.1 Two-layer crustal model

A two-layer crust is shown in Figure 6.7a. The upper layer is limited to a depth of 8 km and is segmented into vertical blocks as is the case in the one-layer crustal model used in the modeling of the aeromagnetic data (Figure 6.5a). The second layer is composed of a homogeneous block that extends to the Curie level (block a26, Figure 6.7a). The homogeneity of the block is justified in that the P-wave velocity through Alpha Ridge for this zone of crust does not vary laterally. Figures 6.7b and 6.7c show the calculated and observed anomalies. Both the calculated and observed aeromagnetic and MAGSAT anomalies match quite well, with respective e_r values of 5.13 nT and 0.086 nT. The magnetizations used in the calculation of the anomaly field, except for two blocks in the upper layer, are all positive, ranging in value from 0 - 7 Am^{-1} (Table 6.2). Since the Alpha Ridge heterogeneous zone extends to a depth of up to 25 km, a model reflecting this situation was computed. For the model too, the calculated and the observed anomalies for both data sets matched.

The two-layer magnetic crust model may therefore be used to explain the anomaly fields observed over Alpha Ridge. It should be noted that block a29 (Figure 6.7a) represents the Eurasia and Makarov Basins while block a30 (Figure 6.7a) represents the Canada Basin. The magnetizations of the blocks (respectively 0 and 0.179 Am^{-1}) are low compared to the lower layer of Alpha Ridge (block a26, with a magnetization

of 1.56 Am^{-1}). The magnetizations for the continental sections of the crust are 4.6 Am^{-1} (block a31, Figure 6.7a, North America portion) and 5.2 Am^{-1} (block a32, Figure 6.7a, Eurasia portion)

6.5.2   Three-layer crustal model

Figure 6.8a shows the three-layer magnetic crustal model for Alpha Ridge. The second layer (block a26) from the two-layer model of the preceding subsection is divided into two blocks so that a three-layer model is examined. The division of the second block into two (blocks a26 and a33,) may be explained by the fact that temperature variations at depth influences the magnetic nature of the block such that the deeper part is less magnetic than the upper part. The boundary between the second (a26) and third (a33) layer is fixed at about 25 km. This layering is fixed in accordance with the seismic data.

Like for the two-layer model, the calculated and observed anomalies match for both the aeromagnetic and MAGSAT data sets with respective e_r values of 5.13 nT and 0.095 nT (Figures 6.8b and 6.8c). Except for blocks a26 and a33, the magnetizations (Table 6.4) are the same as those in the two-layer model (Table 6.3).

As is the case with the two-layer model, the three-layer crustal model may be used to explain the Alpha Ridge anomalies.

6.6   3-D modeling of MAGSAT data

Von Frese et al., (1981) have discussed the use and versatility of 3-dimensional spherical prisms in the modeling of magnetic data at satellite elevations. Noble (1983) used spherical prism in modeling the Ungava satellite magnetic anomaly. In this thesis, a simplified version of the method used by Noble is used to model the Alpha

Ridge MAGSAT anomaly. The mathematical expressions used in the calculation of an anomaly due to a spherical prism are given in the following subsection.

6.6.1   Magnetic field calculation using 3-d bodies

In representing three-dimensional magnetic bodies within the earth's crust using spherical prisms, the prisms are taken to have discrete magnetic dipoles residing within them. This representation is attractive for modeling magnetic data at high altitudes for two main reasons. First, the sphericity of the earth is taken into account. Secondly, the discrete representation of the magnetic body in the form of equivalent point sources simplifies the numerical computations. The following development describing the representation of a magnetic body using spherical prisms is based on the method used by Noble (1983).

Figure 6.9 depicts the geometry involved in calculating anomaly fields due to a magnetic body. The magnetic scalar potential at P due to a single dipole at Q having a dipole moment $\vec{m}$ is given by:

$$A = \frac{\vec{m}.\hat{R}}{4\pi R^2} \qquad (6.7)$$

where $\hat{R}$ is the unit vector directed from P to Q. Taking Q as residing within the magnetic body of volume V, then the potential due to the entire body is given as

$$A = -\frac{1}{4\pi} \int_v \frac{\vec{J}.\hat{R}}{R^2} dv. \qquad (6.8)$$

$\vec{J}$ is the magnetization of the body and is considered to be uniform throughout the body. In vector form, $\vec{J}$ and $\hat{R}$ are respectively

$$\vec{J} = J_x\hat{i} + J_y\hat{j} + J_z\hat{k} \qquad (6.9)$$

and

$$\hat{R} = R_x\hat{i} + R_y\hat{j} + R_z\hat{k}. \qquad (6.10)$$

Substitution of equations (6.9) and (6.10) into equation (6.8) gives

$$A = -\frac{1}{4\pi} \int_v \frac{J_x R_y + J_y R_y + J_z R_z}{R^3} dv. \tag{6.11}$$

The magnetic anomaly of the body measured at the field P is the negative directional derivative of the magnetic potential A, multiplied by μ_0, the permeability of free space. In this thesis, only the vertical component of the magnetic field ΔZ, is discussed.

$$\Delta Z = -\mu_0 \frac{\partial A}{\partial z_p} \tag{6.12}$$

$$= -\frac{\mu_0}{4\pi} \int_v \frac{\partial}{\partial z_p} \frac{\vec{J}.\vec{R}}{R^3} dv \tag{6.13}$$

$$= -\frac{\mu_0}{4\pi} \int_v \frac{J_x(x_q - x_p) + J_y(y_q - y_p) + J_z(z_q - z_p)}{\left((x_q - x_p) + (y_q - y_p) + (z_q - z_p)\right)^{3/2}} dv \tag{6.14}$$

$$= \frac{\mu_0}{4\pi} \int_v \left[\frac{3J_x R_x R_z + 3J_y R_y R_z + J_z(3R_z^2 - R^2)}{R^5}\right] dv. \tag{6.15}$$

The last equation is now in the form

$$\Delta F = \int f dv \tag{6.16}$$

where f represents the integrand and it depends on the position P and Q, and on the magnetization vector $\vec{J}$. Equation (6.16) may now be numerically integrated using gaussian quadrature. The simplest quadrature problem is to construct the equality

$$\int_a^b f(x)dx = \sum_{i=1}^n w_i f(x_i) + T. \tag{6.17}$$

The construction of the equality problem is done by choosing the nodes x_i and the weights w_i such that the truncation error T is as small as possible. Noble (1983) gives a simple example in which the integration interval is $[-1, +1]$ and for n=2. Equation (6.17) then becomes

$$\int_{-1}^{+1} f(x)dx \approx \sum_{i=1}^2 w_i f(x_i). \tag{6.18}$$

Putting $f(x) = x^m$, where $m = 0, 1, 2, 3$ leads to four equations:

$$0 = w_1 x_1^3 + w_2 x_2^3 \qquad (6.19)$$

$$2/3 = w_1 x_1^2 + w_2 x_2^2 \qquad (6.20)$$

$$0 = w_1 x_1 + w_2 x_2 \qquad (6.21)$$

$$2 = w_1.1 + w_2.1 \qquad (6.22)$$

Solving the four equations give $w_1 = w_2 = 1$ and $-x_1 = x_2 = 3^{-1/2}$.

Figure 6.10 illustrates a two dimensional circular sector containing a 2×2 array of dipoles. The dipoles are located at geocentric co-ordinates $(\rho_i, \phi_j, \lambda_k)$ where

$$\rho_i = \rho_Q + \frac{\Delta\rho}{2}.v_i \qquad (6.23)$$

$$\phi_j = \phi_Q + \frac{\Delta\phi}{2}.v_j \qquad (6.24)$$

$$\lambda_k = \lambda_Q + \frac{\Delta\lambda}{2}.v_k \qquad (6.25)$$

where $i, j, k = 1, 2$ and $v_m = \frac{(-1)^m}{\sqrt{3}}$ are the gaussian nodes.

For a volume element of a sphere, equation (6.16) becomes

$$\Delta F(P, Q) = \int \int \int f(P, Q) \rho^2 sin\phi d\rho d\phi d\lambda \qquad (6.26)$$

where ρ, ϕ, λ are as shown in Figure 6.11. Applying gaussian quadrature to equation (6.26) gives

$$\Delta F(P,Q) = \frac{\Delta\lambda}{2} \sum_{i=1}^{n} \left[\frac{\Delta\phi}{2} \sum_{j=1}^{n} \left(\frac{\Delta\rho}{2} \sum_{k=1}^{n} f(P,Q')\rho_i^2 sin\phi_j w_i \right) w_j \right] w_k \qquad (6.27)$$

where $Q' = (\rho_i, \phi_j, \lambda_k)$, the co-ordinates of the subdivisions of the quadrature. For $n = 2$, equation (6.27) becomes

$$\Delta F(P,Q) = \frac{\Delta\lambda\Delta\phi\Delta\rho}{8} \sum_{i=1}^{2} \sum_{j=1}^{2} \sum_{k=1}^{2} f(\rho_i, \phi_j, \lambda_k, Q)\rho_i^2 sin\phi_j \qquad (6.28)$$

with $(\rho_i, \phi_j, \lambda_k)$ as defined in equations (6.23, 6.24, 6.25) and where Q defines the co-ordinates of the center of the prism of dimension $\Delta\lambda$, $\Delta\phi$, and $\Delta\rho$. The quadrature coefficients are $v_1 = -3^{-1/2}$ and $v_2 = 3^{-1/2}$.

The vertical field anomaly, given by equation (6.14) becomes

$$\Delta Z = C_1 \sum_{ijk}^{2} C_2 \left(3J_x R_{x_{ijk}} R_{z_{ijk}} + 3J_y R_{y_{ijk}} R_{z_{ijk}} + J_z[3R_{z_{ijk}}^2 - R_{ijk}^2] \right) \qquad (6.29)$$

where

$$C_1 = \frac{\mu_0}{4\pi} \frac{\Delta\lambda\Delta\phi\Delta\rho}{8} \qquad (6.30)$$

and

$$C_2 = \rho_i^2 sin\phi_j R_{ijk}^{-5}. \qquad (6.31)$$

The separation vector R_{ijk} is directed from the observation point P to the dipole corresponding to i, j, k in the prism having x, y and z components $R_{x_{ijk}}$, $R_{y_{ijk}}$, and $R_{z_{ijk}}$ respectively.

6.6.2 The 3-D models

The MAGSAT anomaly over Alpha Ridge is modeled using crustal layers obtained in the 2-D modeling. The layers are modified into spherical prisms by changing

the coordinates from Cartesian to spherical. The conversion is done as follows. The average width of the ridge obtained from the 2-D models is about 880 km. Taking the profile along which the data are extracted to be a great circle, 880 km corresponds with an angle of 8° extended at the center of the earth. In an east-west direction, Alpha Ridge spans a latitudinal distance of about 90° (see Figure 2.1). The spherical prisms are thus confined to angular dimensions of 90° latitudinally and 8° longitudinally. Figure 6.12 shows the configuration of a one block crustal model.

In the calculation of the MAGSAT anomaly fields, the respective thickness and magnetization values obtained from the two- and three-layer 2-D models were used. The program used in the modeling is given in Appendix C. Figures 6.13 and 6.14 show the calculated MAGSAT anomaly fields for the two and three layers crustal models. The general shape of the anomalies match the observed MAGSAT anomaly shown in Figure 5.2 and all have a peak of about 36 nT.

6.7   Modeling results.

The modeling results indicate that the Alpha Ridge is not a single homogeneous crust. The ridge consists of two or three layered crust. The uppermost layer is laterally heterogeneous. The thickness of this layer cannot be clearly delineated due to the non-uniqueness inherent in modeling potential data. Using seismic and gravity data as constraints, the layer may reach a depth of 25 km. For an 8 km thick upper layer, the positive magnetizations are in the range of 0.0 to 7 Am^{-1}. For a two-layer magnetic crust, the lower layer has a magnetization of 1.59 Am^{-1}. If the magnetic crust is divided into three layers, then the two successive lower layers would have magnetizations of 2.148 and 1.59 Am^{-1} respectively.

In both the two- and three-layer models, the blocks representing the Canada and the Makarov/Eurasia Basins have the same respective magnetizations of 0.179

and 0.0 Am^{-1}. The blocks representing the sections of North America and Eurasia continental crusts also have the same magnetizations of 4.6 and 5.2 Am^{-1} for both models.
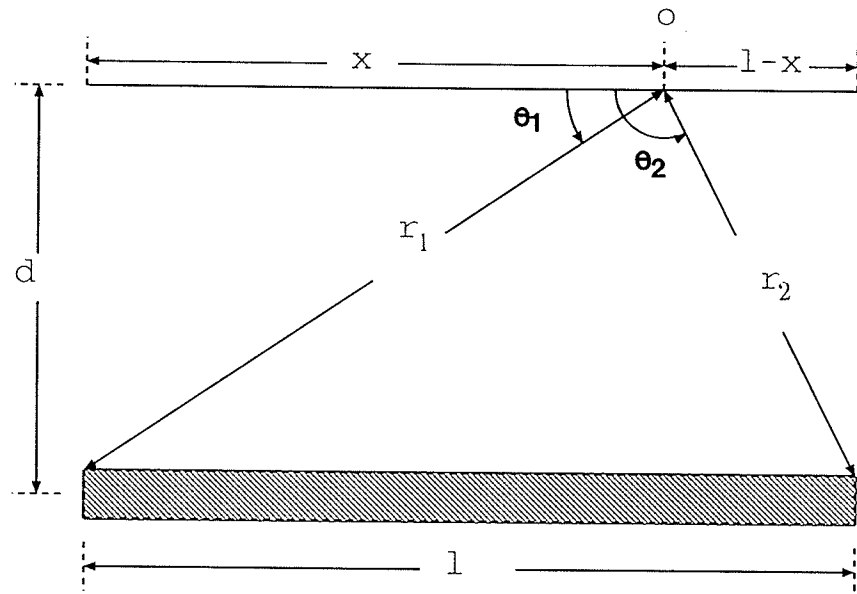
Figure 6.1: Anomaly of a thin horizontal slab

Geometry used in the calculation of the anomaly field $Z(x, d)$ at position $O(x, d)$ of a horizontal sheet of infinite strike. The symbols are explained in the text.
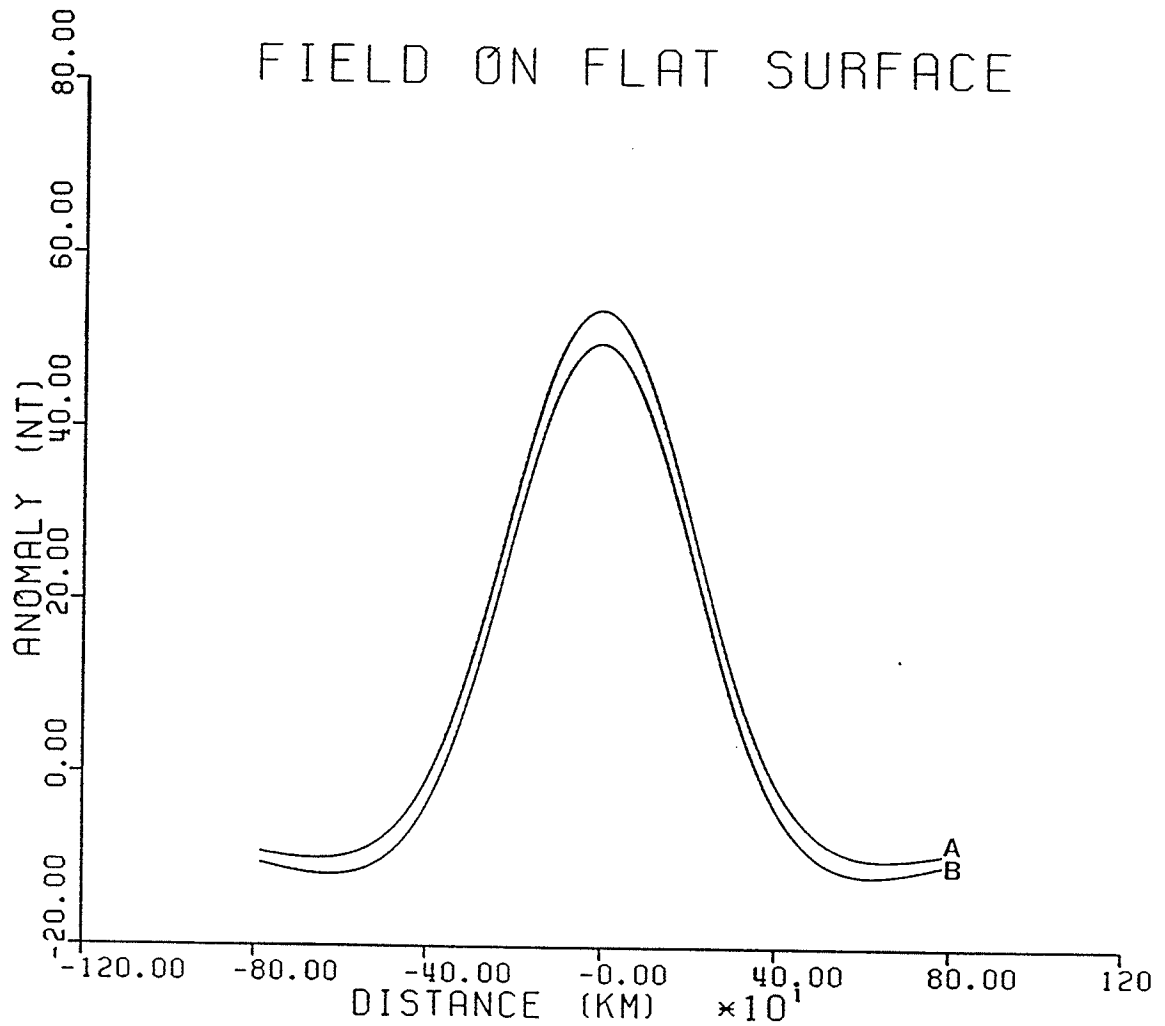
Figure 6.2: Anomaly of infinite and finite strike length slabs

Comparison of the anomaly fields due to a horizontal sheet of infinite strike (A) and a horizontal sheet of finite strike length (B). The thickness and width of both sheets are respectively 18 and 400 km, and the finite length sheet is 1000 km long. The field for the finite sheet is calculated across strike at the middle of the along-strike length. The fields differ by about 8% at the maximum.
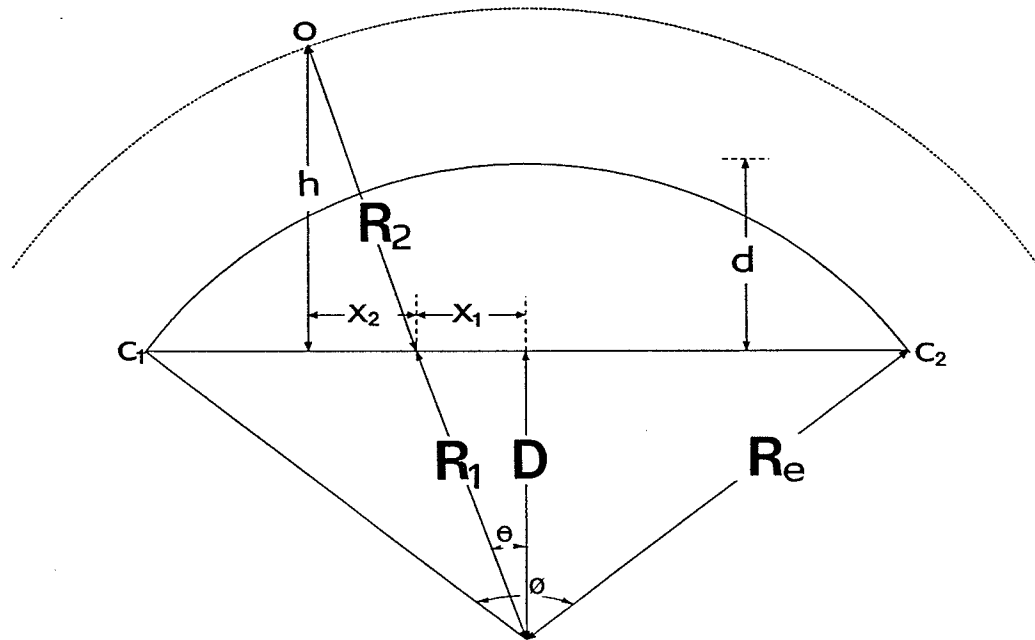
Figure 6.3: Anomaly measurement on a curved surface

Geometry used for calculating a curved observation position at an altitude above a flat surface C_1-C_2. The angle ϕ is between C_1 and C_2. The rest of the symbols are explained in the text.
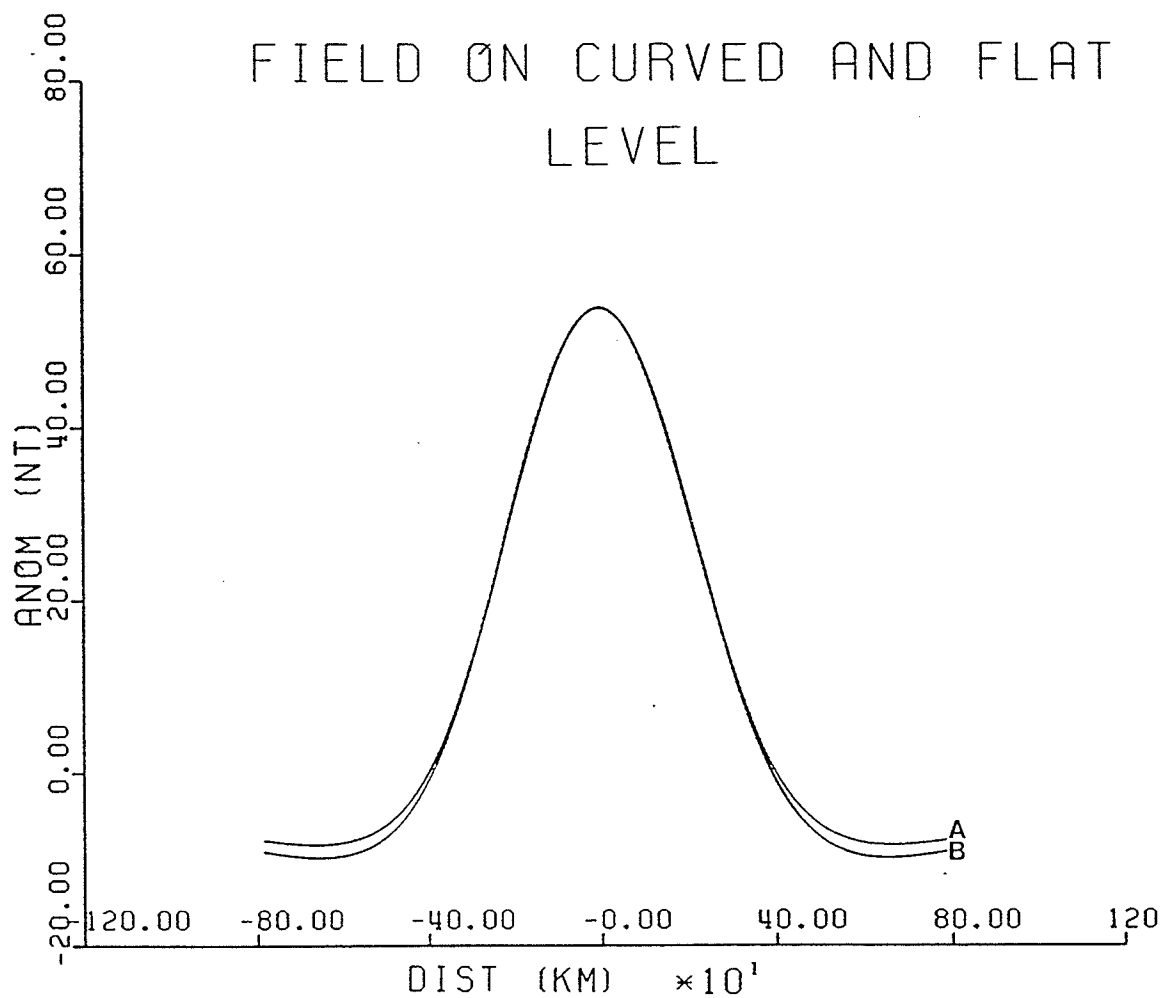
Figure 6.4: Anomaly measurement on a curved and flat surface

Comparison of the vertical anomaly field calculated from the horizontal sheet model on a flat surface (A) with the vertical anomaly component for a curved observation surface (B). The difference from maiximum to minimum is 1.5%, a slight difference.
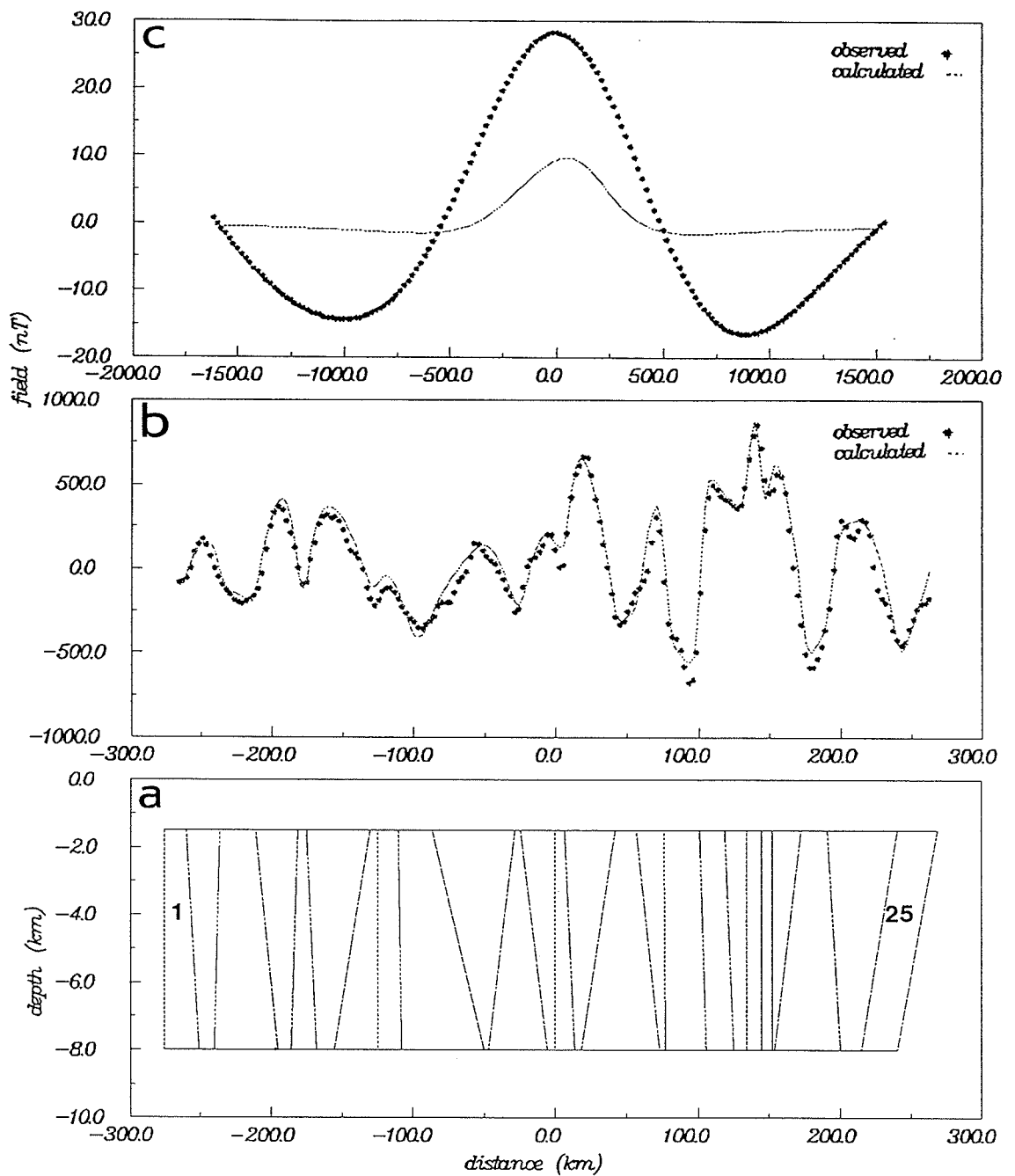
Figure 6.5: Segmented one-layer crustal model

a: Segmented one-layer block model used to represent the Alpha Ridge for obtaining a synthetic vertical field anomaly at both areomagnetic and satellite altitude. b: Observed and calculated fields at aeromagnetic elevation. c: Observed and calculated fields at satellite elevation for the same crustal model.

Table 6.1: Magnetizations for segmented one-layer crustal model

The magnetizations are for the segmented one-layer crustal model shown in Figure 6.5a.

Crustal block number	Magnetization (Am^{-1})
1	0.000
2	1.454
3	0.000
4	3.835
5	0.825
6	3.605
7	0.119
8	0.298
9	−1.230
10	2.555
11	1.454
12	4.361
13	2.822
14	6.028
15	1.170
16	3.860
17	0.000
18	4.851
19	4.972
20	6.925
21	5.330
22	6.028
23	0.000
24	2.285
25	−2.527
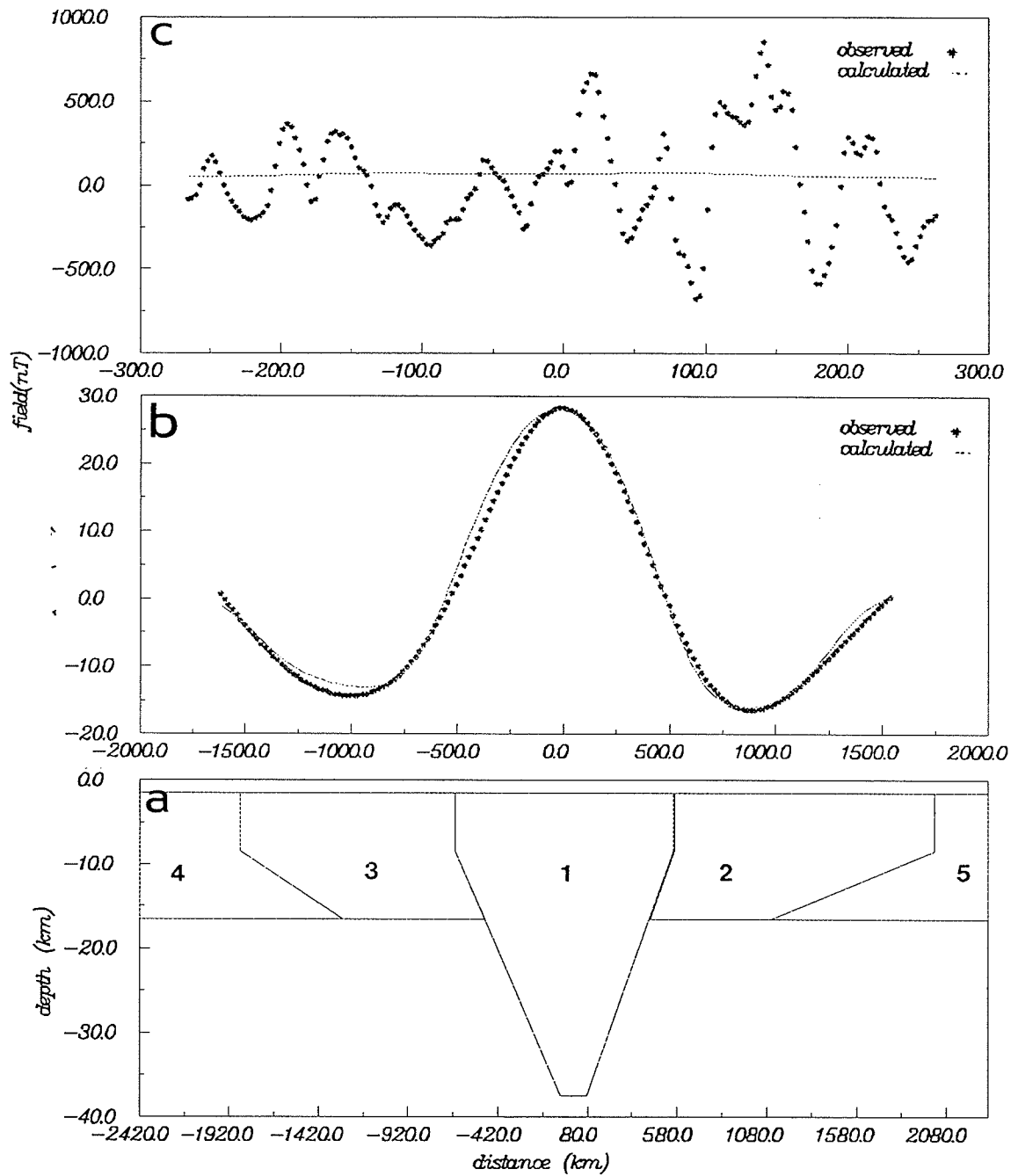
Figure 6.6: Homogeneous one-layer crustal model

a: Homogeneous one-layer block model used to represent the Alpha Ridge for obtaining a synthetic vertical field anomaly at both areomagnetic and satellite altitudes. b: Observed and calculated fields at satellite elevation. c: Observed and calculated fields at aeromagnetic elevation for the same crustal model.

Table 6.2: Magnetizations for homogeneous one-layer crustal model

The magnetizations for the homogeneous one-layer crustal model shown in Figure 6.6a.

Crustal block number	Magnetization (Am^{-1})
1	1.8180
2	0.0000
3	0.1793
4	4.6078
5	5.2115
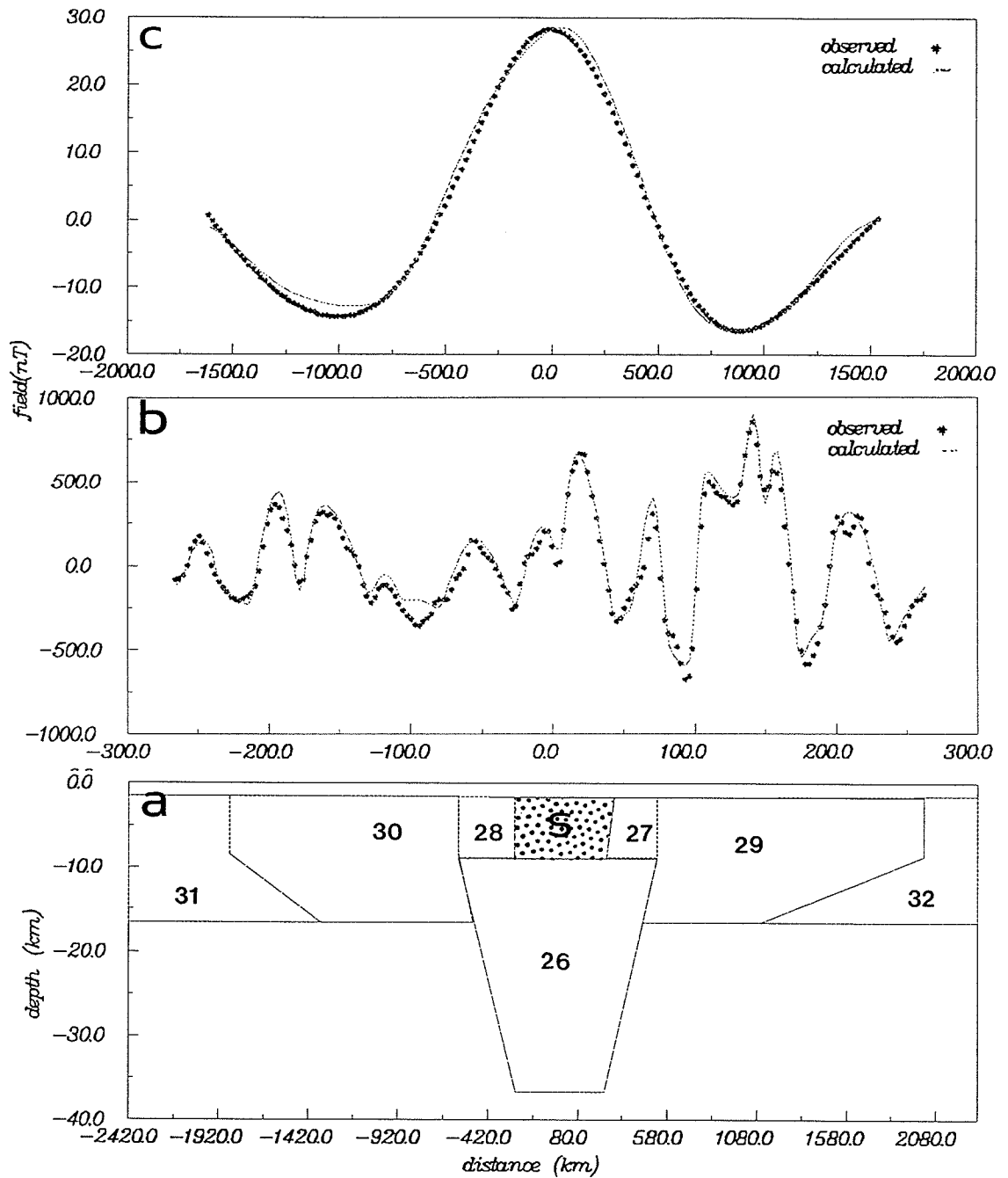
Figure 6.7: Two-layer crustal model

a: Two-layer block model used to represent the Alpha Ridge for obtaining a synthetic vertical field anomaly at both areomagnetic and satellite altitudes. The shaded area S is the heterogeneous one-layer crustal block model of Figure 6.5a. The upper layer (S, a27, a28) is heterogeneous while the lower layer (a26) is homogeneous. b: Observed and calculated fields at aeromagnetic elevation. c: Observed and calculated fields at satellite elevation for the same crustal model.

Table 6.3: Magnetizations for two-layer crustal model

The magnetizations are for the two-layer crustal model shown in Figure 6.7a. The crustal blocks from 1 to 25 refers to the shaded area S of the figure. This shaded area is the same segmented one-layer crustal block of Figure 6.5a.

Crustal block number	Magnetization (Am^{-1})
1	0.0000
2	1.4543
3	0.0000
4	3.7333
5	0.8255
6	3.3476
7	0.1048
8	0.4752
9	−0.6076
10	2.1487
11	0.8833
12	3.8604
13	2.8226
14	5.3302
15	1.1706
16	3.8604
17	0.0000
18	4.8513
19	4.8513
20	6.9252
21	4.1124
22	6.4818
23	0.0000
24	2.2851
25	−1.8705
26	1.5949
27	1.1706
28	1.1706
29	0.0000
30	0.1793
31	4.6078
32	5.2115
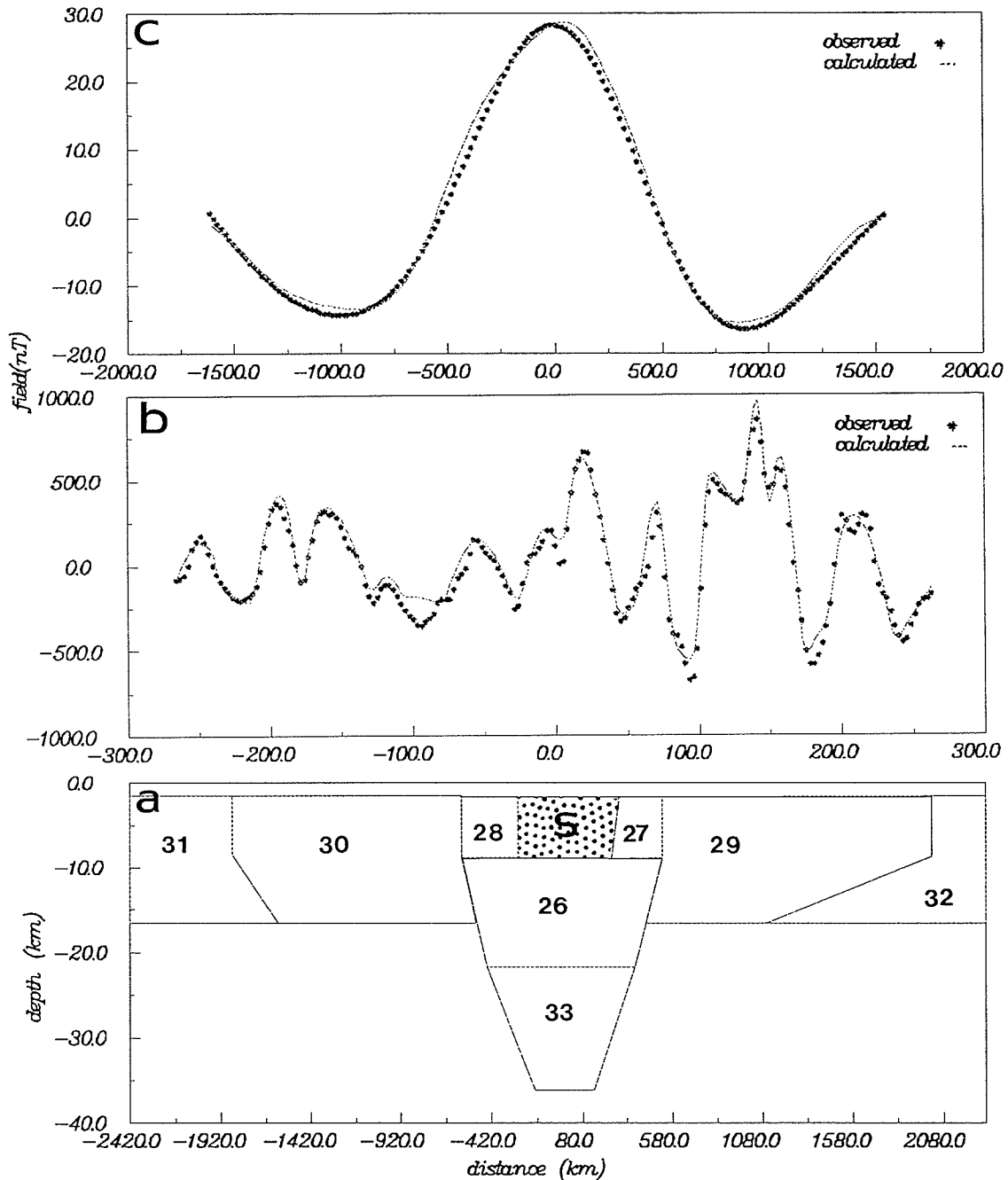
Figure 6.8: Three-layer crustal model

a: Three-layer block model used to represent the Alpha Ridge for obtaining a synthetic vertical field anomaly at both areomagnetic and satellite altitudes. The upper layer (S, a27, a28) is heterogeneous while the lower two layers (a26, a33) are homogeneous. b: Observed and calculated fields at aeromagnetic elevation. c: Observed and calculated fields at satellite elevation for the same crustal model.

Table 6.4: Magnetizations for three-layer crustal model

The magnetizations in this Table are for the three-layer crustal model showm in Figure 6.8a. The crustal blocks from 1 to 25 refers to the shaded area S of the figure. This shaded area is the same segmented one-layer crustal block of Figure 6.5a.

Crustal block number	Magnetization (Am^{-1})
1	0.0000
2	1.4543
3	0.0000
4	3.7333
5	0.8255
6	3.3476
7	0.1048
8	0.4752
9	-0.6076
10	2.1487
11	0.8833
12	3.8604
13	2.8226
14	5.3302
15	1.1706
16	3.8604
17	0.0000
18	4.8513
19	4.8513
20	6.9252
21	4.1124
22	6.4818
23	0.0000
24	2.2851
25	-1.8705
26	2.1487
27	1.1706
28	1.1706
29	0.0000
30	0.1793
31	4.6078
32	5.2115
33	1.5949
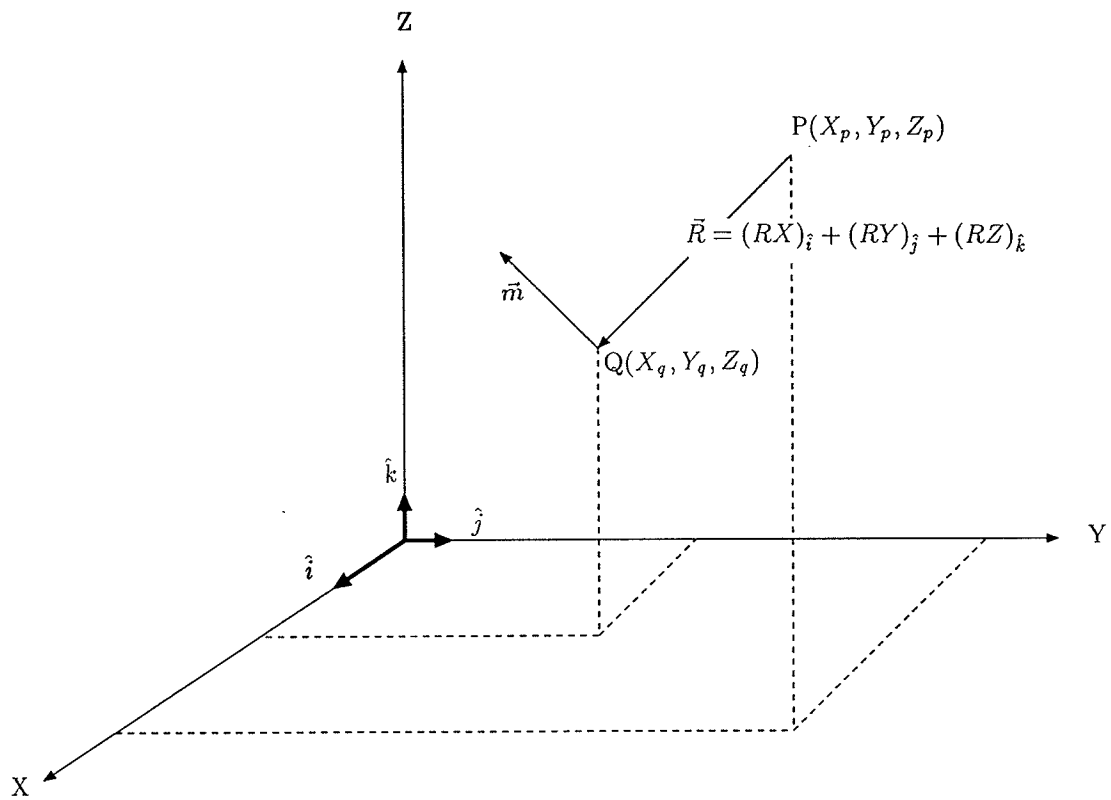
Figure 6.9: Geometry for anomaly calculations

Diagram showing the geometry involved in the calculation of the magnetic field at P due to a magnetic body at position Q.
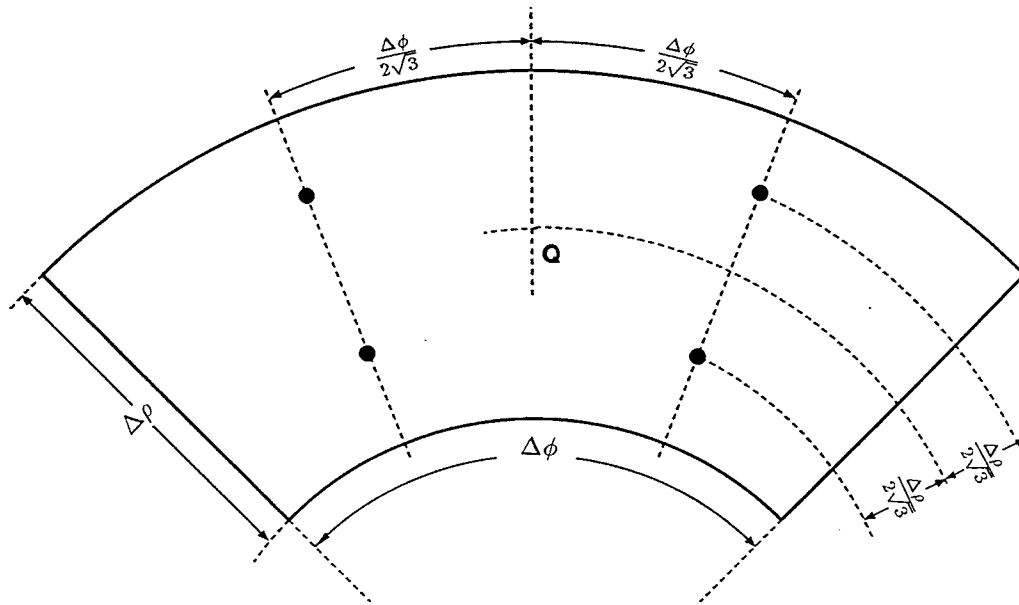
Figure 6.10: Dipole arrangement in a prism section

Diagram showing cross-section of a 2 × 2 array of discrete magnetic bodies. Q is the prism center.
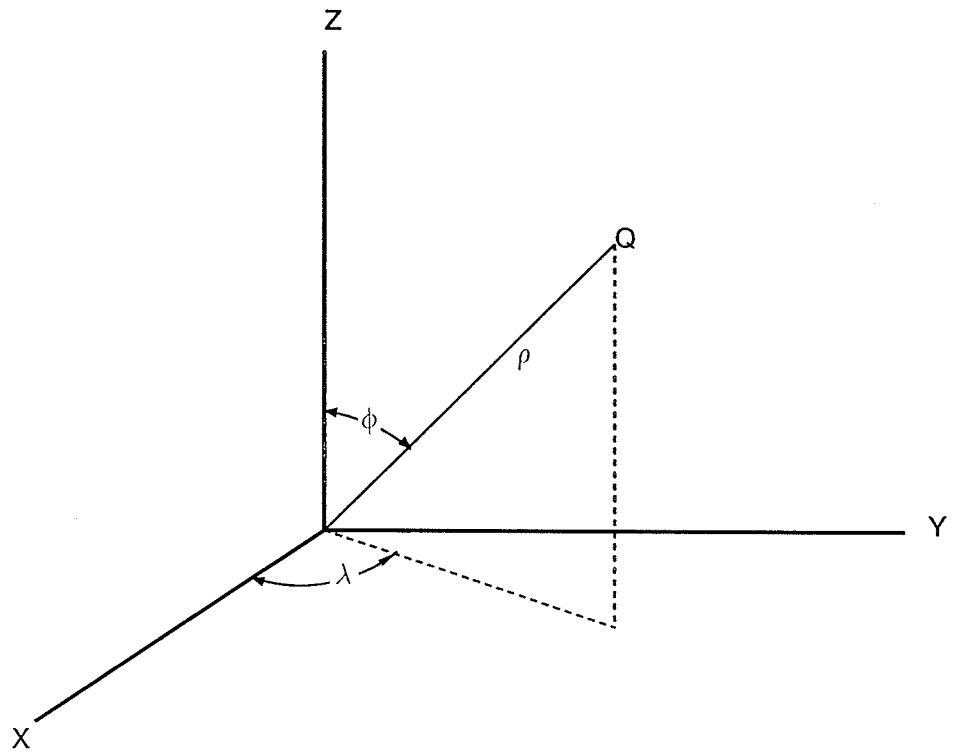
Figure 6.11: Parameters used in spherical geometry calculations

Diagram showing the parameters used in the calculation of of an anomaly field in spherical coordinates. The symbols are explained in the text.
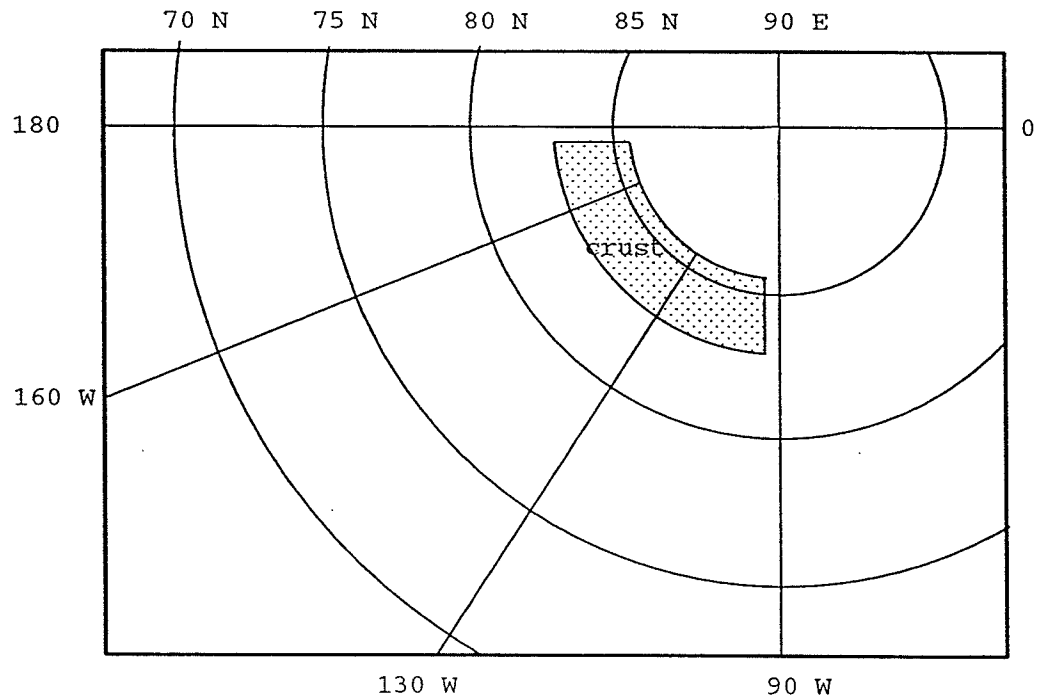
Figure 6.12: Configuration used in 3-D modeling

Configuration of a one block crustal model used in the calculation of the Alpha Ridge anomaly in 3-D at satellite elevations.
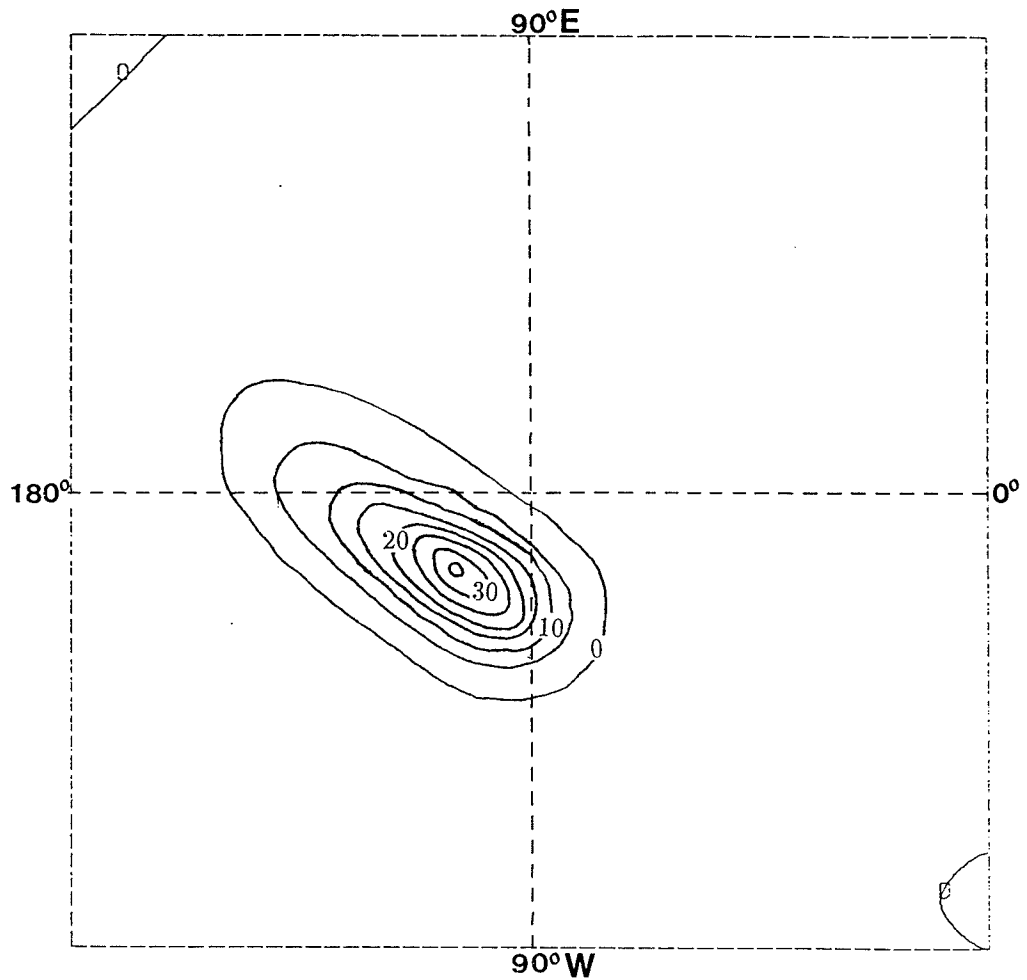
Figure 6.13: Calculated MAGSAT anomaly for two layer model

The calculated MAGSAT anomaly field for the two layers crustal model at an elevation of 328 km. The contour interval is 5 nT.
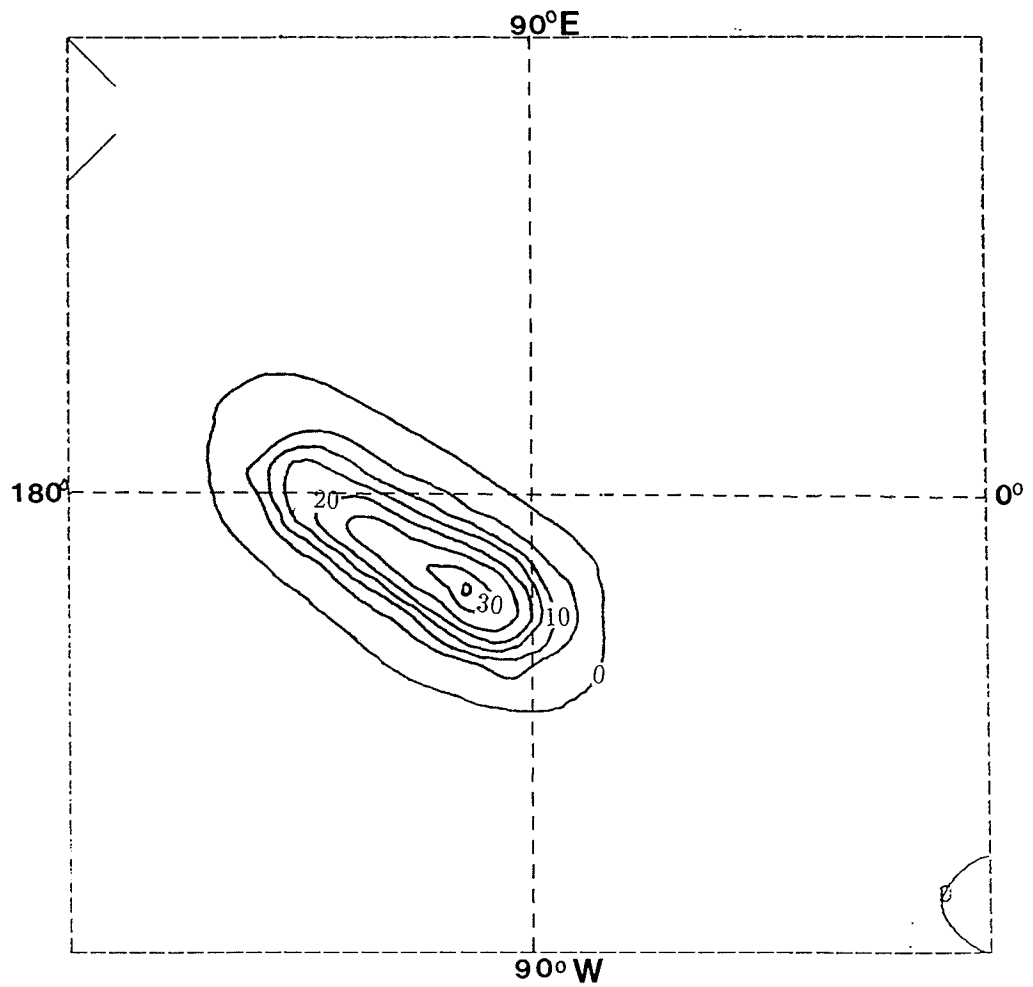
Figure 6.14: Calculated MAGSAT anomaly for three layer model

The calculated MAGSAT anomaly field for the three layers crustal model at an elevation of 328 km. The contour interval is 5 nT.

Chapter 7

Discussion and Conclusion

The combined investigation of the aeromagnetic and MAGSAT data for the Alpha Ridge has given a new perspective in the understanding of the ridge's magnetic nature. As part of the investigation, previous geophysical and geological information pertaining to the ridge was extensively reviewed. Some of the information, particularly heat flow data, was used as constraints in modeling the ridge's magnetic crust.

7.1 Constraints on magnetic modeling

Seismic and gravity data show that the Alpha Ridge is thickest beneath the ridge axis, reaching about 42 km, and thins towards the Canada and Makarov Basins. On the basis of P-wave velocities, the ridge's crust is divided into three layers. The layering has been interpreted to be oceanic in nature. The variation of P-wave velocities in the upper layer was interpreted to indicate that the layer is compositionally heterogeneous. The lower layers were interpreted to be compositionally homogeneous from the smoothness of the P-wave velocities.

Heat flow values over the Alpha Ridge (and the adjacent areas) were of particular

113

importance to the understanding of the ridge's magnetic crust. Using the oceanic crust layering, the heat flow values were extrapolated to the curie level. Critical to the estimation was the curie temperature for magnetite. This temperature was particularly chosen because it gave the maximum possible magnetic crust for the ridge. On this basis, the magnetic crust of the ridge is estimated to be 36 km thick.

7.2   Summary of data investigation

The aeromagnetic and MAGSAT data indicate a highly magnetic Alpha Ridge crust. The MAGSAT anomaly alone, which is one of the strongest on earth to date, delineates the Alpha Ridge to be a magnetic province. The aeromagnetic data show that the positive anomalies are confined to a narrow zone of about 270-300 km that runs along the strike (crest) region of the ridge. The amplitudes of the anomalies reach up to 1800 nT peak to trough. The small almost circular anomalies are up to 20 km in diameter while the elongated ones are about 80 km wide and up to 250 km long. The anomalies are thus irregular to sublinear. There is no clear pattern of alternating positive and negative anomalies as is expected of spreading ocean floors.

Spectral analysis of the data showed that the data has little energy at wavelength of 6-8 km. Components with these wavelengths are interpreted to be noise. The noise may be due to digitization and/or instrumental errors or due to effects that may be attributed to bathymetry or small scale geologic intrusives such as thin highly magnetic dikes. The wavelength of most of the anomalies vary from 80 to 100 km.

The shapes and sizes (and therefore the varied wavelengths of the anomalies) indicate that the source (or sources) from which the anomalies emanate is complex. When wavelengths of up to 25 km are removed from the anomalies, the positive anomalies become dominant. Successive removal of longer wavelength components give results similar to upward continuation. Thus at higher elevations the positive anomalies over

the Alpha ridge dominate. This result concurs with the result obtained by Coles and Haines (1979) for the ridge. The dominance of the positive anomalies at higher elevations is due to the merging of the anomalies. The individual anomalies that are observed at aeromagnetic elevations indicate that there are different sources within the crust. When observed at higher elevations, these sources become indistinguishable due to the merging of the signals.

7.3   Modeling procedure

In modeling the aeromagnetic and MAGSAT data, the magnetic crust obtained for the Alpha Ridge was divided into layers similar to the seismic layers. The upper layer was further vertically segmented so as to reflect the heterogeneity of the layer. The Canada and Eurasia Basins were represented by homogeneous blocks to which different magnetizations were assigned. So that the basins and the Alpha Ridge are better modeled, continental crust representing portions of North America and Eurasia were used. A 2-D program was then used to simultaneously model the data. Results from the 2-D modeling were used in a 3-D program to model the MAGSAT anomaly.

7.4   Modeling results

The combined modeling of the aeromagnetic and MAGSAT data indicates that the Alpha Ridge is not a single homogeneous magnetic crust. The ridge is found to consist of 2 or 3 magnetic crustal layers. If the interpretation of Grantz et al. (1990b) is taken into consideration then it is likely that the ridge's magnetic crust consists of three layers. The upper layer is laterally heterogeneous as is exhibited by the different magnetizations of the sources within the layer. The lower portion of Alpha Ridge may consist of one or two homogeneous magnetic layers.

The thickness of the upper layer cannot be clearly established due to the non-uniqueness inherent in modeling potential data. Magnetic anomaly field calculations involve products of magnetization and volume (equation (6.12)). Thus a small volume and a large magnetization will give results similar to one obtained from using a large volume and a small magnetization. If the lateral heterogeneity is tied with the lateral variations exhibited by seismic results, then the thickness of the upper layer may vary from 8 to 25 km. A thickness of 25 km is unlikely due to the fact that it requires the lower portion of the ridge to have an unacceptably high magnetization. Thus a thickness of about 8 km is a reasonable estimate for the upper layer. The magnetization of the various segments varied from 0 to 7 Am^{-1}. The width of the blocks varied from about 20 to 60 km.

For a one layer lower magnetic crust, extending from 8 km to 36 km, the magnetization is 1.59 Am^{-1}. For a two layer lower magnetic crust, the boundary between the two lower layers is estimated to be at the depth of about 27 km on the basis of seismic data. The magnetization for the two lower layers are respectively 2.14 Am^{-1} (for the middle) and 1.59 Am^{-1} (for the bottom).

The magnetizations for the Canada and Eurasia Basins are respectively 0.17 and 0.00 Am^{-1}. The magnetizations are low compared to those for the Alpha Ridge. The continental crusts have magnetizations of 4.6 Am^{-1} and 5.2 Am^{-1} for the North America and Eurasia portions.

The modeling results show that, at aeromagnetic elevations, the anomalies are strongly influenced by magnetic sources that are within the upper heterogeneous layer. As the observation elevation increases, the anomalies of the upper layer sources merge and the deeper layers begin to be of more influence. Reaching MAGSAT elevations, the deeper broad lower layers become the dominant contributors to the positive anomaly over Alpha Ridge. This is consistent with the FFT results where, at long wavelengths (similar to observing anomalies at higher elevations), positive

anomalies become predominant.

7.5 Discussion of model results

In modeling the large scale magnetic features such as those observed by MAGSAT, the average magnetizations of the features are used since small scale features cannot be resolved at very high elevations. Thus for the Canada and Eurasia basins, which are underlain by normal oceanic crusts, the magnetizations average out to zero or to small positive magnetizations. In investigating oceanic floor magnetization, Thomas (1987) pointed out that the alternating positive and negative magnetization of oceanic layer 2A and 2B average out to zero when observed at elevations greater than 200 km. The lower layer 3A, with a magnetization of 0.5 Am^{-1} (Banerjee, 1984), would contribute more to the anomalies at satellite elevations. Thus the almost zero magnetizations for the basins are consistent with the expected results for normal oceanic floors at satellite elevations (Thomas, 1987). The magnetization of the lower layer(s) for Alpha Ridge (1.59 - 2.14 Am^{-1}) is also consistent with the expected magnetization for long-wavelength anomaly sources (Mayhew, 1985). Although the crusts representing the North America and Eurasia portions have not been constrained, it is interesting to note that the magnetizations (4.6 and 5.2 Am^{-1}) are also within those expected for long-wavelength anomaly sources.

The width extent of the blocks constituting the upper magnetic layer of Alpha Ridge reach up to 60 km. On the basis of seismic velocity, the heterogeneous blocks reach up to 100 km in extent. The width extent of heterogeneities from magnetics and seismic seem different. Since the magnetic and seismic data was not acquired from the same line (or profile), it is difficult to tie the magnetic blocks to seismic blocks. However, since the lateral extents of the blocks are comparatively large (e.g. at the lateral extent of 60 km) there might be correlation between the magnetic and

seimic results.

The varied magnetization of the upper layer of Alpha Ridge may be accounted for if rocks of different composition were emplaced within the layer. From modeling, the magnetizations of the upper layer block are within those of oceanic layer 2 (Thomas, 1987). It is therefore probable that the upper layer of the ridge is composed of igneous rocks of different compositions. The variation in magnetization may also be accounted for if, instead of induced magnetization only, near normal remanence is considered. The accretion process occurring in the Cretaceous normal polarity Superchron would have allowed material injected into the crust to acquire strong remanent magnetization in the direction of the then normal field. The fluctuation in the intensity of the geomagnetic dipole field over the time scale of emplacement would cause the remanent magnetization of the injected material to vary accordingly. The magnetic heterogeneities may therefore be explained from TRM considerations, difference in rock compositions or a combination of the two.

In section 1.6.1, the minerals responsible for magnetic anomalies and how they are affected within the crust, were introduced. The strong anomalies over the Alpha Ridge indicates that the magnetic crust has a high concentration of magnetic minerals. The chief minerals may include magnetite and titaniferous minerals since they are the most magnetic. The presence of water in the upper portion of the ridge would favor serpentinization resulting in multi-domain magnetite with high magnetization. At the deeper portion of the crust, where temperatures are higher, magnetite is likely to be the dominant magnetic mineral.

7.6 Tectonic setting of Alpha Ridge

The Alpha Ridge is a distinctive bathymetric feature of the Amerasia Basin. Seismic, gravity and MT data indicate the ridge's thickness is comparable to that of continents.

Most of the geophysical data however show that the ridge's crust has an oceanic affinity. Gravity, magnetic, bathymetric and heat flow data all indicate that the ridge is not structurally connected to the North American plate in the vicinity of Ellesmere Island. The heat flow values over the ridge are larger than expected for a purely continental crust. These evidence casts doubt as to the continental nature of the ridge.

Seismic P-wave velocities in the crest region of the ridge exhibit characteristics of an oceanic crust. However, the thickness of a normal oceanic crust, which is about 10 km, is much thinner that the Alpha Ridge crust. Thus the magnetic nature of the Alpha Ridge is likely not explainable in terms of a normal oceanic crust.

The average crustal P-wave velocities over Alpha ridge is also found to be similar to those recorded from mid-Pacific oceanic ridges such as the Ontong-Java Plateau. Shallow refraction results show that in the crest zone of Alpha Ridge, the morphology, sediment and basement structure are similar to those of the Manihiki Plateau. Other oceanic ridges similar to the Alpha Ridge include Hess, Magellan and Shatsky plateaus. Hence, in explaining the magnetic nature of Alpha Ridge, an oceanic plateau model may be taken into consideration. Alpha Ridge has also been compared to Iceland-Faeroe Ridge (Forsyth et al., 1986b). In the crest region of the Alpha Ridge, P-waves exhibit similarities in amplitude and velocity-depth structure to P-waves recorded from the Iceland-Faeroe Ridge.

The trace of strong positive MAGSAT anomalies found over Alpha Ridge, Greenland and Iceland, together with the above oceanic plateau/ridge characteristics, suggest that Alpha Ridge and Iceland-Faeroe Ridge are products of a hotspot which is currently situated beneath the Iceland ridge (see section 2.4). Geochemical evidence show that the basement rocks of Alpha Ridge are of volcanic origin associated with aseismic ridges such as Iceland and Hawaii (Van Wagoner et al., 1986). A hotspot origin for Alpha Ridge would explain its magnetic crust structure in terms of thickness

and magnetizations.

Based on the results presented and previous work, the following is a possible scenario to explain the evolution of the Alpha Ridge. A normal oceanic crust, probably associated with the formation of the Amerasia Basin, passed over a hotspot. Magmatic material from the hotspot rose up to the base of the oceanic crust followed by periodic injection of magmatic material into the crust. This intra-plate hotspot activity may have occurred along the entire length of the ridge. It is also possible that the hotspot activity occurred at a spreading axis (oceanic plate margins). If the ridge was originally a spreading axis, the evidence of magnetic lineations has long been obscured by the volcanism associated with the hotspot activities. Periodic injection of magmatic material, possibly of different compositions, or new volcanism caused the magnetization heterogeneities in the basement complex. At depth the magmatic material seemed to have remained homogeneous. Because of high temperatures at depth magnetization is largely by induction. Thus the homogeneity of the lower crust coupled with the constant direction of magnetization may explain the present state of a homogeneous magnetization in the lower magnetic crust.

7.7 Conclusion

Used in conjunction with previous geophysical and geological information, the work presented in this thesis has added to the understanding of the subsurface magnetic structure of the Alpha Ridge as well as to its tectonic evolution.

In this study, the thickness of the Alpha Ridge magnetic crust was determined to be 36 km using heat flow values. Aeromagnetic anomalies were examined using greylevel maps and spectral methods. The aeromagnetic and MAGSAT data were modeled simultaneously using a 2-D forward modeling program (the validity of this process for the MAGSAT data was confirmed using flat earth and spherical earth

geometries). Finally, a 3-D modeling using results obtained from the 2-D models was performed on the MAGSAT data.

The combined investigation of the MAGSAT and aeromagnetic data has enabled the delineation of the Alpha Ridge crust into two magnetic features: an upper layer responsible for the observed aeromagnetic anomalies, and a lower layer which is the major contributor to the MAGSAT anomalies. The upper layer extends to a depth of probably about 8 km. Lateral heterogeneities in magnetization occur within this layer. Such heterogeneities may be attributed to magmatic intrusions into a pre-existing basement complex. Below the upper layer is a crustal layer that is magnetically homogeneous and extends to the curie level. This lower magnetic layer may be divided into two or more layers.

The likely evolutionary mode for Alpha Ridge involves the passage of an oceanic crust over a hotspot. The process of forming the ridge may have been affected by hotspot activity along the entire length of the ridge. Periodic injection of magmatic material, possibly of different compositions, caused the magnetization heterogeneities in the basement complex. The magnetic heterogeneities could also have arisen from TRM considerations. If the ridge was originally a spreading axis or part of a normal oceanic crust, the evidence has long been obscured by the periodic injection of magmatic material. At depth, the magmatic material seemed to have remained homogeneous.

In summary, the Alpha Ridge is oceanic in origin. It was most likely formed by either a combination of sea-floor spreading and plate margin hotspot activity or by intra-plate hotspot activity.

REFERENCES

[1] Agarwal, R. G., 1968, Two-dimensional harmonic analysis of potential fields: Ph. D. thesis, Univ. of Alberta.

[2] Asudeh, I., Green, A. G., and Forsyth, D.A., 1988, Canadian expedition to study the Alpha Ridge complex; Results of the seismic refraction survey: Geophysical Journal, v. 92, 283-301.

[3] Bambrick, J., Jr., 1984, Spectral analysis and filtering techniques applied to a geologic interpretation of high resolution aeromagnetic data from the Timmins area, Ontario, Canada: Ph. D. thesis, Univ. of Toronto.

[4] Banerjee, S. K., 1984, The magnetic layer of the oceanic crust; How thick is it?: Tectonophysics, v. 105, 15-27.

[5] Bhattacharyya, B. K., 1966, Continuous spectrum of the total-magnetic-field anomaly due to a rectangular prismatic body: Geophysics, v. 31, 92-121.

[6] Bhattacharyya, B. K., and Leu, L.-K., 1977, Spectral analysis of gravity and magnetic prismatic bodies: Geophysics, v. 42, 41-50.

[7] Bhimasankaram, V. L., Nagendra, R., Seshagiri, R., 1977, Interpretation of gravity anomalies due to finite inclined dikes using Fourier transforms: Geophysics, v. 42, 51-59.

[8] Berry, M. J., and Mair, J. A., 1980, Structure of the continental crust; a reconciliation of seismic reflection and refraction studies, *in* Strangway, D. W., Ed., The continental crust and its mineral deposits: Geological Association of Canada Special Paper 20, 195-213.

[9] Bott, M. H. P., 1982, The interior of the earth; Its structure, composition and evolution: Elsevier Science Publishing Co., Inc.

[10] Cain, J. C., and Langel, R. A., 1971, Geomagnetic surveys of the Polar Geophysical Observatories, *in* Zmuda, A. J., ed., World magnetic surveys 1957-1969; Paris, International Association of Geomagnetism and Aeronomy Bulletin, no. 28, 65-75.

[11] Carlson, R. L., Christensen, N. I., and Moore, R. P., 1980, Anomalous crustal structure in ocean basins, continental fragments and oceanic plateaus: Earth and Planetary Science Letters, v. 51, 171-180.

[12] Cassano, E., and Rocca, F., 1975, Interpretation of magnetic anomalies using spectral estimation techniques: Geophysical Prospecting, v. 23, 663-681.

[13] Čermák, V., 1975, Temperature-depth profiles in Czechoslovakia and some adjacent areas derived from heat-flow measurements, deep seismic sounding and other geophysical data: Tectonophysics, v. 25, 103-119.

[14] Čermák, V., and Rybach, L., 1982, Thermal conductivity and specific heat of minerals and rocks, *in* Angenheister, G., Ed., Numerical data and functional relationships in science and technology: Physical properties of rocks, v. 1a, Springer-Verlag, 305-371.

[15] Coles, R. L., 1985, Magsat scalar magnetic anomalies at northern high latitudes: Journal of Geophysical Research, v. 90, 2576-2582.

[16] Coles, R. L., and Haines, G. V., 1979, Long-wavelength anomalies over Canada using polynomial and upward continuation techniques: Journal of Geomagnetism and Geoelectricity, v. 31, 545-566.

[17] Coles, R. L., Haines, G. V., Jansen van Beek, G., Nandi, A., and Walker, J. K., 1982, Magnetic anomaly maps from 40°N to 83°N derived from Magsat satellite data: Geophysical Research Letters, v. 9, 281-284.

[18] Coles, R.L., and Taylor , P. T., 1990, Magnetic anomalies, *in* Grantz, A., Johnson, L., and Sweeney, J. F., Eds., The Arctic Ocean region: Geological Society of America, The Geology of North America, v. L, 119-132.

[19] Collins, S. J., Dodds, A. R., and Johnson, B. D., 1974, Gravity profile interpretation using the Fourier transform: Geophysics, v. 39, 862-866.

[20] Cooley, J. W., and Tukey, J. W., 1965, An algorithm for the machine computation of complex Fourier series: Mathematics of Computation, v. 19, 297-301.

[21] Darby, E. K., and Davies, E. B., 1967, The analysis and design of two-dimensional filters for two-dimensional data; Geophysical prospecting, v. 15, 383-406.

[22] Dobrin, M. B., 1988, Introduction to geophysical prospecting: McGraw-Hill Book Co.

[23] Evans, M. E., and McElhinney, M. W., 1969, An investigation of the origin of stable remanence in magnetite-bearing igneous rocks: Journal of Geomagnetism and Geolectricity, v. 21, 757-773.

[24] Forsyth, D.A., Asudeh, I., Green, A. G., and Jackson, H. R., 1986a, Crustal structure of the northern Alpha Ridge beneath the Arctic Ocean: Nature, v. 322, 349-352.

[25] Forsyth, D.A., Morel-a-l'Huissier, P., Asudeh, I., and Green, A. G., 1986b, Alpha Ridge and Iceland - Product of the same plume?: Journal of Geodynamics, v. 6, 197-214.

[26] Good, I. J., 1958, The interaction algorithm and practical Fourier analysis: Journal of the Royal Statistical Society, v. 20, 361-372.

[27] Grantz, A., Johnson, L., and Sweeney, J. F., 1990a, Introduction, *in* Grantz, A., Johnson, L., and Sweeney, J. F., Eds., The Arctic Ocean region: Geological Society of America, The Geology of North America, v. L, 1-3.

[28] Grantz, A., May, S. D., Taylor, P. T., and Lawver, L. A., 1990b, Canada Basin, *in* Grantz, A., Johnson, L., and Sweeney, J. F., Eds., The Arctic Ocean region: Geological Society of America, The Geology of North America, v. L, 379-402.

[29] Gunn, P. J., 1975, Linear transformation of gravity and magnetic fields: Geophysical Prospecting, v. 23. 300-312.

[30] Gupta, V. K., and Ramani, N., 1980, Some aspects of regional-residual separation of gravity anomalies in a precambrian terrain: Geophysics, v. 45., 1412-1426.

[31] Hahn, A., Kind, E. G., and Mishra, D. C., 1976, Depth estimation of magnetic sources by means of Fourier amplitude spectra: Geophysical Prospecting, v. 24, 287-308.

[32] Haines, G. V., 1985a, Spherical cap harmonic analysis: Journal of Geophysical Research, v. 90, 2583-2591.

[33] Haines, G. V., 1985b, Magsat vertical anomalies above 40°N from spherical harmonic analysis: Journal of Geophysical Research, v. 90, 2593-2598.

[34] Hall, D. H., 1968, Regional magnetic anomalies, magnetic units and crustal structure in the Kenora District of Ontario: Canadian Journal of Earth Sciences, v. 5, 1277-1296.

[35] Hall, J. K., 1973. Geophysical evidence for an ancient sea-floor spreading from Alpha Cordillera and the Mendeleyev Ridge, *in* Pitcher, M.G., Ed., Arctic Geology: American Association of Petroleum Geologists Memoirs 19, 542-561.

[36] Heron, E. M., Dewey, F. J., and Pitman, W. C., III, 1974, Plate tectonics model for the evolution of the Arctic: Geology, v. 2, 377-380.

[37] Jackson, H. R., 1985, Seismic reflections from CESAR, *in* Jackson, H. R., Mudie, P. J., and Blasco, S. M., Eds., Initial geological data report on CESAR; Canadian Expedition to Study Alpha Ridge: Geological Survey of Canada, Paper 84-22, 19-23.

[38] Jackson, H. R., Forsyth, D. A., and Johnson, G. L., 1986, Oceanic affinities of the Alpha Ridge, Arctic Ocean: Marine Geology, v. 73, 237-261.

[39] Johnson, G. L., Grantz, A., and Weber, J. R., 1990, Bathymetry and physiography, *in* Grantz, A., Johnson, L., and Sweeney, J. F., Eds., The Arctic Ocean region: Geological Society of America, The Geology of North America, v. L, 63-77.

[40] King, E. R., Zietz, I., and Alldredge L. R., 1966, Magnetic data on the crustal structure of the central Arctic region: Geological Society of America Bulletin, v. 77, 619-649.

[41] Kovacks, L. C., and Vogt, P. R., 1982, Depth to magnetic source analysis of the Arctic Ocean region: Tectonophysics, v. 89, 255-294.

[42] Lachenbruch, A. H., 1970, Crustal temperature and heat production; Implications of the linear heat-flow relation: Journal of Geophysical Research, v. 71, 3291-3300.

[43] Lachenbruch, A. H., and Marshall, B. V., 1966, Heat flow through the Arctic Ocean floor; The Canada Basin - Alpha rise boundary: Journal of Geophysical Research, v. 71, 1223-1248.

[44] Langel, R. A., 1974, Near earth disturbance in total field at high latitudes 1; Summary of data from OGO 2, 4, and 6: Journal of Geophysical Research, v. 79, 2363-2371.

[45] Langel, R. A., 1990, Global magnetic anomaly maps derived from POGO spacecraft data: Physics of the Earth and Planetary Interiors, v. 62, 208-230.

[46] Langel, R. A., Benson, B. J., and Orem, R. M., 1991, The Magsat bibliography: NASA Technical Memorandum 100776.

[47] Langel, R. A., Coles, R. L., and Mayhew, M. A., 1980, Comparisons of magnetic anomalies of lithospheric origin measured by satellite and airborne magnetometers over western Canada: Canadian Journal of Earth Sciences, v. 17, 876-887.

[48] Langel, R. A., and Estes, R. H., 1985, The near-earth magnetic field at 1980 determined from Magsat data: Journal of Geophysical Research, v. 90 2495-2509.

[49] Langel, R. A., and Estes, R. H., 1982, A geomagnetic field spectrum: Geophysical Research Letters, v. 9, 250-253.

[50] Langel, R. A., Estes, R. H., and Mayhew, M. A., 1981, Early results from Magsat: Nature, v. 293, 190-192.

[51] Langel, R., Ousley, G., Berbert, J., Murphy, J., and Settle, M., 1982, The Magsat Mission: Geophysical Research letters, v. 9, 243-245.

[52] Langel, R. A., and Thorning, L., 1982, A satellite magnetic anomaly map of Greenland: Geophysical Journal of the Royal Astronomical Society, v. 71, 876-887.

[53] Langseth, M. G., Lachenbruch, A. H., and Marshall, B. H., 1990, *in* Grantz, A., Johnson, L., and Sweeney, J. F., Eds., The Arctic Ocean region: Geological Society of America, The Geology of North America, v. L, 133-151.

[54] Lourenco, J. S., and Morrison, H. F., 1973, Vector magnetic anomalies derived from measurements of a single component of the field: Geophysics, v. 38, 359-368.

[55] Macnab, R., Verhoef, J., and Srivastava, S., 1992, Magnetic observations from the Arctic and North Atlantic oceans: EOS, v.73, 123-124.

[56] Mankinen, E. D., Larson, E. E., Grommé, C. S., Prèvot, M., and Coe, R. S., 1987, The Steen Mountain (Oregon) geomagnetic transition 3; Its regional significance: Journal of Geophysical Research, v. 90, 8057-8076.

[57] Mankinen, E. D., Prévot, M., Grommé, C. S., and Coe, R. S., 1985, The Steen Mountain (Oregon) geomagnetic transition 1; Directional history, duration of episodes, and rock magnetism: Journal of Geophysical Research, v. 90, 10393-10416.

[58] Mayhew, M. A., 1979, Inversion of Satellite magnetic anomaly data: Journal of Geophysics, v. 45, 119-129.

[59] Mayhew, M. A., Johnson, B. D., and Wasilewski P. J., 1985, A review of problems and progress in studies of satellite magnetic anomalies: Journal of Geophysical Research, v. 90, 2511-2522.

[60] Mudie, P. J., and Blasco, S. M., 1985, Lithostratigraphy of the CESAR cores, *in* Jackson, H. R., Mudie, P. J., and Blasco, S. M., Eds., Initial geological data report on CESAR; Canadian Expedition to Study Alpha Ridge: Geological Survey of Canada, Paper 84-22, 59-100.

[61] Mudie, P. J., Stoffyn-Egli, P., and Van Wagoner, N. A., 1986, Geological constraints for tectonic model of the Alpha Ridge: Journal of Geodynamics, v. 6, 215-236.

[62] Niblett, E. R., Kurzt, R. D., and Michaud C., 1987, Magnetotelluric measurements over the Alpha Ridge: Physics of the Earth and Planetary Interiors, v. 45, 101-118.

[63] Noble, I. A., 1983, Magsat anomalies and crustal structure of the Churchill-Superior boundary zone: M.Sc. thesis, Univ. of Manitoba.

[64] Ostenso, N. A., and Wold, J. R., 1977; A seismic and gravity profile across the Arctic Ocean Basin: Tectonophysics, v. 37, 1-24.

[65] Odegard, M. E., and Berg, J. W., 1965, Gravity interpretation using Fourier integral: Geophysics, v. 30, 424-438.

[66] Parkinson, W. D., 1983, Introduction to geomagnetism: Scottish Academic Press.

[67] Pedersen, L. B., 1978, A statistical analysis of potential fields using a vertical circular cylinder as a dike: Wavenumber domain expressions for potential fields from arbitrary 2, $2\frac{1}{2}$, and 3-dimensional bodies: Geophysics, v. 43, 626-630.

[68] Press, W. H., Flannery, B. P., Teukolsky, S. A., and Vetterling W. T., 1986, Numerical recipes; The art of scientific computation: Cambridge University Press.

[69] Prévot, M., Mankinen, E. D., Coe, R. S., and Grommé, C. S., 1985, The Steen Mountain (Oregon) geomagnetic transition 2; Field intensity variations and discussion of reversal models: Journal of Geophysical Research, v. 90, 10417-10448.

[70] Rao, R. U. M., and Jessop, A. M., 1975, A comparison of the thermal characters of shields: Canadian Journal of Earth Sciences, v. 12, 347-360.

[71] Regan, R. D., Cain, J. C, and Davies, W. M., 1975, A global magnetic anomaly map: Journal of Geophysical Research, v. 80, 749-802.

[72] Riddihough, R. P., Haines, G. V., and Hannaford, W., 1973, Regional magnetic anomalies of the Canadian Arctic: Canadian Journal of Earth Sciences, v. 10, 157-163.

[73] Roy, A., and Aina, A. O., 1986, Some new magnetic transformations: Geophysical Prospecting, v. 34, 1219-1232.

[74] Sengupta, S., 1974, Fourier transforms of magnetic anomalies of two-dimensional bodies: Pure and Applied Geophysics, v. 112, 987-995.

[75] Sharma, B., Geldar, L. P., and Gill, D. E., 1970, Interpretation of gravity anomalies of dike-like bodies by Fourier transformation: Canadian Journal of Earth Sciences, v. 7, 443-459.

[76] Silva, J. B. C., and Cutrim, A. O., 1989, A robust maximum likelihood method for gravity and magnetic interpretation: Geoexploration, v. 26, 1-31

[77] Sobczak, L. W., Hearty, D. B., Forsberg, R., Kristoffersen, Y., Eldholm, O., and May, S. D., 1990, Gravity from 64°N to the North Pole, *in* Grantz, A., Johnson, L., and Sweeney, J. F., Eds., The Arctic Ocean region: Geological Society of America, The Geology of North America, v. L, 101-118.

[78] Spector A., Grant, F. S., Statistical model for interpreting aeromagnetic data: Geophysics, v. 35, 293-302.

[79] Sweeney, J. F., Weber, J. R., and Blasco, S. M., 1982, Continental ridges in the Arctic Ocean; LOREX constraints: Tectonophysics, v. 89, 217-238.

[80] Tarantola, A. 1987, Inverse problem theory; methods for data filling and model parameter estimation: Elsevier Science Publishing Co.

[81] Taylor, P. T., 1983. Magnetic data over the Arctic from aircraft and satellites: Cold Regions Science and Technology, v. 7. 35-40.

[82] Taylor, A., Judge, A., and Allen, V., 1986, Terrestrial heat flow from project CESAR; Alpha Ridge, Arctic Ocean: Journal of Geodynamics, v. 6, 137-176.

[83] Taylor, P. T., Kovacks, L. C., Vogt, P. R., and Johnson, G. L., 1981, Detailed aeromagnetic investigation of the Arctic Basin 2: Journal of Geophysical Research, v. 84, 6323-6333.

[84] Telford, W. M., Geldart, L. P., and Sheriff, R. E., 1990, Applied geophysics: Cambridge University Press.

[85] Treitel, S., Clement, W. G. and Kaul, R. K., 1971 The spectral determination of depth due to buried magnetic basement rocks: Geophysical Journal of the Royal Astronomical Society, v. 24, 415-428.

[86] Thomas, H. H., 1987, A model of ocean basin crustal magnetization appropriate for satellite elevation anomalies: Journal of Geophysical Research, v. 92, 11609-11613.

[87] Van Wagoner, N, A., and Robinson, P. T., 1985, Petrology and geochemistry of a CESAR bedrock sample; Implication for the origin of the Alpha Ridge, *in* Jackson, H. R., Mudie, P. J., and Blasco, S. M., Eds., Initial geological data report on CESAR; Canadian Expedition to Study Alpha Ridge: Geological Survey of Canada, Paper 84-22, 47-58.

[88] Van Wagoner, N, A., Williamson, M. C., Robinson, P T., and Gibson, I. L., 1986, First samples of acoustic basement recovered from the Alpha Ridge, Arctic Ocean: New constraints for the origin of the ridge: Journal of Geodynamics, v. 6, 177-196.

[89] Verba, V. V., Volk, V. E., and Gubernov, A. P., 1990, General geophysical model for the crust of the Arctic Basin (In Russian): DOKLADY AKADEMII NAUK SSSR, v. 315, 442-445.

[90] Vogt, P. R., and Ostenso, N. A., 1970. Magnetic and gravity profiles across the Alpha Cordillera and their relation to Arctic sea-floor spreading: Journal of Geophysical Research, v. 75, 4925-4937.

[91] Vogt, P. R., Taylor P. T., Kovacks, L. C., and Johnson, G. L., 1979, Detailed aeromagnetic investigation of the Arctic Basin: Journal of Geophysical Research, v. 84, 1071-1089.

[92] Vogt, P. R., Taylor P. T., Kovacks, L. C., and Johnson, G. L., 1982. The Canada Basin; Aeromagnetic constraints on the structure and evolution: Tectonophysics, v. 89, 295-336.

[93] Von Frese, R. B., Hinze, W. J., and Braile, L. W., 1981, Spherical Earth gravity and magnetic anomaly analysis by equivalent point source inversion: Earth and Planetary Science Letters, v. 53, 69-83.

[94] Wang, X., and Hansen, R. O., 1990, Inversion of magnetic anomalies of arbitrary three-dimensional bodies: Geophysics, v. 55, 1321-1326.

[95] Weber, J. R., 1986, The Alpha Ridge; Gravity, seismic and magnetic evidence for a homogeneous mafic crust: Journal of Geodynamics, v. 6, 117-136.

[96] Weber, J. R., and Jackson, H. R., 1985, CESAR bathymetry, *in* Jackson, H. R., Mudie, P. J., and Blasco, S. M., Eds., Initial geological data report on CESAR; Canadian Expedition to Study Alpha Ridge: Geological Survey of Canada, Paper 84-22, 15-17.

[97] Weber J. R., and Roots, E. F., 1990, Historical background; Exploration, concepts, and observations, *in* Grantz, A., Johnson, L., and Sweeney, J. F., Eds., The Arctic Ocean region: Geological Society of America, The Geology of North America, v. L, 5-36.

[98] Weber J. R., and Sweeney, J. F., 1990, Ridges and basins in the central Arctic Ocean, *in* Grantz, A., Johnson, L., and Sweeney, J. F., Eds., The Arctic Ocean region: Geological Society of America, The Geology of North America, v. L, 305-336.

[99] Wasilewski, P. J., Thomas, H. H. and Mayhew, M. A., 1979, The Moho as a magnetic boundary: Geophysical Research Letters, v. 6, 541-544.

Appendix A

Aeromagnetic data parameters

The diskette containing the magnetic data obtained from the Geophysical Division of the Geological Survey of Canada is ASCII coded. The program below (Program GETMAG) may be used to read the gridded data from the file HALLMAG.GRD (name of the file containing the magnetic data in the diskette). Figure A.1 illustrates the map and some of the parameters of the gridded data. From the figure, the projection origin is at the coordinates $63.39067°$ N, $92.00°$ W (referred to in the program as (Xlat,Ylat)). The positions (87,141), (87,90), (83,90) and (83,141) are the latitudes and the longitudes (refered to in the program as (Alat,Along)) defining the area of the gridded data. The rest of the variables are defined in the program.

```
      PROGRAM GETMAG
C****************************************************************
C
C     THIS PROGRAM READS BOTH MAGNETIC AND GRAVITY DATA FROM
C     DATASETS HALLMAG.GRD AND HALLBG.GRD
C
C****************************************************************
      REAL ZIN(1000),ALAT(10),ALONG(10),IDENT(8)
C
C     IDENT      : DATA IDENTIFICATION
C     CENMAR     : CENTRAL MERIDIAN
```

134

```
C      PARS         : SOUTHERN PARALLEL
C      PARN         : NORTHERN PARALLEL
C      PROJ         : PROJECTION "MER", "LCP" OR "UTM"
C      GRDSZ        : GRID SIZE IN METERS ON THE GROUND
C      NCORN        : NUMBER OF COORDINATES
C      LINNDIR      : LINE DIRECTION (DEGREES FROM NORTH)
C      ROTANG       : ROTATION ANGLE OF GRID
C      ALAT, ALONG  : LAT. AND LONG. OF COORDINATES
C      DTYPE        : DATA TYPE
C      ZIN          : ARRAY OF DATA VALUES
C      YLAT         : LATITUDE OF PROJECTION ORIGIN
C      XLONG        : LONGITUDE OF PROJECTION ORIGIN
C
       READ(9,500) IDENT
C      WRITE(*,500) IDENT
500    FORMAT(8A10)
       READ(9,501) CENMER,PARS,PARN,PROJ,GRDSZ,NCORN,LINDIR,ROTANG,
     +             DTYPE
C      WRITE(*,501) CENMER,PARS,PARN,PROJ,GRDSZ,NCORN,LINDIR,ROTANG,
C    +             DTYPE
501    FORMAT(3F10.5,A10,F10.2,2I5,F10.3,A10)
       READ(9,504) (ALAT(I),ALONG(I),I=1,NCORN)
C      WRITE(*,504) (ALAT(I),ALONG(I),I=1,NCORN)
504    FORMAT(8F10.5)
       READ(9,505) YLAT,XLONG
C      WRITE(*,505) YLAT,XLONG
505    FORMAT(2F10.5)
C
C      IO : GRID ORIGIN (# OF COLS - X DIR.) wrt PROJECTION ORIGIN.
C      JO :    "    "    ("  "  ROWS - Y "  )  "      "          "
C      IL : GRID LIMITS ("  "  COLS )          "      "          "
C      JL :    "    "    ("  "  ROWS )          "      "          "
C      NC : NUMBER OF COLUMNS
C      NR : NUMBER FO ROWS
C          NOTE:
C          TO CALCULATE THE NORTHING AND EASTING OF THE GRID ORIGIN:
C          NORTHING = JO*GRDSZ
C          EASTING  = IO*GRDSZ
C
       READ(9,502) IO,IL,JO,JL,NR,NC
       WRITE(*,502) IO,IL,JO,JL,NR,NC
502    FORMAT(6I10)
       DO 10 N=1,NC
          INC=N-1
          READ(9,503) (ZIN(I),I=1,NR)
          DO 707 I=1,NR
C            READ(9,503) ZIN(I)
             INR=I-1
             XNVAL=FLOAT(JO+INR)*GRDSZ
```

```
                  YEVAL=FLOAT(IO+INC)*GRDSZ
C                   IF(ZIN(I).EQ.-9999.0000) GOTO 707
                  WRITE(20,70) XNVAL,YEVAL,ZIN(I)
707         CONTINUE
C           WRITE(*,503) (ZIN(I),I=1,NR)
10      CONTINUE
503     FORMAT(8F10.3)
C
25      WRITE(*,110)
110     FORMAT(1H0,'END OF JOB')
100     CONTINUE
C
        STOP
        END
```
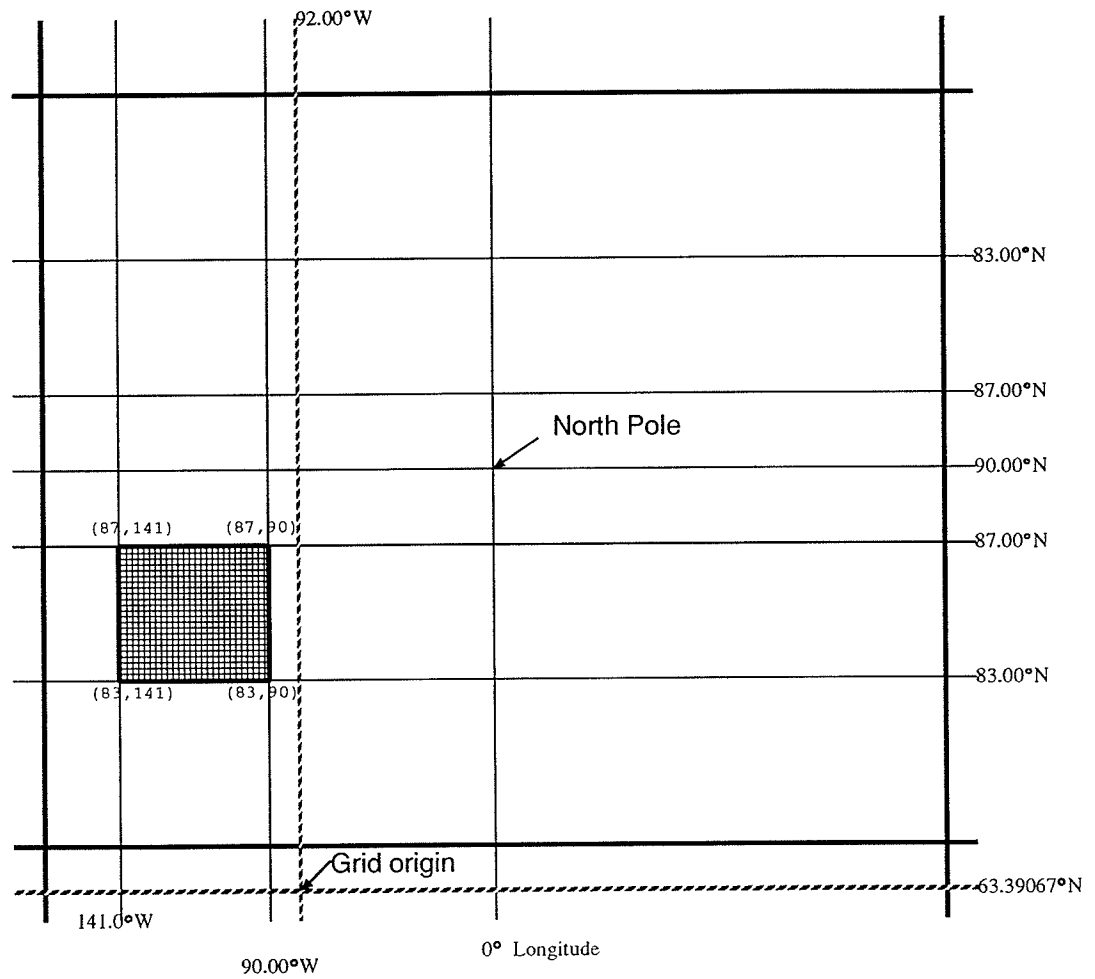
Figure A.1: Map of gridded data

The positions (87,141), (87,90), (83,90) and (83,141) are the coordinates (latitude,longitude) that define the area of the gridded data (shaded area).

Appendix B

Fitting a straight line to data

The equation of a regression line is esxpressed as

$$y = a + bx. \tag{B.1}$$

For the magnetic data described in Chapter 4, y represents the magnetic field observed at a distance x from some reference point. The parameters a and b are to be estimated from the data. Methods used in finding these parameters include least squares and robust estimations. Both methods are discussed by Tarantola (1987). The method of least squares give better parameter estimates if the data being investigated exhibit gaussian errors. On the other hand, if the errors in the data are non-gaussian, the robust methods give better parameter estimates.

The following program estimates the parameters a and b using both the least squares and robust methods. Most of the Subroutines are taken form Press et al., (1986). The program may be used for fiting a straight line to any data.

```
          PROGRAM REGRES
C*********************************************************************
C*                                                                  *
C*    THIS PROGRAM FITS A REGRESSION LINE USING (1) LEAST SQUARES    *
C*    AND (2) ROBUST METHOD.                                         *
C*                                                                  *
C*    VARIABLE DICTIONARY:                                           *
C*    XVAR:              INDEPENDENT VARABLE                         *
C*    YVAR:              DEPENDENT VARIABLE                          *
C*    AFIT:              INTERCEPT FROM LEAST SQUARES                *
C*    BFIT:              SLOPE FROM LEAST SQAURES                    *
C*    AROB:              INTERCEPT FROM ROBUST ESTIMATION            *
C*    BROB:              SLOPE FROM ROBUST ESTIMATION                *
C*********************************************************************
C     GENERAL VARIABLES
      PARAMETER (NMAX=400 )
      REAL XVAR(400),YVAR(400)
C     LEAST SQUARES VARIABLES
      REAL AFIT,BFIT
      REAL ASIGMA,BSIGMA,CHISQ,QPROB,SIGMA(400)
C     ROBUST ESTIMATION VARIABLES
      REAL AROB,BROB,DEROB
C
C     READ  x and y
C
      OPEN(8,FILE='mag.dat')
      READ(8,*) NDATA
      DO 10 I=1,NDATA
      READ(8,*) XVAR(I),YVAR(I)
10    CONTINUE
C
C     DO LEAST SQ. CALCULATION
C
      DUMMY=0
      CALL FIT(XVAR,YVAR,NDATA,SIGMA,DUMMY,AFIT,BFIT,ASIGMA,
     +          BSIGMA,CHISQ,QPROB)
      WRITE(*,21) AFIT,ASIGMA
      WRITE(*,22) BFIT,BSIGMA
21    FORMAT(' THE VALUE a IS ',20X,F12.4,2X,'+ -',2X,F10.5)
22    FORMAT(' THE VALUE B IS ',20X,F12.4,2X,'+ -',2X,F10.5)
23    FORMAT(' CHISQUARE VALUE IS',2X,F12.4)
24    FORMAT('  VALUE IS',2X,F12.4)
C
C     CALCULATE ROBUSTLY
C
      CALL MEDFIT(XVAR,YVAR,NDATA,AROB,BROB,DEROB,IDUM1)
      WRITE(*,*) ' ROBUST ESTMATION '
      WRITE(*,25) AROB
      WRITE(*,26) BROB
```

```
C        WRITE(*,27) DEROB
25       FORMAT(' THE VALUE a IS ',20X,F12.4)
26       FORMAT(' THE VALUE B IS ',20X,F12.4)
27       FORMAT(' CHISQUARE VALUE IS',2X,F12.4)
C
601      CONTINUE
         STOP
         END
C
         SUBROUTINE MEDFIT(X,Y,NDATA,A,B,ABDEV,IDUM1)
C*****************************************************************
C        SUBROUTINE ACCEPTS DATA X(I),Y(I) AND SIG(I). THE DATA ARE   *
C        FIT TO A STRAIGHT LINE (y = ax + b) BY MINIMIZING CHI-SQUARE. *
C        RETURNED: THE UNCERTAINTIES A AND B; SIGA,SIGB,              *
C        THE CHI-SQUARE; CHISQ,                                       *
C        AND THE GOODNESS-OF-FIT PROBABILITY Q;QPROB                  *
C                                                                     *
C*****************************************************************
         PARAMETER (NMAX=1000)
         EXTERNAL ROFUNC
         COMMON /ARRAYS/ NDATAT,XT(NMAX),YT(NMAX),ARR(NMAX),AA,ABDEVT
         DIMENSION X(NDATA),Y(NDATA)
         SX=0.
         SY=0.
         SXY=0.
         SXX=0.
         DO 11 J=1,NDATA
           XT(J)=X(J)
           YT(J)=Y(J)
           SX=SX+X(J)
           SY=SY+Y(J)
           SXY=SXY+X(J)*Y(J)
           SXX=SXX+X(J)**2
11       CONTINUE
         NDATAT=NDATA
         DEL=NDATA*SXX-SX**2
         AA=(SXX*SY-SX*SXY)/DEL
         BB=(NDATA*SXY-SX*SY)/DEL
         CHISQ=0.
         DO 12 J=1,NDATA
           CHISQ=CHISQ+(Y(J)-(AA+BB*X(J)))**2
12       CONTINUE
         SIGB=SQRT(CHISQ/DEL)
         B1=BB
         F1=ROFUNC(B1)
C        WRITE(*,*) B1,F1
         B2=BB+SIGN(3.*SIGB,F1)
         F2=ROFUNC(B2)
C***************** THIS IF IS MY OWN! FOR DATA WITHOUT ERRORS
```

```
           IF(IDUM1.EQ.0) GO TO 4
C****************************************************************
1          IF(F1*F2.GT.0.)THEN
             BB=2.*B2-B1
             B1=B2
             F1=F2
             B2=BB
             F2=ROFUNC(B2)
             GOTO 1
           ENDIF
4          SIGB=0.01*SIGB
2          IF(ABS(B2-B1).GT.SIGB)THEN
             BB=0.5*(B1+B2)
             IF(BB.EQ.B1.OR.BB.EQ.B2)GOTO 3
             F=ROFUNC(BB)
             IF(F*F1.GE.0.)THEN
               F1=F
               B1=BB
             ELSE
               F2=F
               B2=BB
             ENDIF
             GOTO 2
           ENDIF
3          A=AA
           B=BB
           ABDEV=ABDEVT/NDATA
           RETURN
           END
C
           FUNCTION ROFUNC(B)
           PARAMETER (NMAX=1000)
           COMMON /ARRAYS/ NDATA,X(NMAX),Y(NMAX),ARR(NMAX),AA,ABDEV
           N1=NDATA+1
           NML=N1/2
           NMH=N1-NML
           DO 11 J=1,NDATA
             ARR(J)=Y(J)-B*X(J)
11         CONTINUE
           CALL SORT(NDATA,ARR)
           AA=0.5*(ARR(NML)+ARR(NMH))
           SUM=0.
           ABDEV=0.
           DO 12 J=1,NDATA
             D=Y(J)-(B*X(J)+AA)
             ABDEV=ABDEV+ABS(D)
             SUM=SUM+X(J)*SIGN(1.0,D)
12         CONTINUE
           ROFUNC=SUM
```

```
      RETURN
      END
C
      SUBROUTINE SORT(N,RA)
C-------------------------------------------------------------------
C     SORTS AN ARRAY RA OF LENGNTH N INTO ASCENDING NUMERICAL ORDER
C     USING THE HEAPSORT ALGORITHM. N IS INPUT; RA IS REPLACEDON
C     OUTPUT BY ITS SORTED ARRANGEMENT.
C-------------------------------------------------------------------
      DIMENSION RA(N)
      L=N/2+1
      IR=N
10    CONTINUE
      IF(L.GT.1)THEN
         L=L-1
         RRA=RA(L)
      ELSE
         RRA=RA(IR)
         RA(IR)=RA(1)
         IR=IR-1
         IF(IR.EQ.1)THEN
            RA(1)=RRA
            RETURN
         ENDIF
      ENDIF
      I=L
      J=L+L
20    IF(J.LE.IR)THEN
         IF(J.LT.IR)THEN
            IF(RA(J).LT.RA(J+1))J=J+1
         ENDIF
         IF(RRA.LT.RA(J))THEN
            RA(I)=RA(J)
            I=J
            J=J+J
         ELSE
            J=IR+1
         ENDIF
         GO TO 20
      ENDIF
      RA(I)=RRA
      GO TO 10
      END
C
      FUNCTION GASDEV(IDUM)
C-------------------------------------------------------------------
C
C     RETURNS A NORMALLY DISTRIBUTED DEVIATE WITH ZERO MEAN AND
C     AND UNIT VARIANCE, USING RAN1(IDUM) AS THE SOURCE OF
```

```
C      UNIFORM DEVIATES.
C
C-------------------------------------------------------------
C      EXTERNAL RAN1
       DATA ISET/0/
       IF(ISET.EQ.0) THEN
1          V1=2.*RAN1(IDUM)-1.
           V2=2.*RAN1(IDUM)-1.
           R=V1**2 + V2**2
           IF(R.GE.1.)GO TO 1
           FAC=SQRT(-2.*LOG(R)/R)
           GSET=V1*FAC
           GASDEV=V2*FAC
           ISET=1
       ELSE
           GASDEV=GSET
           ISET=0
       ENDIF
C      PRINT *, 40.0
       RETURN
       END
C
       FUNCTION RAN1(IDUM)
C-------------------------------------------------------------
C
C      RETURNS A UNIFORM RANDOM DEVIATE BETWEEN 0.0 AND 1.0. SET
C      IDUM TO ANY NEGATIVE VALUE TO INITIALIZE OR REINITIALIZE THE
C      SEQUENCE
C
C-------------------------------------------------------------
       DIMENSION R(97)
       PARAMETER(M1=259200,IA1=7141,IC1=54773,RM1=1./M1)
       PARAMETER(M2=134456,IA2=8121,IC2=28411,RM2=1./M2)
       PARAMETER(M3=243000,IA3=4561,IC3=51349)
       DATA IFF /0/
       IF(IDUM.LT.0.OR.IFF.EQ.0) THEN
           IFF=1
           IX1=MOD(IC1-IDUM,M1)
           IX1=MOD(IA1*IX1+IC1,M1)
           IX2=MOD(IX1,M2)
           IX1=MOD(IA1*IX1+IC1,M1)
           IX3=MOD(IX1,M3)
           DO 11 J=1,97
               IX1=MOD(IA1*IX1+IC1,M1)
               IX2=MOD(IA2*IX2+IC2,M2)
               R(J)=(FLOAT(IX1)+FLOAT(IX2)*RM2)*RM1
11         CONTINUE
           IDUM=1
       ENDIF
```

```
      IX1=MOD(IA1*IX1+IC1,M1)
      IX2=MOD(IA2*IX2+IC2,M2)
      IX3=MOD(IA3*IX3+IC3,M3)
      J=1+(97*IX3)/M3
      IF(J.GT.97.OR.J.LT.1)PAUSE
      RAN1=R(J)
      R(J)=(FLOAT(IX1)+FLOAT(IX2)*RM2)*RM1
C      PRINT *,100.0
      RETURN
      END
C
      SUBROUTINE FIT(X,Y,NDATA,SIG,MWT,A,B,SIGA,SIGB,CHI2,Q)
C-----------------------------------------------------------------
C
C     SUBROUTINE ACCEPTS DATA X(I),Y(I) AND SIG(I). THE DATA ARE
C     FIT TO A STRAIGHT LINE ( y = ax + b ) BY MINIMIZING CHI-SQUARE.
C     RETURNED: THE UNCERTAINTIES A AND B; SIGA,SIGB,
C     THE CHI-SQUARE; CHISQ,
C     AND THE GOODNESS-OF-FIT PROBABILITY Q;QPROB
C
C-----------------------------------------------------------------
      DIMENSION X(NDATA),Y(NDATA),SIG(NDATA)
      REAL A,B,SIGA,SIGB,CHI2,Q
C     INTIALIZE SUMS TO ZERO
      SX=0.
      SY=0.
      ST2=0.
      B=0.
C     ACCUMULATE SUMS........
      IF(MWT.NE.0) THEN
C          ....WITH WEIGTHS
          SS=0.
          DO 11 I= 1,NDATA
             WT=1./(SIG(I)**2)
             SS=SS+WT
             SX=SX+X(I)*WT
             SY=SY+Y(I)*WT
11        CONTINUE
      ELSE
C          ....WITHOUT WEIGHTS
          DO 12 I=1,NDATA
             SX=SX+X(I)
             SY=SY+Y(I)
12        CONTINUE
          SS=FLOAT(NDATA)
      ENDIF
      SXOSS=SX/SS
C      WRITE(6,100) SX,SY,SS,SXOSS
100   FORMAT(2X,4(2X,F10.2))
```

```
           IF(MWT.NE.0) THEN
              DO 13 I=1,NDATA
                 T=(X(I)-SXOSS)/SIG(I)
                 ST2=ST2+T*T
                 B=B+T*Y(I)/SIG(I)
13            CONTINUE
           ELSE
              DO 14 I=1,NDATA
                 T=X(I)-SXOSS
                 ST2=ST2+T*T
                 B=B+T*Y(I)
14            CONTINUE
           ENDIF
C          SOLVE FOR A,B,ASIGMA,BSIGMA
           B=B/ST2
           A=(SY-SX*B)/SS
C           WRITE(6,101) A,B
C101        FORMAT(' ',2(2X,F10.2))
           SIGA=SQRT((1.+SX*SX/(SS*ST2))/SS)
           SIGB=SQRT(1./ST2)
C           WRITE(6,100) A,B,SIGA,SIGB
C          CALCULATE CHI-SQUARE
           CHI2=0.
           IF(MWT.EQ.0) THEN
              DO 15 I=1,NDATA
                 CHI2=CHI2+(Y(I)-A-B*X(I))**2
15            CONTINUE
C          FOR UNWEIGHTED DATA EVALUATE TYPICAL SIG USING CHI2
C          AND ADJUST THE STANDARD DEVIATIONS.
              Q=1.
              SIGDAT=SQRT(CHI2/(NDATA-2))
              SIGA=SIGA*SIGDAT
              SIGB=SIGB*SIGDAT
           ELSE
              DO 16 I=1,NDATA
                 CHI2=CHI2+((Y(I)-A-B*X(I))/SIG(I))**2
16            CONTINUE
              Q=GAMMQ(0.5*(NDATA-2),0.5*CHI2)
           ENDIF
C           C=A
C           A=B
C           B=C
           RETURN
           END
C
C
           FUNCTION GAMMQ(A,X)
C-------------------------------------------------------------------
C
```

```
C       CALL BY SUBROUTINE FIT.
C       RETURNS THE INCOMPLETE GAMMA FUNCTION Q(a,x)= 1 - P(a,x)
C
C------------------------------------------------------------------
        IF(X.LT.0..OR.A.LE.0)PAUSE
        IF(X.LT.A+1.)THEN
C           USE THE SERIES REPRESENTATION
            CALL GSER(GAMSER,A,X,GLN)
C           TAKE COMPLIMENT OF GAMSER
            GAMMQ=1.-GAMSER
        ELSE
C           USE THE CONTINUED FRACTION REPRESENTATION
            CALL GCF(GAMMQ,A,X,GLN)
        ENDIF
        RETURN
        END
C
        SUBROUTINE GSER(GAMSER,A,X,GLN)
C------------------------------------------------------------------
C
C       RETURNS THE INCOMPLETE GAMMA FUNTION P(a,x) EVALAUTED BY
C       SERIES REPRESENTATION AS GAMSER. ALSO RETURNS ln[(a) AS
C       GLN
C
C------------------------------------------------------------------
        PARAMETER (ITMAX=100,ESP=3.E-7)
        GLN=GAMMLN(A)
        IF(X.LE.0.)THEN
            IF(X.LT.0.)PAUSE
            GAMSER=0.
            RETURN
        ENDIF
        AP=A
        SUM=1./A
        DEL=SUM
        DO 11 N=1,ITMAX
            AP=AP+1
            DEL=DEL*X/AP
            SUM=SUM+DEL
            IF(ABS(DEL).LT.ABS(SUM)*EPS)GO TO 1
11      CONTINUE
        PAUSE 'A too large,ITMAX too small'
1       GAMSER=SUM*EXP(-X+A*LOG(X)-GLN)
        RETURN
        END
C
        SUBROUTINE GCF(GAMMCF,A,X,GLN)
C------------------------------------------------------------------
C
```

```
C       RETURNS THEE INCOMPLETE GAMMA FUNCTION Q(a,x) EVALUATED BY
C       BY ITS CONTINUED FRACTION REPRESENTATION AS GAMMCF. ALSO
C       RETURNS ln[(a).
C
C---------------------------------------------------------------
        PARAMETER (ITMAX=100,EPS=3.E-7)
        GLN=GAMMLN(A)
        GOLD=0.
        AO=1.
        A1=X
        BO=0.
        B1=1.
        FAC=1.
        DO 11 N=1,ITMAX
            AN=FLOAT(N)
            ANA=AN-A
            AO=(A1+AO*ANA)*FAC
            BO=(B1+BO*ANA)*FAC
            ANF=AN*FAC
            A1=X*AO+ANF*A1
            B1=X*BO+ANF*B1
            IF(A1.NE.0.)THEN
                FAC=1./A1
                G=B1*FAC
                IF(ABS((G-GOLD)/G).LT.EPS)GO TO 1
                GOLD=G
            ENDIF
11      CONTINUE
        PAUSE 'A too large, ITMAX too small'
1       GAMMCF=EXP(-X+A*ALOG(X)-GLN)*G
        RETURN
        END
C
        FUNCTION GAMMLN(XX)
C---------------------------------------------------------------
C
C       RETURNS THE VALUE ln{T(xx) FOR xx>0.
C
C---------------------------------------------------------------
        REAL*8 COF(6),STP,HALF,ONE,FPF,X,TMP,SER
        DATA COF,STP/76.18009173D0,-8650532033D0,24.011409822D0,
     +      -1.231739516D0,.120858003D-2,-.536382D-5,2.50662827465D0/
        DATA HALF,ONE,FPF/0.5D0,1.0D0,5.5D0/
        X=XX-ONE
        TMP=X+FPF
        TMP=(X+HALF)*LOG(TMP)-TMP
        SER=ONE
        DO 11 J=1,6
            X=X+ONE
```

```
          SER=SER+COF(J)/X
11    CONTINUE
      GAMMLN=TMP+LOG(STP*SER)
      RETURN
      END
```

Appendix C

MAGSAT data and Programs

C.1 The MAGSAT data

.

The MAGSAT data obtained from G. V. Haines of the Geophysics Division, Geological Survey of Canada, is contained in an ASCII coded diskette as the file MAGSAT.ZRS. The following program may be ued to read the data.

```
      PROGRAM MAG
C*******************************************************************
C     THIS PROGRAM READS MAGSAT DATA FROM THE FILE MAGSAT.ZRS.    *
C     IT IS CAPABLE OF READING  DATA FOR A SPECIFIC REGION        *
C     USES SUBROUTINE EQAREA  FOR EQUAL AREA  PROJECTION.         *
C*******************************************************************
      REAL OBSLAT,OBSLON,OBSALT,OBSX,OBSY,OBSZ,ZVAL
      REAL LITLAT,LAT,BIGLAT
C
C     OBSLAT : LATITUDE
C     OBSLON : LONGITUDE
C     OBSALT : ELEVATION
c     OBSX   : X-LOCATION
C     OBSY   : Y-LOCATION
C            : X AND Y DEFINE THE POSITION OF ZVAL
C     ZVAL   : THE MAGNETIC ANOMALY AT (X,Y)
C
```

```
C       LITLAT/BIGLAT DEFINE THE REGION OF INTEREST TO BE EXTRACTED.
        LITLAT = 60.0
        BIGLAT = 90.0
        READ(18,*) NUM
        DO 10 I=1,7524
           READ(18,*) OBSALT,OBSLAT,OBSLON
C          READ(17,*) OBSLAT,OBSLON
C*
C*         CONVERT OBSERVATION POSITION TO XY COORDINATES
C*         FOR EQUAL AREA POLAR STEREOGRAPHIC PROJECTION.
C*
           CALL EQAREA(OBSLAT,OBSLON,OBSALT,OBSX,OBSY)
C       IF ( (OBSLAT .LT. LITLAT) .OR. (OBSLAT .GT.BIGLAT) ) GOTO 10
C           WRITE(12,35) OBSALT,OBSLAT,OBSLON,OBSX,OBSY,OBSZ,ZVAL
            WRITE(12,35) OBSLAT,OBSLON,OBSX,OBSY,ZVAL
35      FORMAT(7(F10.2))
10      CONTINUE
        STOP
        END
C*
        SUBROUTINE EQAREA(RLAT,RLONG,RO,X,Y,Z)
C
C       THE VALUE OF OLAT AND OLONG ARE TO BE CHANGED TO THE
C       CENTRE OF THE AREA OF INTEREST
C
        OALAT=40.50
        OLONG=270.50
C        OALAT=90.00
C        OLONG=0.0
C        RO=6378.16
C        RO=6371.2
        RO=6356.912
        PI=4.0*ATAN(1.0)
        RATE=PI/180.0
        A=OALAT*RATE
        B=RLAT*RATE
        C=(RLONG-OLONG)*RATE
        D=1.0+SIN(A)*SIN(B)+COS(A)*COS(B)*COS(C)
        R=RO*(1.0-0.003367*SIN(A)**2+0.0000071*(SIN(2.0*A))**2)
        X=2.0*R*(COS(A)*SIN(B)-SIN(A)*COS(B)*COS(C))/D
        Y=2.0*R*(COS(B)*SIN(C))/D
        RETURN
        END
C
        RETURN
        END
```

C.2 Modeling program

The following program MAG is a simplified version of that developed by Noble (1883).

It calculates the vertical anomaly field for a given spherical prism. The equations used

were discussed in Chapter 6.

```
      PROGRAM MAG
C*******************************************************************
C     THIS PROGRAM CALCULATES THE VERTICAL COMPONENT OF THE        *
C     MAGNETIC FIELD ANOMALY USING SPHERICAL PRISMS.               *
C                                                                  *
C*******************************************************************
C
C     THE DIPOLE VARIABLES
C
C     DELRHO: RADIAL DIMENSION OF PRISM
C     DELTHE: LONGITUDINAL ANGULAR DIMENSION OF PRISM
C     DELPHI: LATITUDINAL ANGULAR DIMENSION OF PRISM
C     MIDRHO,MIDLAT,MIDLON: CENTER OF PRISM
C     DIPXDIPY,DIPZ: CARTESIAN LOCATION OF DIPOLES
C
      REAL DELRHO(100),DELTHE(100),DELPHI(100),GAUSS(2)
      REAL DIPRHO,DIPLAT,DIPLON,DIPX,DIPY,DIPZ
      REAL MIDRHO(1000),MIDLAT(1000),MIDLON(1000)
C
C     OBSERVATION VARIABLES
C
C     OBSLAT,OBSLON,OBSALT: SPHERICAL CO-ORD OF OBSERVATION POINT
C     OBSX,OBSY,OBSZ: CARTESIAN  CO-ORD OF OBSERVATION POINT
      REAL OBSLAT,OBSLON,OBSALT,OBSX,OBSY,OBSZ
C
C     OTHERS
C     JX,JY,JZ,JS                 : MAGNETIZATION VARIABLES
C     OPLOTX,OPLOTY,XPLOT,YPLOT: VARIABLES TO HOLD PLOTTING POINTS
C


      REAL ZFIELD(2000),RX,RY,RZ,JX,JY,JZ,JS(100),R2,R5
      REAL XPLOT(2000),YPLOT(2000),X(2000),Y(2000)
C*
C*
C*    CONSTANTS AND COUNTERS
C
C     MU                          : PERMEABILITY OF FREE SPACE
C     DECL                        : DECLINATION
C     INCL                        : INCLINATION
```

```
C      B                              : EARTH FIELD
C
       INTEGER I,J,K,IRHO,JLAT,KLON,IDP,DIPNUM
       REAL MU,DECL,INCL,B
       REAL CONST1,CONST2,CONST3,PI,CONVRT,DELH
C
C*
C*     STATE THE CONSTANTS
C*
       PI = 3.1415926536
       CONVRT = PI/180.0
       INCL=90.0
       DECL=0.0
       B=60000.0/1000000000.0
       MU=4.0*PI/10000000.0
       DELH=1000.
C
C*     PRISM CONSTANTS
C
       GAUSS(1)= 1.0/(3.0**(1.0/2.0))
       GAUSS(2)= -GAUSS(1)
C*
C*     READ PRISM INFORMATION
C*
       READ(5,*) DIPNUM
       DO 15 I=1,DIPNUM
       READ(5,*) MIDRHO(I),MIDLAT(I),MIDLON(I),
      +DELRHO(I),DELTHE(I),DELPHI(I),JS(I)
C      CONVERT FROM KM TO M
       MIDRHO(I)=MIDRHO(I)*DELH
       DELRHO(I)=DELRHO(I)*DELH
C      WRITE(6,*) MIDRHO(I),MIDLAT(I),MIDLON(I),DELTHE(I),DELPHI(I)
  15   CONTINUE
C
C      READ OBSERVATION INFORMATION
C
C      STATE OBSERVATION ALTITUDE (m)
       OBSALT=6700*DELH
C
C
C      CALCULATION OF FIELD
C      STEP 1: FIND POSITION OF OBSERVATION POINT.
C      MU=4*PI*E-7 ; MU/4*PI = E-7
C
C*      READ(17,8) OBSNUM
C*      DO 10 I=1,OBSNUM
       DO 10 I=1,1316
C      INITIALIZE FIELD TO ZERO
       ZFIELD(I)=0.0
```

```
            READ(17,*) OBSLAT,OBSLON
C*           WRITE(6,*) OBSLAT,OBSLON,OBSALT
C
C           CONVERT OBSERVATION POSITION TO XY COORDINATES
C           FOR EQUAL AREA POLAR STEREOGRAPHIC PROJECTION.
C
            CALL EQAREA(OBSLAT,OBSLON,OBSALT,OPLOTX,OPLOTY)
            XPLOT(I)=OPLOTX
            YPLOT(I)=OPLOTY
C*           WRITE(6,*) OBSLAT,OBSLON,OPLOTX,OPLOTY
C
C           CONVERT OBSERVATION POSITION FROM SPHERICAL EARTH
C           TO FIXED X,Y, AND Z COORDINATES.
C
            OBSLAT=90.0-OBSLAT
            CALL DETXYZ(OBSALT,OBSLAT,OBSLON,OBSX,OBSY,OBSZ)
C
C           FIND COORDINATES OF DIPOLE AND MAGNETIZATION
C
            DO 16 IDP=1,DIPNUM
            JX=JS(IDP)*COS(INCL*CONVRT)*COS(DECL*CONVRT)
            JY=JS(IDP)*COS(INCL*CONVRT)*SIN(DECL*CONVRT)
            JZ=JS(IDP)*SIN(INCL*CONVRT)
            CONST1=(DELRHO(IDP)*(DELTHE(IDP)*CONVRT)*(DELPHI(IDP)
        *          *CONVRT))/80000000.0
            DO 20 IRHO=1,2
            DIPRHO=MIDRHO(IDP) + (DELRHO(IDP)/2.0)*GAUSS(IRHO)
            DO 30 JLAT=1,2
            DIPLAT=MIDLAT(IDP) + (DELTHE(IDP)/2.0)*GAUSS(JLAT)
            DIPLAT=90-DIPLAT
            DO 40 KLON=1,2
            DIPLON=MIDLON(IDP) + (DELPHI(IDP)/2.0)*GAUSS(KLON)
C
C           CONVERT EARTH SPHERICAL COORDINATES OF DIPOLE
C           TO FIXED X,Y, AND Z COORDINATES.
C
            CALL DETXYZ(DIPRHO,DIPLAT,DIPLON,DIPX,DIPY,DIPZ)
C           WRITE(6,*) DIPLAT,DIPLON,DIPRHO,DIPX,DIPY,DIPZ
C
C           FIND SEPERATION VECTOR AND COMPONENTS
C
            RX=DIPX-OBSX
            RY=DIPY-OBSY
            RZ=DIPZ-OBSZ
            R2=(RX*RX + RY*RY + RZ*RZ)**(1/2.0)
            R5=R2**5
C           WRITE(6,*) RX,RY,RZ
C
C           CALCULATE THE ANOMALY
```

```fortran
C
      CONST2=CONST1*DIPRHO*DIPRHO*SIN(DIPLAT*CONVRT)/R5
      CONST3=CONST2*(JX*3.0*RX*RZ
     +         + JY*3.0*RY*RZ + JZ*((3.0*RZ*RZ)-R2*R2))
      ZFIELD(I)=ZFIELD(I)+CONST3
  40  CONTINUE
  30  CONTINUE
  20  CONTINUE
  16  CONTINUE
  10  CONTINUE
C
C     CONVERT INTO nT AND WRITE
C
      DO 111 I=1,1316
      ZFIELD(I)=ZFIELD(I)*1000000000.0
C     WRITE FOR PLOTING
      WRITE(12,*) XPLOT(I),YPLOT(I),ZFIELD(I)
111       CONTINUE
C
      STOP
      END
C
      SUBROUTINE EQAREA(RLAT,RLONG,RO,X,Y)
C********************************************************************
C     (see previous program)
C********************************************************************
C
      SUBROUTINE DETXYZ(RHO,COLAT,ELONG,X,Y,Z)
C********************************************************************
C                                                                  *
C     THIS SUBROUTINE CONVERTS RADIAL DISTANCE (RHO),              *
C     GEOCENTRIC CO-LATITUDE (COLAT), AND EAST LONGITUDE (ELONG)   *
C     TO EARTH FIXED CO-ORDINATES X,Y, AND Z.                      *
C     THE X-AXIS PIERCES THE EARTH SURFACE AT THE INTERSECTION     *
C     OF GREENWICH MERIDIAN AND THE EQUATOR. THE Z-AXIS CONCIDES   *
C     WITH THE NORTH ROTATIONAL AXIS.                              *
C                                                                  *
C     INPUT: RHO, COLAT, ELONG.                                    *
C                                                                  *
C     OUTPUT: X, Y, Z.                                             *
C                                                                  *
C********************************************************************
C
      PI = 3.1415926536
      CON = PI/180.0
C
      COSLAT=COS(COLAT*CON)
      SINLAT=SIN(COLAT*CON)
      COSLON=COS(ELONG*CON)
```

```
      SINLON=SIN(ELONG*CON)
C
      X=RHO*COSLON*SINLAT
      Y=RHO*SINLON*SINLAT
      Z=RHO*COSLAT
C
      RETURN
      END
```

The following subroutines from the Computer Services at the University of Manitoba were used:

a) IMSL Subroutine IQHSCV; used for interpolating data.

b) Subroutine SMOCON; used for contouring the data.